The Dissertation Committee for Lauren Cristy Andrews Certifies that this is the approved version of the following dissertation:

Spatial and Temporal Evolution of the Glacial Hydrologic System of the Western Greenland Ice Sheet: Observational and Remote Sensing Results

Committee:

Ginny A. Catania, Supervisor

Meinhard Bayani Cardenas

Matthew J. Hoffman

Charles S. Jackson

David Mohrig

Spatial and Temporal Evolution of the Glacial Hydrologic System of the Western Greenland Ice Sheet: Observational and Remote Sensing Results

by

Lauren Cristy Andrews, B.A.

Dissertation

Presented to the Faculty of the Graduate School of

The University of Texas at Austin

in Partial Fulfillment

of the Requirements

for the Degree of

Doctor of Philosophy

The University of Texas at Austin

December 2015

Dedication

To John and Joe.

"Walking across any glacier is a hazardous undertaking, and this one was particularly trying."

- Jean Bowie Shor, *After You, Marco Polo*

Acknowledgements

I thank my advisor, Ginny Catania, for giving me the freedom to explore and the boundaries to move my understanding forward. I would also like to thank Bayani Cardenas, Charles Jackson, and David Mohrig for their classes, advice, and reviews. Science is never an individual experience, and without the knowledge and insight of Matthew Hoffman, Joseph MacGregor, and Jason Gulley, I might be still lost in the weeds. In particular, Matthew Hoffman spent more hours on the phone helping me think through problems than was strictly necessary.

To the scientists who provided valuable advice, Bob Hawley, Tom Neumann, Leigh Stearns, and Martin Lüthi: thank you. Fieldwork wouldn't hold its appeal without a number of individuals, including Kristin Schild, Blaine Morriss, and Claudia Ryser. I shared the experience of being a graduate student with a wide array of wonderful individuals, including Lindsay Olinde, Benj Wagman, Liz Logan, Katie Delbecq, Mason Fried, Brendan Murphy, Denis Felikson, John Nowinski, and Justin Heister.

The staff of the Institute for Geophysics and CH2MHill Polar Services are amazing. Their assistance will be remembered with gratitude, whether it involved two tons of cargo or Greenlandic receipts. Much of this work was supported by United States National Science Foundation grant OPP 0908156 and National Geographic Society grant 9067-12. I also benefited from the financial support of a number of fellowships, including the Gale White and Ewing/Worzel Fellowships from the Institute for Geophysics.

These things are never finished without acknowledging the unwavering support and understanding of family and friends. John Andrews and Joseph MacGregor, a thank you will never convey how much you mean to me.

Spatial and Temporal Evolution of the Glacial Hydrologic System of the Western Greenland Ice Sheet: Observational and Remote Sensing Results

Lauren Cristy Andrews, Ph.D.

The University of Texas at Austin, 2015

Supervisor: Ginny A. Catania

The Greenland Ice Sheet is losing mass at an accelerating rate due to a combination of increased surface melting and changes in dynamical behavior, both of which are associated with changing climate. In the ablation zone, seasonal melting results in a dynamic ice-sheet response as supraglacial meltwater reaches the ice–bed interface via moulins and crevasses. Meltwater delivery to the bed increases subglacial water pressure and decreases basal traction, leading to regional ice acceleration. However, these processes and their future evolution are poorly constrained. An improved understanding of the complex relationship between the glacial hydrologic system and ice velocity will ultimately improve predictions of ice-sheet mass change.

In this dissertation, I use a suite of techniques to quantify the response of the glacial hydrologic system to changes in melt supply on daily to inter-decadal timescales. Moulins represent the primary englacial connection between the ice surface and its bed. As such, they play a critical role in determining the location of subglacial channels in the ablation zone. I observe inter-decadal persistence in moulin locations, which can result in positive feedbacks that allow for rapid growth at the onset of the melt season and encourage persistence of subglacial channels. These observations suggest that inter-

decadal variability in the relationship between supraglacial melt production and ice velocity is caused by altering the rate at which efficient subglacial drainage pathways develop. Further, my observations indicate that daily changes in ice velocity are mirrored by moulin water levels, but this pattern does not hold at seasonal timescales. This relationship suggests that the channelized portion of the subglacial hydrologic system adjusts rapidly to the available meltwater; therefore, long-term trends in ice velocity are the result of increasing hydrologic connectivity of poorly connected regions of the bed, lowering regional subglacial water pressure. Finally, the subglacial hydrologic system experiences variability on multiple timescales, some of which are not accounted for in existing models of this system. By modeling the mechanisms causing both diurnal to seasonal and changes in moulin water level, I further constrain the physical processes impacting mass change in land-terminating regions of the Greenland Ice Sheet.

Table of Contents

List of Tables xi

List of Figures xii

Chapter 1. Introduction 1

1.1. Glacier Dynamics 2

1.1.1. Historical Basis 2

1.1.1.1 Glacier Motion 2

1.1.1.2 Subglacial Hydrology 4

1.1.2. Conceptual Model 7

1.2. Greenland Ice Sheet Ablation Zone 9

1.2.1. Ice-sheet Response to Melting 9

1.2.2. GrIS Ice Velocity 10

1.3. Importance and Scope 12

Chapter 2. Multi-decadal moulin variability and implications for subglacial drainage of the Greenland Ice Sheet 17

2.1. Abstract 17

2.2. Introduction 17

2.2. Data and Methods 19

2.2.1. Data 20

2.2.2. Moulin Identification 20

2.3 Supraglacial Drainage Basin Delineation 22

2.2.4. Subglacial Drainage 24

2.3. Results and Analysis 25

2.3.1. Moulin Distribution 25

2.3.2. Supraglacial Basins 28

2.3.3. Moulin Connection to Subglacial Flow Paths 29

2.4. Discussion 29

2.4.1. Changing Moulin Distribution 29

2.4.2. Characteristics of Matched Moulins 30

2.4.3 Subglacial Implications 31
2.5. Conclusions 33
2.6. Acknowledgements 34
2.7. Author Contributions 34

Chapter 3. Direct observations of evolving subglacial drainage beneath the Greenland Ice Sheet 44
3.1. Introductory Paragraph 44
3.2. Main Text 45
3.3. Extended Methods 53
3.3.1. Seasonal Data Presentation 53
3.3.2. Borehole Drilling and Instrumentation 53
3.3.3. Moulin Instrumentation and Measurements 55
3.3.4. Coincident Observations 57
3.3.5. Ice Velocity and Bed Separation 57
3.3.6. Melt Events 59
3.3.7. Cross-Correlation Analysis 60
3.3.8. Subglacial Channel Geometry 61
3.3.9. Potential Mechanisms for Borehole Diurnal Variability 64
3.3.10. Flow Coupling and Mechanical Support Transfer 65
3.3.11. Moulin–Velocity Hysteresis 66
3.3.12. GULL Borehole Observations 66
3.4. Acknowledgements 66
3.5. Author Contributions 67

Chapter 4. Modeled and observed seasonal evolution of drainage efficiency in the Paakitsoq Region of western Greenland 79
4.1. Abstract 79
4.2. Introduction 79
4.3. Data and Methods 83
4.3.1. Remote-Sensing and Field Observations 83
4.3.1.1. Drainage Basin Delineation 84
4.3.1.2. Supraglacial Drainage 85

4.3.1.3. Moulin Hydraulic Head 88
4.3.1.4. Ice Velocity 88
4.3.2. Subglacial Drainage Model 89
4.3.2.1. Channelized Drainage 90
4.3.2.2. Subglacial Storage 93
4.3.2.3. Subglacial Overpressurization 95
4.4. Results and Analysis 96
4.4.1. Supraglacial Hydrology 96
4.4.2. GPS Observations 96
4.4.3. Model Results 98
4.4.3.1 Modeled Subglacial Characteristics 98
4.4.3.2 Comparison of Modeled Subglacial Characteristics and Observed Ice Velocity 100
4.4.3.3. Modeled and Observed Moulin Hydraulic Head 101
4.5. Discussion 102
4.5.1. Seasonal Evolution of the Subglacial Hydrologic System 102
4.5.1.1 Onset of Summer Ice Motion 102
4.5.1.2 Transition to Efficient Subglacial Drainage 103
4.5.2. Modeled and Observed Moulin Hydraulic Head 105
4.6. Conclusions 107
4.7. Acknowledgements 108
4.8. Author Contributions 108
Chapter 5. Conclusions 119
5.1. Synthesis 119
5.2. Summary of this Dissertation 119
5.3. Direction of Future Work 121
References 124

List of Tables

Table 2.1. Mann-Whitney U test results for supraglacial basin size. 43

Table 3.1. Site coordinates and characteristics 76

Table 3.2. Cross-correlation analysis for boreholes, moulins, and ice velocity 77

Table 3.3. Parameters used in conduit-geometry calculations 78

Table 4.1. Parameters used in 1D subglacial model 118

List of Figures

Figure 1.1. Schematic of the glacial hydrologic system 15

Figure 1.2. Conceptual relation between subglacial hydrology and seasonal ice acceleration 16

Figure 2.1. Paakitsoq Region, Western Greenland 35

Figure 2.2. Representative moulins and associated supraglacial features 36

Figure 2.3. Moulin surface drainage basins 37

Figure 2.4. Moulins present in both 1985 and 2011 38

Figure 2.5. Getis-Ord Gi* cluster analysis for matched and unmatched moulins 39

Figure 2.6. Moulin and drainage basin densities 40

Figure 2.7. Subglacial flow pathways and moulin association 41

Figure 2.8. Conceptual model of moulin formation and downstream advection 42

Figure 3.1. Study area in the western ablation zone of the Greenland Ice Sheet 68

Figure 3.2. Borehole and moulin head and ice-surface velocity during 2011 and 2012 69

Figure 3.3. Relationships between hydraulic head and ice-surface velocity 70

Figure 3.4. Borehole and moulin head and ice-surface velocity over two melt seasons 71

Figure 3.5. Components of vertical motion 2011 and 2012 72

Figure 3.6. Modeled hydraulic head and conduit geometry 73

Figure 3.7. Long-term relationship between moulin head and ice velocity for 2012 and 2011 74

Figure 3.8. Borehole hydraulic heads and ice velocity at GULL during 2011 75

Figure 4.1. Study area in the Paakitsoq Region of western Greenland.....109

Figure 4.2. Modeled daily ablation for three locations in the study domain 110

Figure 4.3. 24-h GPS-derived ice surface velocities and surface melt rates for 2011 111

Figure 4.4. 24-h GPS-derived ice surface velocities and surface melt rates for 2012 112

Figure 4.5. 6-h GPS-derived ice surface velocities and surface melt rates for 2011 113

Figure 4.6. 6-h GPS-derived ice surface velocities and surface melt rates for 2012. 114

Figure 4.7. Modeled fraction of overburden and subglacial channel geometry for 2011 and 2012 115

Figure 4.8. Observed and modeled moulin hydraulic head in 2011 and 2012 116

Figure 4.9. Non-uniform channel development and diurnal ice velocity 117

Chapter 1. Introduction

The interaction of water and ice modulates glacier and ice-sheet behavior on both short and long timescales via multiple processes. Ongoing anthropogenic climate change has accelerated these interactions, resulting in increasingly negative glacier and ice-sheet mass balance [*Vaughan et al.*, 2013]. Despite clear indications of mass loss for nearly all glaciated regions of Earth, the nature of future interactions between these ice masses and the water generated by their continued disintegration is poorly constrained. This challenge is perhaps best exemplified at the ice–bed interface, where the evolution of the subglacial hydrologic system in response to a changing meltwater supply results in substantial spatiotemporal variability in ice flow.

This dissertation focuses on the processes affecting ice flow in the ablation zone of the western Greenland Ice Sheet (GrIS). Each melt season (late May through August), the GrIS ablation zone experiences complex changes in ice motion as surface melt is routed through actively changing supraglacial, englacial, and subglacial hydrologic systems. The ultimate goal of this study is to better constrain the processes that cause the observed dynamic response of the GrIS, so that we may better predict their long-term evolution and impact on mass change. To achieve this advance, I combine direct field observations, high-resolution remote sensing data and numerical modeling, and aim to develop a holistic understanding of key ice-dynamic and hydrologic mechanisms and their relationships.

1.1. GLACIER DYNAMICS

1.1.1. Historical Basis

1.1.1.1 Glacier Motion

Glaciers accumulate mass at higher elevations through snowfall and lose mass (ablate) at lower elevations due to surface melting, iceberg calving or submarine melting [*van der Veen*, 1999]. Driven by gravity, creep deformation, basal sliding, and subglacial till deformation cause ice flow from the accumulation area to the ablation area [*Cuffey and Paterson*, 2010]. In particular, basal motion, either through the deformation of subglacial sediments or sliding along the ice-bed interface, can account for a substantial component of glacier and ice sheet motion. Though the mechanisms driving basal sliding, are complex, the role of meltwater in accelerating basal motion, was recognized by the early pioneers of modern glaciology [e.g., *Forbes*, 1859].

Though glaciers and ice sheets can be underlain by a sediments and bedrock with varying properties [*Cuffey and Paterson*, 2010], this introduction focuses on role of water in facilitating acceleration of glacier sliding over bedrock. When basal ice is near the pressure melting point, a film of liquid water forms at the ice-bed interface. Classical, hard-bedded sliding theory hypothesizes that this film of water is unable to support basal shear stresses resulting from glacier flow, thus any drag or inhibition of basal flow is caused by bed undulations [*Weertman*, 1957, 1979; *Nye*, 1969, 1970; *Kamb*, 1970; *Fowler*, 1981] or debris bridging the water film [*Fowler*, 1981; *Schweizer and Iken*, 1992]. As ice moves over these aspersions via viscous creep and regulation, subglacial cavities form on the lee side of bedrock obstacles [*Lliboutry*, 1968]. The size of these subglacial cavities should be dependent on the effective subglacial pressure, defined as ice overburden pressure minus subglacial water pressure. Thus, basal drag, τ_b, is a function of ice motion at the bed, u_b, and effective pressure, p_e, such that:

$$\tau_b = C u_b^m p_e^n \quad , \tag{1.1}$$

where, C and m are positive constants dependent on basal roughness and ice rheology, and n is the Glen's flow law exponent for ice [*Budd et al*., 1979; *Bindschadler*, 1983; *Cuffey and Paterson*, 2010]. Field observations of ice velocity and subglacial pressure generally validate the relation in Equation 1.1 [e.g., *Iken and Bindschadler*, 1986]. However, this and similar power law relations are physically unrealistic in that basal drag can increase without bound with increasing basal sliding or effective pressure. As ice flows, basal drag is generated by high compressive stresses on the upstream side of a bedrock bump, which are necessarily balanced by low compressive stresses on the lee side [*Iken*, 1981; *Schoof*, 2005]. However, when the subglacial pressure exceeds ice overburden pressure, cavitation acts to as a negative feedback, inhibiting basal drag [*Iken*, 1981; *Schoof*, 2005; *Gagliardini et al*., 2007]. This limit on basal drag is independent of ice velocity; thus if the driving stress of the glacier or ice sheet exceeds the local basal drag, longitudinal and lateral stresses become important to ice flow. In these instances, changes in basal motion are largely controlled by changing stress distribution beneath and within the ice [e.g., *Howat et al*., 2008].

Redistribution of stresses within and beneath the ice column is aided by spatially heterogeneous water supply. While ice at the pressure melting point supplies a small amount of subglacial water, summer melting can provide a large and variable volume of meltwater. Observations of borehole water pressure and surface motion led to the recognition that increased surface velocity and subglacial cavity growth are associated with an increase in meltwater supply delivered by moulins and crevasses [*Iken et al*., 1983; *Iken and Bindschadler*, 1986]. Variation in meltwater supply can result in the transfer of stresses to and from hydraulically active regions of the bed over hours to days [*Murray and Clarke*, 1995; *Kavanaugh and Clarke*, 2001; *Amundson et al*., 2006; *Howat*

et al., 2008]. Reorganization of basal stresses can be correlated, not just with the volume of subglacial cavities, but with the state of the subglacial hydrologic system. If locally available meltwater exceeds the capacity of the subglacial hydrologic system, subglacial pressures increase and basal drag decreases, resulting in stress transfer to other regions of the bed [*Mair et al*., 2001, 2002a]. However, if the capacity of the subglacial system evolves to more rapidly conduct available meltwater and locally decrease effective pressure, local basal drag can increase [*Mair et al*., 2001, 2002a]. Thus, the state of the subglacial hydrologic system can impact both subglacial pressure and the spatial distribution of basal drag.

1.1.1.2 Subglacial Hydrology

Observations of borehole pressure and ice velocity used to validate theoretical sliding relationships also reveal a dynamic subglacial hydrologic system [e.g., *Müller and Iken*, 1973; *Iken and Truffer*, 1997]. Glaciers and ice sheets with beds at the pressure melting point are generally believed to have liquid water at the ice-bed interface whether it is contained in subglacial cavities [e.g., *Lliboutry*, 1968; *Walder*, 1986; *Kamb*, 1987], as a thin water film [e.g., *Weertman*, 1966, 1969], or within subglacial till [*Boulton and Jones*, 1979]. While many of these cavities may be isolated from surface meltwater and each other either completely [e.g., *Weertman*, 1964; *Iken and Truffer*, 1997] or ephemerally [e.g., *Murray and Clarke*, 1995], interconnected cavities grow with an increase in meltwater supply delivered by moulins and crevasses [*Iken et al*., 1983]. This cavity growth increases subglacial storage of water, which can directly influence ice motion [*Iken et al*., 1983; *Kamb et al*., 1994; *Bartholomaus et al*., 2008]. Water movement within these potentially extensive interconnected cavities is generally considered inefficient [*Fountain and Walder*, 1998]. However, substantial efficient water flow can occur in channels incised in ice (Röthlisberger or R-channels) [*Röthlisberger*,

1972; *Hooke*, 1984] or bedrock (Nye or N-channels) [*Nye*, 1973], whose locations are determined by both the basal topography and the overlying ice [*Shreve*, 1972].

The characteristics of the inefficient and efficient drainage components of the subglacial hydrologic system depend on local basal conditions, such as bedrock lithology and the presence or absence of till. Although direct visual observations of this system are limited, the theoretical foundation of subglacial water drainage has generally proved to be consistent with such observations. There are observations of past and active subglacial cavities (inefficient flow) [e.g., *Engelhardt et al*., 1978; *Walder and Hallet*, 1979; *Anderson et al*., 1982; *Rea and Whalley*, 1994], R-channels (efficient flow) [*Engelhardt et al*., 1978; *Walder and Hallet*, 1979; *Gulley et al*., 2014] and N-channels (efficient flow) [e.g., *Walder and Hallet*, 1979]. Water flow through subglacial till may also be an important mechanism affecting basal lubrication [e.g., *Walder and Fowler*, 1994; *Harper and Humphrey*, 1995].

Theoretical and observational work indicates that the form of the subglacial drainage network can impact the efficiency of subglacial water flow and the relation between discharge capacity and subglacial pressure. Inefficient drainage via interconnected subglacial cavities, water films, and porous flow will display increasing subglacial pressure with increasing discharge [*Hubbard and Nienow*, 1997]. However, efficient drainage via ice R- or N- channels displays a slight inverse relationship, with increasing discharge leading to decreasing subglacial pressure [*Röthlisberger*, 1972; *Hooke*, 1984]. This contrasting behavior is the result of different mechanisms dominating their formation. The capacity of an inefficient drainage system is determined by the balance between ice-bed separation due to basal motion and creep closure due to the pressure of the overlying ice. Thus, cavity formation is favored by high subglacial pressures and bed roughness [*Nye*, 1970]. Water flow between inefficient drainage

elements is restricted by bed roughness and close contact between the bed and overlying ice, limiting melting due to energy dissipated by flowing water. In contrast, the capacity efficient, ice-incised subglacial channels are primarily driven by the balance between melting and creep closure because once the radius of the subglacial channel is greater than the bedrock roughness elements, opening cannot be generated through sliding. Instead, the relatively large hydraulic radius of subglacial channels allows for fast turbulent flow and any energy generated from turbulent flow in excess of that needed to maintain the water temperature at the pressure melting can be used to enlarge the subglacial channel radius.

Inefficient and efficient drainage elements are thought to coexist and evolve over the duration of the melt season [*Hubbard and Nienow*, 1997; *Fountain and Walder*, 1998]. Efficient subglacial drainage elements are unstable at low discharges and creep closed over winter [*Walder*, 1986; *Fountain and Walder*, 1998]. Thus, early in the melt season inefficient drainage dominates, as confirmed by slow transit velocities and disperse concentration returns during dye-tracing studies [e.g., *Nienow et al*., 1998; *Chandler et al*., 2013]. Though efficient subglacial elements may remain active near the terminus where water volumes can be relatively large and creep closure rates are low. Increases in meltwater supply will increase subglacial pressures and allow subglacial cavity growth [e.g., *Iken et al*., 1983; *Bartholomaus et al*., 2011]. If the meltwater flux increases rapidly enough, ice-incised channels will form [*Kamb*, 1987; *Schoof*, 2010] and subglacial discharge becomes efficient. As long as the supply of meltwater is sufficient, melt will counteract creep closure and efficient drainage will persist. Dye-tracing studies consistently support this temporal evolution and also suggest an upstream progression of this subglacial transition [e.g., *Nienow et al*., 1998; *Chandler et al*., 2013]; however, the

details of the spatial and temporal variability of the subglacial hydrologic system are poorly constrained.

1.1.2. Conceptual Model

The presence, distribution and flow of water plays a fundamental from in ice motion under both alpine glaciers [e.g., *Iken and Bindschadler*, 1986] and ice sheets [e.g., *Kamb*, 2001]. Though large portions of Antarctica and some glaciers do not experience surface melting, on the GrIS and many alpine glaciers, the timing of melt production and its accommodation within the supraglacial hydrologic system directly influences basal stress distribution, and thus basal sliding. During the summer melt season, above-freezing temperatures result in melting on the GrIS's subaerial surface (forming supraglacial meltwater). This meltwater either flows over the ice surface or percolates through the overlying snow and firn where it can be retained within an aquifer [*Forster et al*., 2014] or can flow horizontally along an impermeable layer (Figure 1.1). On bare ice, this meltwater frequently coalesces into supraglacial streams, where enhanced heat transfer results in channel incision into the ice surface [*Karlstrom et al*., 2013]. Most of these streams drain into either supraglacial lakes or directly into englacial conduits [*Smith et al*., 2015], though in some instances they can carry water supraglacially to the terminus. Englacial conduits (moulins or crevasses) allow water to move through the glacier. While water may be stored, and potentially refreeze within crevasses, much of this water reaches the bed [*Smith et al*., 2015], though how directly depends on the formation mechanism of the conduit [*Gulley et al*., 2009].

Once water reaches the ice–bed interface, its flow is generally characterized as either inefficient/slow/distributed or efficient/fast/channelized, based on water velocity and the ability of the subglacial hydrologic system to drain available meltwater [*Fountain and Walder*, 1998; *Flowers*, 2015]. Prior to the onset of summer melting, the only

available water is from basal melting and englacial storage. This limited supply water suggests that the subglacial hydrologic system likely maintains itself in an inefficient configuration [*Walder*, 1986; *Fountain and Walder*, 1998]. Though subglacial channels may be stable near the terminus [*Rennermalm et al*., 2013a] where ice overburden pressures are low and discharge is collected from a large upstream catchment. The spatially extensive distribution of water within inefficient drainage features results in low hydraulic radii. As a result, these features operate at high water pressure (at or near ice overburden pressure) and water flow within/between them is driven by small pressure gradients. Slow flow within these inefficient features limits melting of the overlying ice induced by turbulent dissipation of energy [*Walder*, 1986].

Large perturbations in water supply associated with the onset of summer supraglacial melting overwhelm this inefficient drainage system, increasing subglacial water pressure and ice velocity due to enhanced basal sliding (Figure 1.2) [e.g., *Iken and Bindschadler*, 1986; *Mair et al*., 2002; *Bartholomaus et al*., 2008]. When the inefficient subglacial hydraulic system is unable to accommodate more water, increased hydraulic gradients allow for increased water velocity. At high flow velocities, basal melting due to the dissipation of turbulent energy exceeds sliding-driven cavity opening and efficient subglacial pathways evolve [*Röthlisberger*, 1972; *Schoof*, 2010]. The formation and evolution of efficient drainage pathways increase hydraulic radii and reduce subglacial water pressure, leading to decreasing basal sliding and ice surface velocity (Figure 1.2) [e.g., *Mair et al*., 2002; *Bartholomaus et al*., 2008]. Increased drainage efficiency also reduces the impact of subsequent melt events on ice velocity because larger volumes of water are necessary to perturb the subglacial hydrologic system [e.g., *Bartholomaus et al*., 2008]. Thus, seasonal subglacial hydrologic system evolution typically results in

initially rapid ice acceleration due to increased basal sliding, followed by a more gradual deceleration associated with increased subglacial drainage efficiency (Figure 1.2).

While this conceptual model qualitatively describes seasonal ice acceleration, a number of unknowns remain. Of particular interest is the possible coexistence of multiple subglacial drainage types, due to heterogeneous water delivery and bed conditions [*Harper and Humphrey*, 1995; *Gulley et al*., 2012]. Further, most borehole studies indicate that substantial regions of the bed remain undrained [e.g., *Murray and Clarke*, 1995; *Harbor et al*., 1997; *Fountain and Walder*, 1998; *Mair et al*., 2002; *Hart et al*., 2015], indicating that they are not connected to the active components of the subglacial hydrologic system (whether efficient or inefficient). Yet, these unconnected regions are far from inactive [*Iken and Truffer*, 1997]. Thus, this conceptual model fails to recognize the importance of those unconnected regions of the bed, which likely constitute the majority of the bed.

1.2. Greenland Ice Sheet Ablation Zone

1.2.1. Ice-sheet Response to Melting

Despite the well-observed pattern of seasonal ice acceleration on alpine glaciers, until recently ice-sheet dynamic changes were believed to occur over much longer timescales when not in direct contact with the ocean [*Alley and Whillans*, 1984]. This reasoning suggested that mass loss in land-terminating regions of ice sheets would primarily be driven by surface mass loss (melting), with ice-dynamic changes being of little importance [*Ritz et al*., 1997].

While significant surface melting and moulins have long been observed within the GrIS ablation zone [e.g., *Thomsen*, 1986; *Thomsen et al*., 1988; *Carver et al*., 1994; *Greuell*, 2000], early studies suggested that seasonal variations in ice velocity were either

limited [*Reeh and Olesen*, 1986] or absent for the GrIS [*Echelmeyer and Harrison*, 1990]. However, subsequent long-term high-resolution observations documented strong seasonal ice acceleration tied to indirect measures of seasonal surface melt, indicating that the GrIS does undergo surface-melt-induced acceleration in a manner similar to alpine glaciers [*Zwally et al*., 2002]. Accelerated ice flow can drive additional ice-sheet thinning, increasing mass loss by allowing inward migration of the ablation zone and accentuating the ice sheet response to climate change [*Zwally et al*., 2002; *Bell*, 2008]. This seasonal ice acceleration of the GrIS is now well documented [e.g., *Zwally et al*., 2002; *van de Wal et al*., 2008; *Bartholomew et al*., 2010; *Hoffman et al*., 2011], but its ultimate impact on GrIS mass balance is still largely unknown.

1.2.2. GrIS Ice Velocity

The GrIS has the potential to contribute 7 m to sea-level rise [*Cuffey and Marshall*, 2000]. Therefore, constraining long-term dynamic changes of this ice sheet is critical to understanding the future of a key component of Earth's climate system and sea-level budget. Because surface-melt-induced acceleration of ice flow is a dynamic process, quantifying the future mass changes associated with subglacial hydrologic system is difficult and current studies suggest that its impact on mass loss could either positive or negative [*Shannon et al*., 2013]. Therefore, the scientific community has focused on exploring the subglacial processes that could impact both intra- and inter-annual variability in ice flow within the ablation zone and its relation to melt.

Summer ice velocity in the GrIS ablation zone often display a similar pattern to those observed on alpine glaciers; rapid ice acceleration, followed by a gradual decline, indicating that the subglacial hydrologic system has overall increased its drainage efficiency [e.g., *Bartholomew et al*., 2010; *Hoffman et al*., 2011]. This mechanism, i.e., a transition from an inefficient distributed drainage system to and efficient channelized

system, is invoked to explain the observed velocity patterns [e.g., *van de Wal et al*., 2008; *Bartholomew et al*., 2010; *Chandler et al*., 2013]. However, recent work suggests that channelization due to ice incision may be delayed or restricted in regions where both surface and bed slopes are low, because of limited potential energy available for melting [*Meierbachtol et al*., 2013; *Dow et al*., 2014]. Thus, the increased drainage efficiency of the subglacial hydrologic system inferred from surface ice velocity patterns [e.g., *Bartholomew et al*., 2010; *Hoffman et al*., 2011; *van de Wal et al*., 2015] may be instead due to features unaccounted for in our current conceptual model of the subglacial hydrologic system. Potential mechanisms include increasing drainage efficiency within the inefficient system due to increased cavity opening [*Meierbachtol et al*., 2013; *Hoffman and Price*, 2014], till processes [*Bougamont et al*., 2014; *Walter et al*., 2014] or expansion of the inefficient system at the expense of regions of the bed unconnected to the active subglacial hydrologic system [*Andrews et al*., 2014; *Tedstone et al*., 2015].

All of these proposed processes would act to reduce subglacial water pressure over large regions, leading to reduced ice velocity near the end and after the cessation of surface melting and potentially compensating for acceleration earlier in the melt season [*Sole et al*., 2013; *Tedstone et al*., 2013]. Thus, evolving drainage efficiency of all components of the subglacial hydrologic system likely determines the mass-balance effect of surface-melt-induced ice acceleration. However, this effect is limited to regions and timescales that permit significant subglacial hydrologic system evolution. Near or above the equilibrium line, ice velocity has been observed to accelerate without a commensurate late-season deceleration, possibly due the inability of the subglacial system to drain the available water over the course of the melt season, resulting net water storage and increasing annual ice displacement attributed [*Doyle et al*., 2014]. Further, late-season melt or precipitation events have the ability to cause rapid subglacial

pressurization and ice acceleration [*Doyle et al*., 2015], potentially increasing pressures within an inefficient subglacial hydrologic system and returning ice velocity to winter background levels more rapidly than previously envisioned.

1.3. IMPORTANCE AND SCOPE

The nature of the GrIS subglacial hydrologic system and its impact on long-term ice flow is clearly complex yet societally relevant. Current work defines similarities and differences between alpine glacier and GrIS subglacial hydrology, which ultimately impact how the ablation zone of the GrIS responds to climate change. Therefore, in this dissertation, I focus on the mechanisms that induce both sub-daily and long-term ice-velocity changes, so as to provide information on the physical processes impacting mass loss in land-terminating regions of the GrIS. Chapters 2-4 have been prepared or submitted for journal publication.

Chapter 1 (this chapter) introduces key concepts in glacier hydrology and explores its relationship to ice surface velocity. The current conceptual model used is explained and compared with observations from the GrIS. Key unknowns and areas requiring further study are identified.

In Chapter 2, I explore spatial changes in the supraglacial hydrologic system over 26 years to better understand how changes in this component of the system influence the subglacial hydrologic system. The supraglacial hydrologic system is composed of firn aquifers, lakes, rivers, crevasses and moulins (Figure 1.1). Although supraglacial features can store melt on both short and long timescales [e.g., *Forster et al*., 2014; *Koenig et al*., 2015], moulins efficiently drain the vast majority of available supraglacial melt to the ice–bed interface [*Smith et al*., 2015]. This phenomenon results in spatial patterns of ice velocity that are related to both moulin locations and subglacial hydrologic potential [*Palmer et al*., 2011]. However, because moulin locations depend on both meltwater

supply [*Gulley et al*., 2012; *Clason et al*., 2015] and high extensional strain rates [*Catania et al*., 2008; *Poinar et al*., 2015], their spatial persistence over multiple melt seasons is unknown. I combine historic aerial photos and modern satellite images to locate moulins and evaluate their multi-decadal persistence. Using surface digital elevation models (DEMs) in conjunction with moulin locations, I show that moulin density and drainage basin size do not uniformly increase or decrease, respectively, in response to increasing surface melt, as has previously assumed. Instead, moulin density more likely responds to changes in ice dynamics.

In Chapter 3, I step into the realm of subglacial hydrology proper using direct observations of moulin water levels, borehole pressure, supraglacial melt, and ice surface velocity in a portion of the western GrIS to examine subglacial hydrologic system evolution [*Andrews et al*., 2014]. According to the prevailing conceptual model, increasing drainage efficiency should result in both a decline in pressure within the channelized system as well as a decline in ice velocity [*Bartholomew et al*., 2010; *Cowton et al*., 2013]. However, during the latter part of the melt season, there is no decline in channelized pressure commensurate with declining ice velocity. This result confirms modeling studies suggesting that changes in drainage efficiency can occur elsewhere in the subglacial hydrologic system [*Meierbachtol et al*., 2013; *Dow et al*., 2014]. Borehole pressures indicate they are unconnected from the active portion of the subglacial hydrologic system, but over time some regions of the bed may connect to hydrologically active regions. This mechanism reduces subglacial water pressure and increases basal friction over larger areas [*Iken and Truffer*, 1997]. These observations suggest that large regions of the bed are unconnected to the active subglacial hydrologic system, yet they still play a significant role in the evolution of that system.

Expanding upon Chapter 3, in Chapter 4 I develop a one-dimensional model to explore the extent to which channelization can accommodate the available meltwater within the subglacial hydrologic system. I force this model using a combination of observed moulin locations, realistic supraglacial discharge, and bed and surface elevations, to explore whether channelization alone can explain GPS-derived ice velocity patterns in the study area. These results suggests that evolving drainage capacity of the distributed system is essential to reproduce observed moulin water level ice velocity patterns.

In Chapter 5, I present the key conclusions from Chapters 2-4 and contextualize these conclusions within the overall scope of this dissertation and within the current literature. I further consider potential avenues for future research using the insights presented herein.

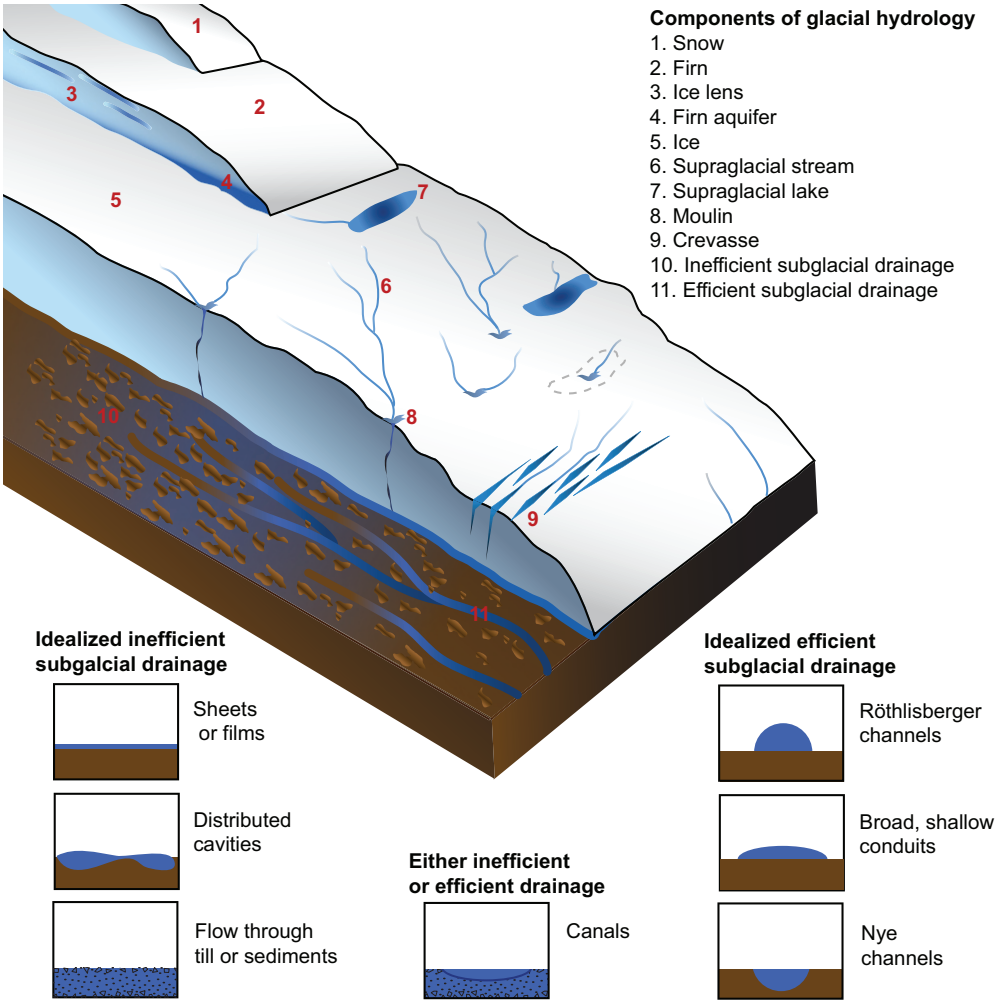

Figure 1.1. Schematic of the glacial hydrologic system. In the ablation zone, the ice surface melts and subsequent water is routed through the snow or firn, or over the ice surface via supraglacial streams. This supraglacial water can be impounded in lakes or immediately drained to the bed through moulins and crevasses. Water at the ice-bed interface can flow in a number of different ways, generally characterized as inefficient or efficient. Modeling the subglacial system requires the idealization of these flow characteristics. Inefficient flow can be represented as sheets distributed cavities or porous flow while efficient drainage can be represented as R-channels, N-channels or broad, low ceilinged conduits. When sediment is involved, flow can be either inefficient or efficient depending on defined characteristics. The ice sheet diagram is adapted from [*Rennermalm et al.*, 2013b]. The idealized subglacial features are adapted from [*Flowers*, 2015]. Not to scale.

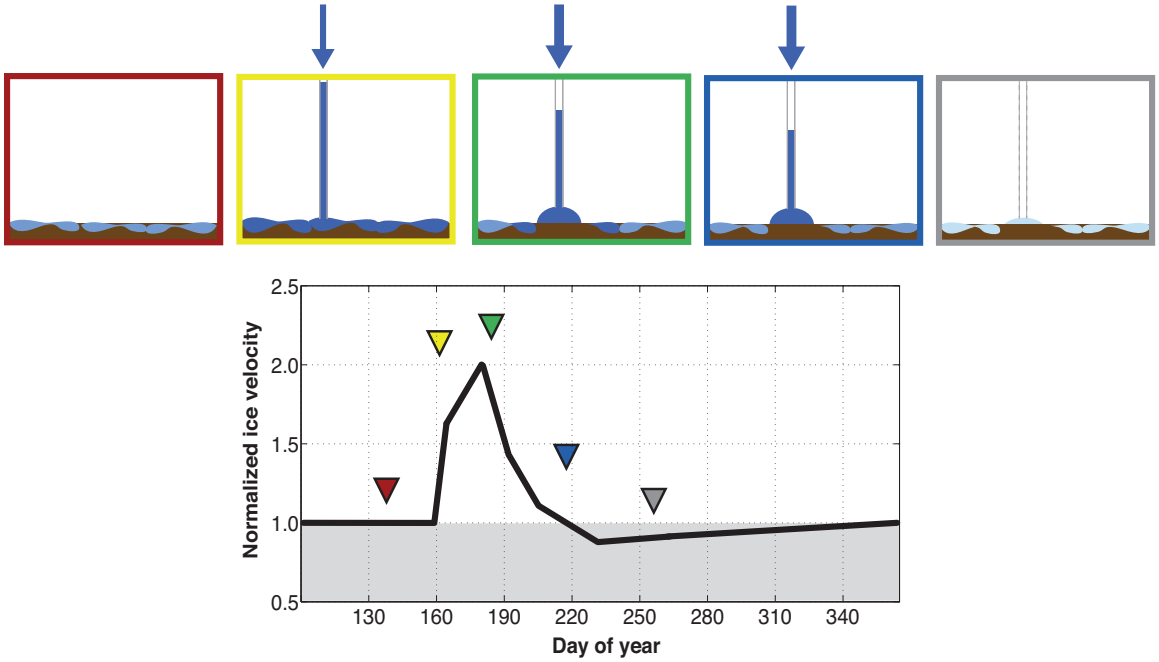

Figure 1.2. Conceptual relation between subglacial hydrology and seasonal ice acceleration. Ice velocity is presented as a fraction of the background value measured in later winter and early spring. Before the onset of seasonal melting, the subglacial hydrologic system conducts a limited amount of water in an inefficient configuration (red box) resulting in a quiescent period for the subglacial hydrologic system and ice velocities (red triangle, days 100 – 160). The onset of above freezing air temperatures results in the production of surface melt which is routed to the ice-bed interface via moulins and crevasses. This water overwhelms the inefficient subglacial hydrologic system, increasing subglacial pressures (yellow box), causing widespread bed separation and ice acceleration (yellow triangle, day 160). A continued supply of water and bed separation allow for the initiation of ice-incised subglacial channels. Once the efficient system can readily accommodate the available water (green box) ice velocities begin to decline (green triangle, day ~180). Continued development of efficient subglacial channels results in a regional reduction in subglacial pressure (blue box) and ice velocity (blue triangle, day ~ 220). Following the cessation of surface melting, any subsequent subglacial drainage can further reduce subglacial pressures and ice velocities (grey box and triangle). Not to scale.

Chapter 2. Multi-decadal moulin variability and implications for subglacial drainage of the Greenland Ice Sheet

2.1. ABSTRACT

The development and configuration of the subglacial hydraulic system under the ablation zone of the western Greenland Ice Sheet (GrIS) modulates seasonal surface-melt-driven perturbations in ice surface velocity. Subglacial evolution is strongly dependent on the spatial distribution of meltwater delivery to the ice-bed interface. Moulins act as point sources, directly delivering nearly all meltwater to the ice sheet bed. Therefore, constraining the change in moulin location over time is critical to understanding long-term patterns of subglacial drainage. We characterize changes in the spatial distribution of moulins and their associated drainage basins in the Paakitsoq Region of the GrIS from 1986 to 2011, 26 years. We find that, despite increasing supraglacial melt, the number of moulins and supraglacial drainage basin size does not change significantly. Further, a large percentage of moulins are spatially persistent over the 26-year observation window. Spatially persistent moulins reform approximately every three years and are more likely to be located in the vicinity of potential subglacial flow paths. These characteristics suggest that the configuration of efficient subglacial drainage pathways can be constant over long periods, potentially allowing for the formation of Röthlisberger channels and removal of sediments, which are not currently acknowledged as mechanisms of increased subglacial efficiency within many models of subglacial hydrology.

2.2. INTRODUCTION

The Greenland Ice Sheet (GrIS) mass loss continues to decline at an accelerating rate [*van den Broeke et al.*, 2009; *Velicogna*, 2009; *Velicogna et al.*, 2014] due to a combination of dynamic thinning (increasing ice velocities and outlet glacier calving) and

decreasing surface mass balance (SMB). SMB changes account for 52% to 68% of the total mass loss [*Csatho et al*., 2014; *Velicogna et al*., 2014], and are primarily due to increasing air temperatures, which increase the surface melt rates and spatial extent of the ablation area [*McGrath et al*., 2013] and reduce the ice surface albedo [*Tedesco et al*., 2011; *Box et al*., 2012]. Increased losses in SMB can directly influence long-term ice dynamics through evolution of the subglacial hydrologic system [e.g., *Bartholomew et al*., 2012; *Andrews et al*., 2014], by introducing heat to the ice column via moulins and crevasses [*Phillips et al*., 2013; *Harrington et al*., 2015; *Lüthi et al*., 2015], and by altering the ice surface profile over [e.g., *Shannon et al*., 2013].

As moulins can drain the majority of the ablation zone [*Smith et al*., 2015], predicting future SMB-driven dynamical changes may be linked to our ability to understand the distribution and variability of moulins over time. Moulin formation is dependent on the local stress field [*Catania et al*., 2008; *Price et al*., 2008; *Colgan et al*., 2011a; *Clason et al*., 2015; *Poinar et al*., 2015] and the routing of available supraglacial melt [*Phillips et al*., 2011; *Banwell et al*., 2012; *Arnold et al*., 2014; *Clason et al*., 2015], which is controlled by local meteorological conditions and physical characteristics of the ice surface. Despite downstream advection due to ice motion, moulins can reactivate over multiple melt seasons as long as they reconnect to an adequate surface meltwater supply [*Catania and Neumann*, 2010]. If a supraglacial water supply becomes unavailable due to ice motion, moulins will reform at previous locations of high extensional strain [*McGrath et al*., 2011]. This balance between advection and re-occupation should allow moulins to maintain a quasi-steady location despite local ice motion, although this has not been shown. Further, moulins act as the primary englacial connection between supraglacial melt and subglacial drainage; therefore, understanding moulin density is critical to understanding englacial storage may influence long-term trends in ice motion.

The importance of a moulin to the subglacial system depends on its discharge, which in turn is dependent on surface topography and melt gradients. Here, we use a combination of high-resolution datasets to characterize the distribution of moulins and the associated supraglacial drainage basins in the Paakitsoq Region of western GrIS for the 2011 summer melt season. We compare these data to similar observations from 1985 in order to examine changes in the pattern of meltwater delivery over 26 years during which melt production increased [*van Angelen et al.*, 2013]. An increase in moulin density and hence a decrease in supraglacial drainage basin size will result in larger regions of the bed receiving direct meltwater input. In contrast, consistent drainage basin size and density can result in an increase in meltwater delivery to these locations over time. Both potential outcomes can alter the timing of subglacial drainage system development and thus influence the ice sheet dynamic response to meltwater. Constraining these changes will provide insight into the spatial distribution of melt supply to the subglacial system and will inform process-based modeling of the subglacial hydrologic system. Combining observations of moulin position and drainage ability provides a clear picture of the long-term evolution of the supraglacial and englacial hydrologic system.

2.2. Data and Methods

Our study focuses on Sermeq Avangnardleq, part of the Paakitsoq Region in western Greenland. Encompassing 990 km^2, the region exhibits annual ice velocities on the order of 100 m a^{-1} [*Hoffman et al.*, 2011; *Andrews et al.*, 2014]. Regionally, the equilibrium line altitude (ELA) has varied between ~1,000 m to 1,800 m over the past two decades [*Mernild et al.*, 2010; *McGrath et al.*, 2013]. Using remote sensing observations, we identify moulin locations and supraglacial drainage basin sizes in 2011 and 1985 in order to constrain changes in supraglacial drainage patterns. The defined

study area is limited by the extent of 1985 aerial photography and mapping (Figure 2.1) [*Kjær et al*., 2012].

2.2.1. Data

We produce two data sets for both 1985 and 2011; moulin locations and their associated drainage basin size and distribution. For the 1985 dataset, we utilize moulin locations identified by *Thomsen* [1986] and an ice surface digital elevation model (DEM) constructed by Kjær et al. [2012], both of which are derived from an aerial photography survey in July 1985 performed by the Geological Survey of Greenland in conjunction with the University of Maine [*Thomsen*, 1986; *Thomsen et al*., 1988]. For 2011, moulin locations are obtained using WorldView-2 (WV-2) imagery provided by the Polar Geospatial Center. Images ranged in date from June 17 to July 7, 2011 except for a small region uncovered in 2011, where a July 6, 2010 image was used. In areas of overlap the most recent image was used. For 2011 surface topography, we utilize an ice surface DEM constructed from the same WV-2 imagery using search-space minimization techniques [*Noh and Howat*, 2015]. This DEM is nominally from 2011, but utilizes imagery spanning 2010 to 2013 due to limited satellite coverage in any given year. In addition to these two datasets, we use basal topography derived from mass conservation [*Morlighem et al*., 2014] to calculate subglacial hydrologic potential.

2.2.2. Moulin Identification

To determine moulin distribution we take advantage of a photogrammetric map of moulin locations, supraglacial streams, crevasses and supraglacial drainage basins constructed by *Thomsen* [1986] using aerial photos from 1985 and stereo-plotting techniques. The *Thomsen* [1986] map was scanned and georeferenced based on the coordinate grid. We then digitized the identified moulins at a 1:3,000 scale (Figure 2.1).

The positional accuracy of the digitized moulins can be affected by the scale of features and their representation as well as errors in the original mapping and subsequent digitization [*James et al*., 2012]. In order to constrain positional accuracy of moulins from the *Thomsen* [1986] map, we estimate the cumulative positional errors (σ_C) following *Cheung and Shi* [2004]:

$$\sigma_C = \sqrt{\sigma_S^2 + M^2(\sigma_M^2 + \sigma_d^2)}\,, \tag{2.1}$$

where, σ_S is the error introduced during the initial data collection, σ_M is the map error, σ_d is the digitization error, and M is the map scale. Note that the original map error and the digitization error are scaled linearly by the scale of the map. The original aerial photos were collected at 1:150,000 scale, which results in an approximate resolution and precision of 2 m [*Motyka et al*., 2010]. The *Thomsen* [1986] map is at a scale of 1:75,000, which results in a positional accuracy of approximately 0.6 mm for mapped features [*Marsden*, 1960] and manual digitization results in an error of approximately 0.2 mm. Combined, these errors result in a cumulative positional error ellipse of 47 m for the digitized location of each moulin in 1985.

To create a moulin position dataset for 2011, moulin locations were identified manually in WV-2 imagery. WV-2 imagery has a resolution of 50 cm; therefore, there is an inherent resolution difference between 1985 and 2011 imagery (2 m for the 1985 map and 50 cm for the 2011 map). This resolution difference results in an offset in identifiable moulin sizes between 1985 and 2011. To overcome this bias, we resample the WV-2 imagery to 2 m resolution using bilinear interpolation and identify moulins from this new dataset at a resolution of 1:3,000 (Figure 2.1). Moulin locations were identified primarily by the abrupt termination of supraglacial streams; however, several additional features improve our ability to detect moulins, including the presence of refrozen spray downstream of a moulin and evidence of lake drainage including bathtub rings (Figure

2.2). Following Equation 2.1, we estimate the moulin positional error to be approximately 24 m for the 2011 dataset.

2.3 Supraglacial Drainage Basin Delineation

In order to determine the supraglacial drainage basins associated with each moulin in 1985 and 2011, we apply a modified flow accumulation workflow to DEMs from each time period [*Tarboton et al*., 1991]. *Kjær et al*. [2012] constructed a DEM from the original 1985 air photos using robust photogrammetric techniques, resulting in a 25 m resolution and a vertical error of ~5.5 m. The extent of this DEM is limited by the 1985 snow line as snow cover limits feature identification. For 2011 data, we resample the 10-m DEM constructed using WV-2 imagery [*Noh and Howat*, 2015] to 25-m using bilinear interpolation to match the resolution of the 1985 DEM. We then vertically correct both DEMs to the Greenland Ice Mapping Project (GIMP) DEM [*Howat et al*., 2014] in off-ice regions. Displacements are uniformly distributed over bedrock regions, with a mean error of 6.38 m and 6.41 m and standard deviation of 7.82 m and 7.01 m for 1985 and 2011, respectively. A vertical downshift of 6.4 m for both the 1985 and 2011 DEMs allows for an accurate analysis of subglacial hydraulic potential using mass conserving bed elevations which are referenced to the GIMP DEM [*Morlighem et al*., 2014].

Supraglacial drainage basins were determined using ArcGIS 10.1 [*ESRI*, 2014] through the following steps: 1) flow direction determination; 2) flow accumulation calculation; 3) moulin location adjustment; and 4) watershed delineation. Flow direction for a grid cell is determined relative to the surrounding eight grid cells, following the approach presented in *Jenson and Domingue* [1988]:

$$S_m = \frac{dz}{dl} \cdot 100 \quad , \tag{2.2}$$

where the steepest descent, S_m, is equal to the change in elevation, z, over the distance between the center point of the grid cell of interest and an adjacent grid cell, l. For 25 m grid cells, l is equal to 25 m for orthogonal cells and approximately 35 m for diagonal cells. Previous work has filled sinks in order to route meltwater off the surface of the ice [e.g., *Lewis and Smith*, 2009], or assumed that sinks will always hydrofracture to drain stored water [e.g., *Banwell et al.*, 2013]. However, recent work indicates that knowledge of moulin locations is important in determining supraglacial drainage basins [*Yang et al.*, 2015]. Therefore, we utilize moulin locations in conjunction with the DEMs and surface routing algorithm to delineate supraglacial drainage basins.

When determining water flow direction from the surface DEMs, surface depressions are filled in order to route water over the surface until a moulin is reached. Though this complete 'filling' of surface depressions is not necessarily indicative of supraglacial lake size [*Yang et al.*, 2015], this process does reflect the observations that not all depressions have moulins and some supraglacial lakes can drain over the ice surface to downstream moulins [*Tedesco et al.*, 2013b; *Poinar et al.*, 2015]. In instances where moulins are located within surface depressions, the entire depression, including regions downstream of the moulin are included in calculations of its supraglacial drainage basin size.

One potential issue arising with this methodology is an offset between the moulin location and the DEM-derived flow path. This offset can be caused by error in DEM production, moulin location and, in 2011, the offset in timing between DEM construction and moulin location, or by the inherent smoothing caused by representing a surface with a grid cells with a unique value. Therefore, in order to properly assign moulins a drainage area, we allow moulins to shift up to 150 m to the highest flow accumulation pathway.

Increasing this distance does not significantly change the distribution or size of supraglacial drainage basins.

A second potential issue is the presence of crevasse fields which either store or drain supraglacial water [*Colgan et al.*, 2011a]. Here, we do not consider the potential importance of crevassing and instead treat the ice as impermeable except for moulin locations. Though not considered directly here, we acknowledge that there may be a change in crevasse extent within our study area, which can influence englacial drainage patterns. Further, the distribution of moulins does provide a natural boundary for crevassing at the terminus (Figure 2.1) and, the increase in crevassing between 1985 and 2011 is limited, approximately 13%, and focused on the southern edge of the study area [*Colgan et al.*, 2011a].

2.2.4. Subglacial Drainage

Subglacial water flows along gradients in the hydraulic potential, ϕ, following *Shreve* [1972],

$$\phi = k\rho_i g(h - z) + \rho_w gz \quad , \tag{2.3}$$

where g is the acceleration due to gravity; ρ_i and ρ_w are the density of ice and liquid water, respectively; h is the surface elevation from the 1985 and 2011 DEMs; z is the elevation of the ice-bed interface [*Morlighem et al.*, 2014]; and k is a spatially uniform fraction of floatation. Though subglacial erosion rates can alter subglacial topography, estimated erosion rates in slow moving regions of the ablation zone would result in changes of less than 0.2 m over the 26 year observation window [*Cowton et al.*, 2012], an order of magnitude smaller than the annual surface melt rates in our study area and below the resolution of subglacial basal topography. For the purposes of these calculations, we assume that k is equal to 0.91 the ratio of ice pressure to water pressure at floatation. It should be noted that a spatially and temporally uniform fraction of floatation is generally

unrealistic considering the high variability in subglacial water pressures observed in both this study area [*Andrews et al*., 2014; *Ryser et al*., 2014a, 2014b] and other regions of the ablation zone of western Greenland [*Cowton et al*., 2013; *Meierbachtol et al*., 2013]. However, subglacial channels are thought to initiate when subglacial pressures are high at the beginning of the melt season.

Using the calculated subglacial hydraulic potential, we determine the subglacial flow accumulation pathways and subglacial drainage basins using steps, including filling infrequent depressions in hydraulic potential, similar to those used for the determination of supraglacial watersheds: 1) determine subglacial hydraulic potential flow direction, and 2) calculate flow accumulation. These potential subglacial flow pathways for 1985 and 2011 are then compared to moulin locations in those same years.

2.3. Results and Analysis

2.3.1. Moulin Distribution

In 1985, *Thomsen* [1986] observed 287 individual moulins in the study region, and in 2011, we observe 270 moulins within the study region, resulting in densities of 1 moulin per 3.45 km^2 and 3.66 km^2, respectively (Figure 2.1). In order to examine temporally persistent moulins, we identify moulins that are similarly located (i.e. 'matched moulins') in 1985 and 2011 using a modified nearest neighbor search algorithm. We identify the 2011 moulin in closest proximity to each 1985 moulin and repeat this process by identifying the 1985 moulin in closest proximity to each 2011 moulin. A match was only identified if the two moulins were identified as nearest neighbors in both iterations (Figure 2.4A). Repeating this process eliminates misidentification of moulin pairs. As an additional check, pairs were manually validated if a moulin in the same timeframe was determined to be closer than the matched moulin

in the other time frame. This occurred in less than 10% of the identified moulin pairs and resulted in the elimination of approximately half these pairs when the local spatial pattern of moulin distribution was too complex to confidently identify a matched pair. We identify 154 matched pairs, more than 50% of all moulins in either year, with observed distances between the matched 2011 and 1985 moulins ranging between 10 ± 100 m and 1,235 ± 100 m with the majority of matched moulins less than 200 m apart (Figure 2.4B). This analysis allows us to assign moulins 1985 and 2011 datasets to three categories: 1) present in 1985, but absent in 2011; 2) present in 2011, but absent in 1985; and 3) present in both 2011 and 1985. Though, each of these three categories provides information regarding ice dynamics, the following analysis focuses on identifying moulins in category 3 (present in both 2011 and 1985), as distances between moulins in different time steps can provide information on the average occupation time of moulins in this region.

Conceptually, the distance between the 1985 and 2011 matched moulins will be associated with ice flow speed and local surface topography, which drives supraglacial meltwater routing. Over the course of 26 years, we expect moulins to advect and reform multiple times. As a result, some moulins may have recently reformed, while others may be near the end of their viability (i.e. are advecting away from their water source). Therefore, if we assume that the moulins are randomly distributed within this process in both 1985 and 2011, we would expect the distance between moulins to representative of the average lifespan of moulins within the dataset. Normalizing the observed distances between 1985 and 2011 using the modern (2008-2009) fall velocity field [*Joughin et al.*, 2010a, 2010b] results in a median moulin lifespan of 3.4 years (Figure 2.4C). The error for moulin displacement is ±100 m. When accounting for this positional error in moulin location the minimum median age of matched moulins is 1.3 years and the maximum

median age is 5.9 years. Outliers (at 29 and 38 years) may be either incorrectly matched or experienced significant changes in ice velocity over the 26-year observation window.

To further explore the regional patterns in matched moulin distance, we perform a cluster analysis, Getis-Ord Gi*, order to identify statistically significant clustering in the nearest neighbor distance for matched moulins (Figure 2.5A) [*Getis and Ord*, 1992]. In this analysis, the Getis-Ord Gi* statistic is used to compare the distances between assigned nearest neighbor with surrounding nearest neighbor distances. If short distances are adjacent to other short distances, the region is characterized as having low nearest neighbor distances between moulins and vice versa.

Moulins without an identifiable temporal nearest neighbor (i.e. unmatched) compose approximately 50% of moulins in either time period (Figure 2.4A). Unlike the matched moulin comparison, this suggests the appearance and disappearance of moulins during the 26-y time period. In order to analyze any change in moulin distribution between 1985 and 2011, we again use the Getis-Ord Gi* statistic. Matched moulins in each year are assigned a nominal value of one and unmatched moulins in each year are assigned a nominal value of zero. Using this numeric assignment allows for analysis using the Getis-Ord Gi* statistic for all moulins (matched and unmatched). This analysis reveals regions that have experienced moulin loss or gain over the observation window (Figure 2.5B). We observe statistically significant clustering of 1985 moulins without 2011 pairs near the terminus of Sermeq Avannarleq and clustering of 2011 moulins without 1985 pairs in the southern edge of the study area near Jakobshavn Isbræ (Figure 2.5B). These changes in moulin distribution near Jakobshavn Isbræ are correlated with substantial changes in potential subglacial flow path orientation associated with the acceleration and thinning of Jakobshavn Isbræ [*Motyka et al.*, 2010; *Colgan et al.*, 2011a], which drew down elevation in the southern portion of our study area. These

clustering observations are further elucidated in an examination of moulin density within specific elevation bands, where there is a decline in moulin density between 1985 and 2011 except between 400 and 600 m.a.s.l. (Figure 2.6A).

2.3.2. Supraglacial Basins

Supraglacial drainage basins are delineated by ice surface topography (Figures 2.3A and 2.3B). At relatively large length scales, ice surface topography is the transmission of basal topography controlled by ice thickness and the fraction of ice motion controlled by basal sliding [*Gudmundsson*, 2003; *Lampkin and VanderBerg*, 2011]. As supraglacial basin size exerts considerable control on the volume of water reaching the bed at a given location, it may influence the subglacial hydrologic system.

In order to determine if supraglacial drainage basins change in character regionally, we examine the number of basins with centroids in 100 m elevation bands (Figure 2.6B) and utilize the Mann-Whitney U test [*Hollander and Wolfe*, 1999] to determine if basin sizes differ in a statistical sense between 1985 and 2011. Moulin basin sizes do not exhibit a normal distribution due to characteristics of the natural system, which is why we use the Mann-Whitney U test, a nonparametric test used to determine if two samples (in this case 1985 and 2011 basin sizes) originate from the same population. This analysis suggests that supraglacial drainage basins do not demonstrate any statistical difference between 1985 and 2011 as a whole or when subdivided into elevation bands (Figure 2.6B; Table 2.1). However, there are substantial changes in identified moulin density near the terminus, which reduces the area that we can identify as being drained by moulins. Despite these spatial changes in moulin distribution between 1985 and 2011, drainage basin sizes remain statistically similar. This holds true within subdivided elevation zones.

2.3.3. Moulin Connection to Subglacial Flow Paths

Persistence of a moulin in a particular location is associated with both a supply of supraglacial water [e.g., *Clason et al*., 2015]. As subglacial flow potential is strongly related to ice surface topography (Equation 2.3), there should be a correlation between observed matched moulins and expected subglacial flow pathways. In order to examine this possibility, we examine the spatial relationship between lows in subglacial hydrologic potential, likely regions of efficient subglacial drainage, and moulin locations (Figures 2.7A and 2.7B). We find that matched moulins are more likely to be located close to subglacial channels than unmatched moulins (Figure 2.7C) indicating that long-term occupation of moulins may be important for establishing the more efficient subglacial drainage pathways.

2.4. DISCUSSION

2.4.1. Changing Moulin Distribution

It is often assumed that the number of moulins within a given area will increase with increasing melt volumes [*McGrath et al*., 2011; *Phillips et al*., 2011]. However, despite increases in regional summer air temperature [*Hanna et al*., 2012] and decreasing ice surface albedo [*van Angelen et al*., 2013], which result in increasing SMB loss in our study area, we do not observe an increase in total moulin density or indication that supraglacial drainage basins are declining in size over the entire study area (Figure 2.6A; Table 2.1). In fact, we observe a slight decline in moulin densities between 1985 and 2011, except between 300 to 700 m.a.s.l. It is likely that this decrease is the result of increased crevassing near the terminus of Sermeq Avannarleq and at the southern edge of the study area [*Colgan et al*., 2011a] associated with the thinning and acceleration of Jakobshavn Isbræ in the 1990's [*Motyka et al*., 2010].

Near the terminus of Sermeq Avangnardleq, we observe a decrease in moulin density at low elevations (~100 – 400) and an increase in moulin density at moderate elevations (~400 – 600) (Figure 2.6A). This corresponds well with clustering of unmatched 1985 moulins near the terminus of Sermeq Avangnardleq (Figure 2.5B). We also observe clustering of unmatched moulins in 2011 (indicating that the moulins appeared between 1985 and 2011) along the southern edge of the study area (Figure 2.5B). These shifts in moulin location and changes in supraglacial drainage basin size are also associated with substantial changes in the subglacial hydraulic potential flow pathways (Figures 2.7A and 2.7B) demonstrating the close link between supraglacial and subglacial hydrologic conditions. Dynamic thinning in southern regions of the study area was driven by the 1998 acceleration of Jakobshavn Isbræ [*Motyka et al.*, 2010]. Thinning and increased extension through this region resulted in a substantial change to the subglacial flow pathways, with more subglacial water being directed south toward Jakobshavn Isbræ.

2.4.2. Characteristics of Matched Moulins

Beyond the two regions of unmatched moulins, moulins in the northern extent of the study area frequently have an identifiable match (Figure 2.5B). This temporal persistence may be important to the development of the subglacial hydrologic system. Changes in moulin position over time can have a significant impact on both the supraglacial [*Smith et al.*, 2015] and subglacial hydrologic system [*Gulley et al.*, 2012]; however, previous studies either only characterize the spatial extent of crevassed areas [*Colgan et al.*, 2011a] or constrain moulin position for a single drainage basin [*McGrath et al.*, 2011]. Field and remote sensing observations suggest that there can be a string of abandoned moulins downstream of active moulins [*Holmlund*, 1988; *McGrath et al.*, 2011; *Chu*, 2014] indicating that moulins continue to reform in the same surface location.

These strings of abandoned moulins are not universal and frequently do not correspond to annual ice displacement [*Chu*, 2014]. Further, additional observations suggest that moulins can be re-activated year after year [*Catania and Neumann*, 2010]. The combination of previous observations and clustering of short match distances in regions of slow ice motion (Figure 2.5A) suggest that under a pattern of relatively constant flow speed and direction and pattern of supraglacial drainage, moulins can remain active for a number of years (Figures 2.4C and 2.8). While our results suggest that some moulins in this region reform frequently, a large number of moulins are reactivated each melt season over multiple years. The median length of time moulins in this region are likely to be active is approximately 3.4 years. These values match well with observations of abandoned moulin string spacing [*McGrath et al*., 2011] and are similar, though lower than the calculations of moulin occupation time, by Catania and Neumann [2010].

These low occupation times for paired moulins suggest that approximately half the time, moulins have a high likelihood of being present in a relatively small area, which is likely bounded by regions of extensional strain (Figure 2.8) [*Catania et al*., 2008]. This region is likely to remain relatively constant over long periods as changes must be caused by either changes in ice dynamics [*Poinar et al*., 2015] or substantial ice thinning, which can increase large-scale ice surface roughness [*Gudmundsson*, 2003]. The pattern of moulin reoccupation and formation thus results in a quasi-stationary supply of meltwater to the bed of the ice sheet, which can impact long-term characteristics of the subglacial hydrologic system.

2.4.3 Subglacial Implications

Over 50% of moulins within our study area can be readily matched between 1985 and 2011, indicating that a large number moulins are quasi-static that supraglacial melt water is being introduced to the bed at similar locations over long periods of time. This,

paired with the correlation between matched moulin locations and subglacial flow paths (Figure 2.7), suggests persistence in subglacial channel location. This correlation is expected as moulins form in regions of high extensional strain [*Catania et al*., 2008] and surface topography plays a significant role in the determination of subglacial hydrologic potential.

In Greenland, it is generally assumed that efficient subglacial channels are formed through the melting of ice as turbulent water flow dissipates energy [*Röthlisberger*, 1972] and creep closure eliminates GrIS subglacial channels shortly after the cessation of melt each year [e.g., *Fountain and Walder*, 1998; *Meierbachtol et al*., 2013; *Dow et al*., 2014], though there are some notable exceptions [*Colgan et al*., 2011b]. This classic R-channel formation is limited by high ice overburden pressure and low surface slopes [*Meierbachtol et al*., 2013; *Dow et al*., 2014] or in regions of highly deformable ice. However, the formation of efficient subglacial flow pathways is not limited to this classic model, and there is ample evidence indicating that subglacial erosion is strongly associated with subglacial water drainage [*Chu et al*., 2009; *Cowton et al*., 2012] and evidence for potentially expansive subglacial till under the GrIS [*Dow et al*., 2013; *Walter et al*., 2014]. Both channels formed through bedrock incision [*Nye*, 1976] and the preferential removal of fine sediments [*Walder and Fowler*, 1994; *Gulley et al*., 2012] can precondition the glacier bed. If moulins and subglacial conduits are spatially persistent over long timescales, the repeated annual subglacial flows can alter the bed characteristics in these locations resulting in a positive feedback allowing subglacial channels to form readily in defined areas while reducing the likelihood of additional channel formation.

The observed stability of moulin locations and supraglacial drainage basin sizes despite increasing supraglacial melt production has dynamical impacts on the seasonal

evolution of the subglacial hydrologic system. Changes in the subglacial system are generally driven by increasing melt intensity [*Bartholomew et al*., 2012; *Chandler et al*., 2013; *Andrews et al*., 2014], while the observed persistence of moulin locations suggests limited changes in the efficient subglacial hydrologic system. Thus, increased supraglacial drainage due to changing climactic and supraglacial conditions will result in and increase in the volume of water drained by moulins. Only moulins supply a discharge large enough to result in subglacial channel formation [*Werder et al*., 2013]. Therefore, an increase in the volume of water drained by each moulins results not in an increase in the spatial extent of subglacial channelization [e.g., *Sundal et al*., 2011], but more likely an increase in maximum subglacial channel capacity and a reduction in the time to develop these subglacial channels [*Gulley et al*., 2012]. This potentially explains observations of decreasing summer displacement with increasing melt intensity [*van de Wal et al*., 2008] and the total summer displacement being accommodated by decreasing winter displacement [*Sole et al*., 2013; *Tedstone et al*., 2013, 2014] without the need to invoke increasing moulin density to increase the spatial extent of subglacial channels. Thus, interannual variability in summer ice acceleration may not be the result of substantial reorganization or spatial expansion of the supraglacial and subglacial hydrologic systems, but more likely result from changes in meltwater supply to consistent regions of the GrIS bed.

2.5. Conclusions

Between 1985 and 2011, a large subset of moulins (>50%) are quasi-static, with calculations suggesting that these moulins remain active for a median length of 3.5 years. Moulins with persistent englacial drainage are more likely to be in the vicinity of expected subglacial flow paths, which suggests long-term stability in the subglacial drainage system. Near the terminus, moulin location is less likely to be persistent and in

regions of dynamic change large increases or decreases in moulin density can occur. A reduction of moulin density due to an increase in crevasse extent can influence the volume of englacial storage, potentially impacting gradients in subglacial hydrologic potential.

Analysis of the distribution of moulin locations and their supraglacial drainage basins and careful consideration of the implications associated with the stability of the supraglacial system can provide information that is critical to better understanding the relationship between supraglacial melt production and seasonal ice acceleration in the ablation zone of the GrIS.

2.6. Acknowledgements

This project was supported by United States National Science Foundation grant OPP-0908156. L. C. Andrews was also supported by UTIG Ewing-Worzel and Gale White Graduate Student Fellowships. The University of Minnesota Polar Geospatial Center, funded under NSF OPP collaborative agreement ANT-1043681, provided WorldView imagery.

2.7. Author Contributions

L. C. Andrews designed and implemented this study and wrote the manuscript. L. C. Andrews and G. A. Catania discussed the results and edited the manuscript.

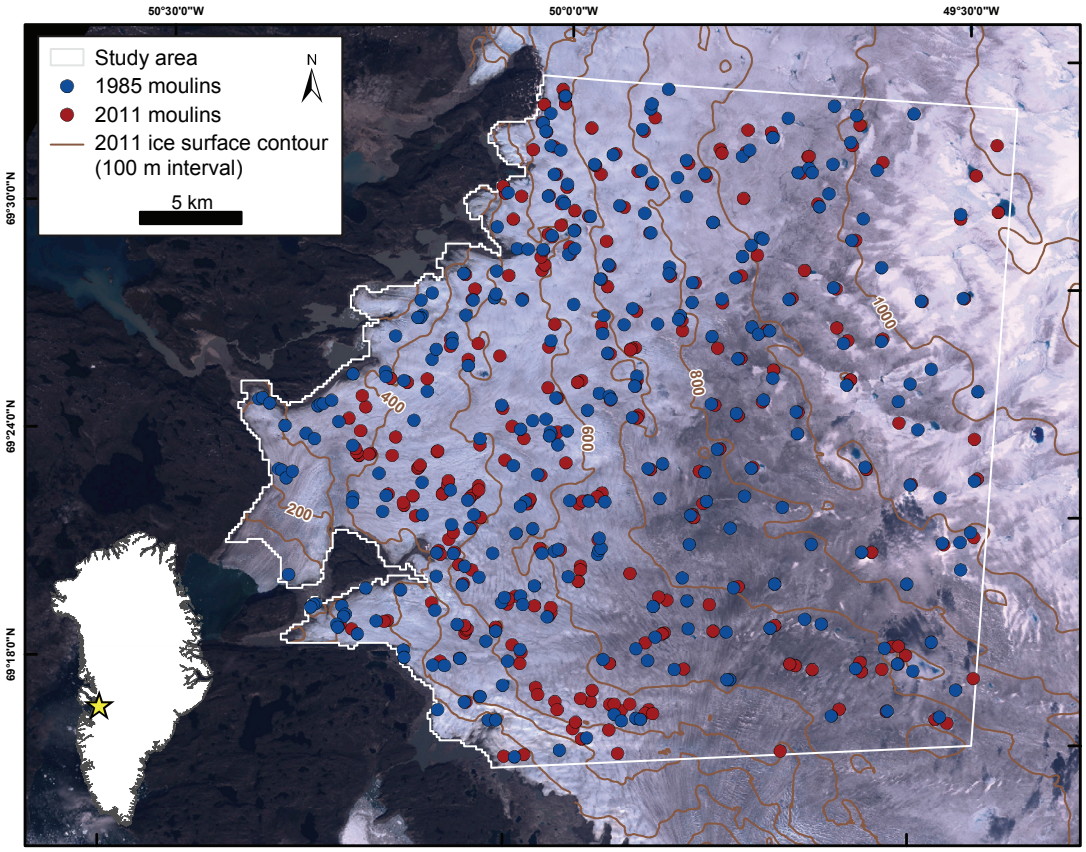

Figure 2.1. Paakitsoq Region, Western Greenland. Identified moulins are marked with blue (1985) and red (2011) circles. Modern ice surface contours (brown) from the 2011 DEM [Ahn and Howat, 2011]. The study area (light grey) is limited by the extent of the 1985 snow line [*Kjær et al.*, 2012]. The background image is a 2001 Landsat 7 ETM+ image, representative of ice surface conditions in between the study time steps.

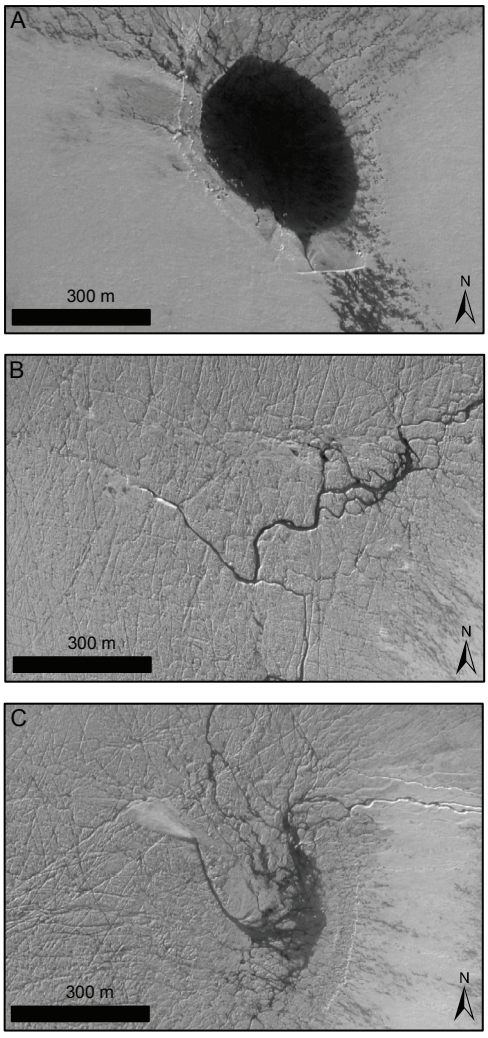

Figure 2.2. Representative moulins and associated supraglacial features. A) Supraglacial lake draining into a nearby moulin resulting from a crevasse. Note the bathtub ring associated the high water mark of the supraglacial lake. B) Abrupt termination of a complex supraglacial stream. There is also evidence of an inactive supraglacial stream downstream of the moulin. C) Refrozen spray associated with a moulin. During 2011, this area was not a supraglacial lake. Though in previous years it has been.

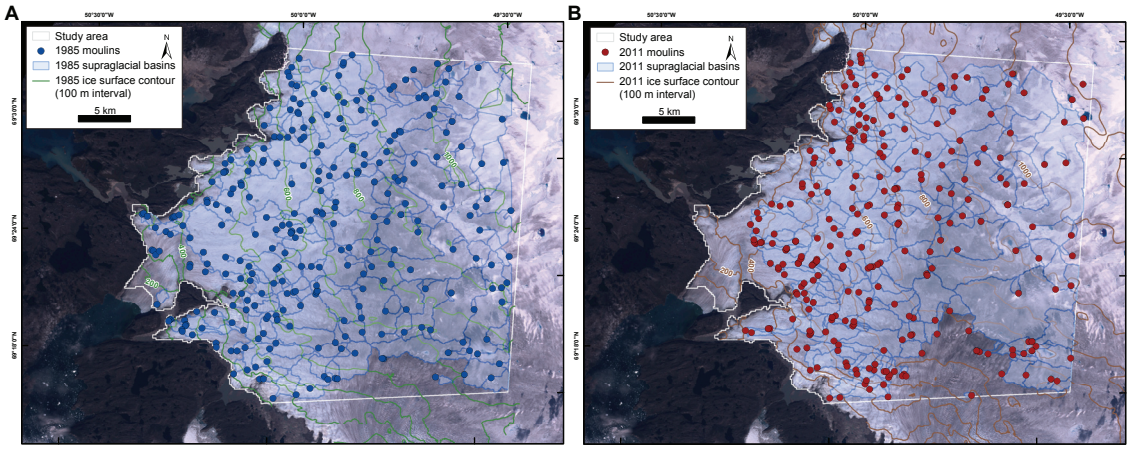

Figure 2.3. Moulin surface drainage basins. A) 1985 and B) 2011. Ice surface contours for both time steps are as indicated. Supraglacial drainage basins (delineated by the blue lines and fill) near the study boundary are impacted by the limits of surface DEMs; however, they account for only a small fraction of the total number of drainage basins and are impacted equally in both time steps.

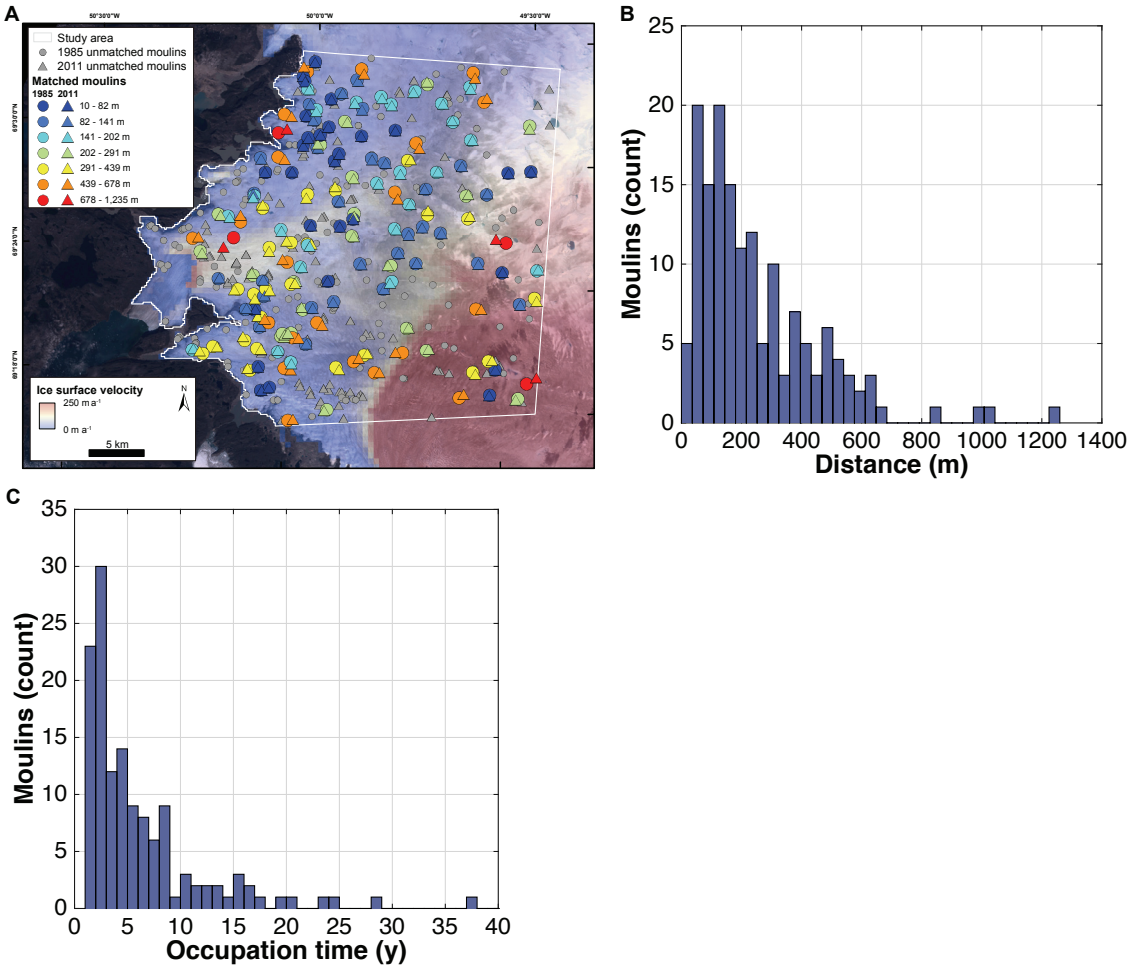

Figure 2.4. Moulins present in both 1985 and 2011. A) Distances between matched moulins (as indicated in legend). Unmatched moulins are represented as grey circles (1985) and triangles (2011). Based on positional error calculations, the distance between moulins has an error of ± 100 m. B) Histogram of matched moulin distances. C) Occupation time of matched moulins calculated using distances between matched moulins and a modern (2008-2009) velocity field [*Joughin et al.*, 2010a]. The median ice velocity in the vicinity of matched moulins is 59 m a^{-1}.

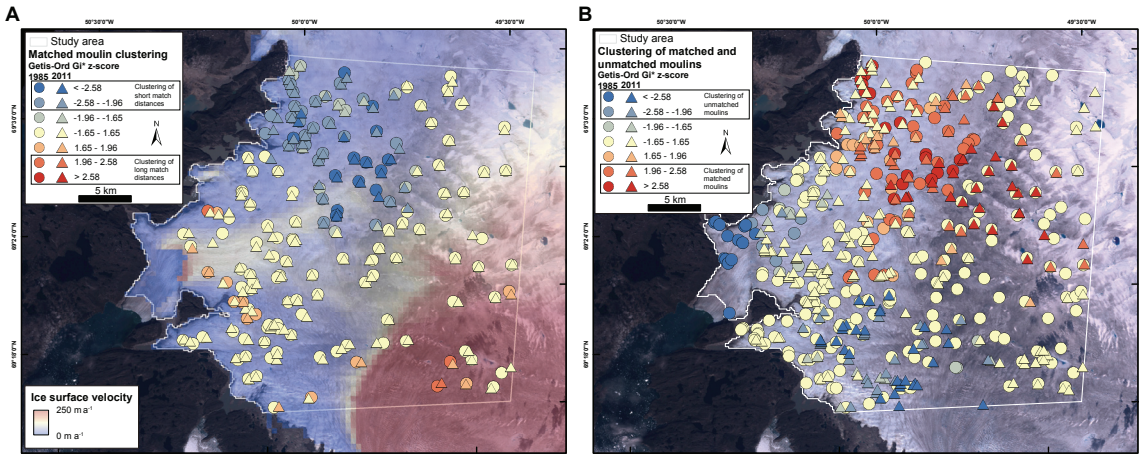

Figure 2.5. Getis-Ord Gi* cluster analysis for matched and unmatched moulins. A) Results from Getis-Ord Gi* cluster analysis for the distances between matched moulins. Short distances and slow ice velocities are clustered in the northern portion of the study area (blues), while limited clustering of long distances (reds) are observed in the south. B) Using cluster analysis on all moulins, matched moulins are shown to cluster from the north to central parts of the study area (reds), while unmatched moulins are shown to cluster to the south and near the terminus of Sermeq Avannarleq (blues).

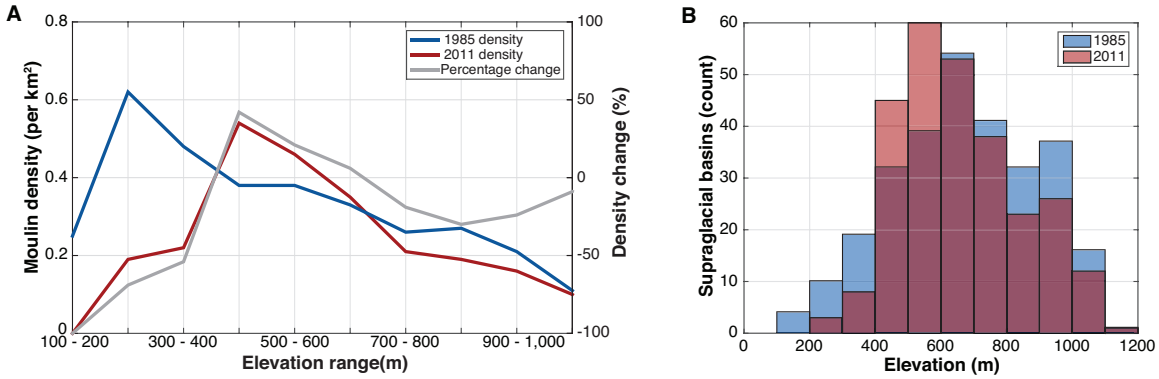

Figure 2.6. Moulin and drainage basin densities. A) Moulin density within 100 m elevation bands for 1985 (blue) and 2011 (red) and percentage change in density between 1985 and 2011 (grey). B) Histogram of basin centroids within 100 m elevation bands for 1985 (blue) and 2011 (red).

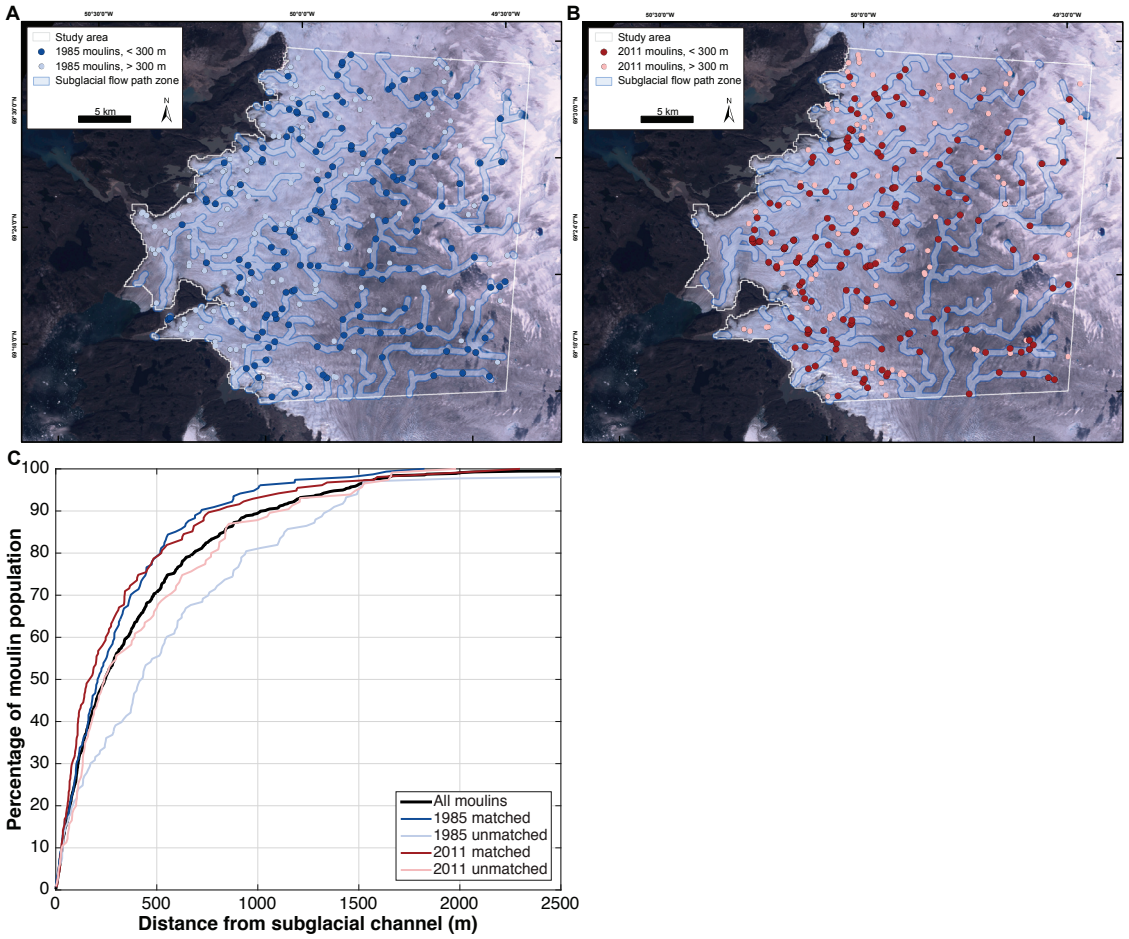

Figure 2.7. Subglacial flow pathways and moulin association. Approximate subglacial flow pathways (300 m width) and 1985 (A) and 2011 (B) moulins contained within these bounds are indicated by blue (A) and red (B) circles. Moulins outside these bounds are indicated as light blue (A) and pink (B) circles C) Distribution of moulin distances from the nearest subglacial channel. A higher percentage of matched moulins in 1985 and 2011 (blue and red, respectively) fall within any given distance from a subglacial channel than unmatched moulins (light blue and pink, respectively).

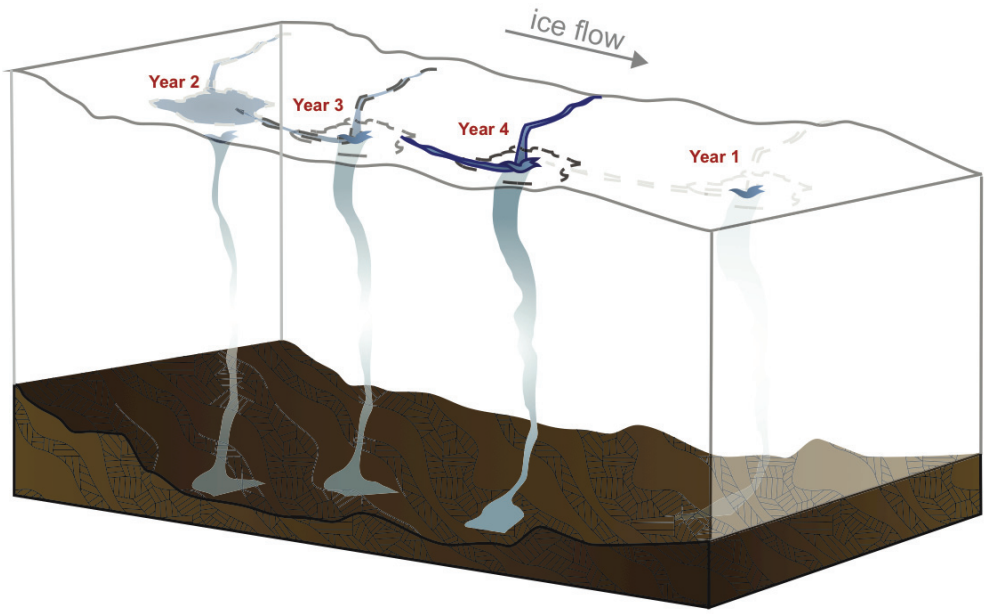

Figure 2.8. Conceptual model of moulin formation and downstream advection. Ice flow is from left to right. The advection and reformation of moulins can occur over multiple years. Here the moulin is initially at its furthest extent from the available melt water. The following year the moulin reforms upstream of its previous location. Over multiple years, it is advected downstream due to ice flow. The timescale of this process will be dependent on melt supply and surface ice velocities. Not to scale.

Elevation range (m)	h - value*	p - value^	Statistical change	Percent change in density
0 - 100	NA	NA	NA	-100
100 - 200	NA	NA	NA	-69
200 - 300	0	0.91	No difference	-54
300 - 400	0	0.12	No difference	42
400 - 500	0	0.59	No difference	21
600 - 700	0	0.82	No difference	6
700 - 800	0	0.70	No difference	-19
800- 900	0	0.13	No difference	-30
900 - 1000	0	0.46	No difference	-24
1000 - 1100	0	0.39	No difference	-9
ALL	0	0.42	No difference	-4

Table 2.1. Mann-Whitney U test results for supraglacial basin size.

Chapter 3. Direct observations of evolving subglacial drainage beneath the Greenland Ice Sheet

This chapter was previously published in *Nature*[1].

3.1. Introductory Paragraph

Seasonal acceleration of the Greenland Ice Sheet is influenced by the dynamic response of the subglacial hydrologic system to variability in meltwater delivery to the bed [*Bartholomew et al.*, 2010; *Sundal et al.*, 2011] via crevasses and moulins (vertical conduits connecting supraglacial water to the bed of the ice sheet). As the melt season progresses, the subglacial hydrologic system drains supraglacial meltwater more efficiently [*Bartholomew et al.*, 2010; *Sundal et al.*, 2011; *Chandler et al.*, 2013; *Cowton et al.*, 2013], decreasing basal water pressure [*Cowton et al.*, 2013] and moderating the ice velocity response to surface melting [*Bartholomew et al.*, 2010; *Sundal et al.*, 2011]. However, limited direct observations of subglacial water pressure [*Lüthi et al.*, 2002; *Cowton et al.*, 2013; *Meierbachtol et al.*, 2013; *Ryser et al.*, 2014b] mean that the spatiotemporal evolution of the subglacial hydrologic system remains poorly understood. Here we show that ice velocity is well correlated with moulin hydraulic head but is out of phase with that of nearby (0.3–2 kilometers away) boreholes, indicating that moulins connect to an efficient, channelized component of the subglacial hydrologic system, which exerts the primary control on diurnal and multi-day changes in ice velocity. Our

[1] Andrews, L. C., G. A. Catania, M. J. Hoffman, J. D. Gulley, M. P. Lüthi, C. Ryser, R. L. Hawley, and T. A. Neumann (2014), Direct observations of evolving subglacial drainage beneath the Greenland Ice Sheet, *Nature*, *514*(7520), 80–83, doi:10.1038/nature13796.

G. A. Catania, J. D. Gulley, M. P. Lüthi, R. L. Hawley and T. A. Neumann designed this study. L. C. Andrews, R. L. Hawley, M. J. Hoffman, M. P. Lüthi, C. Ryser and J. D. Gulley performed the fieldwork. L. C. Andrews analyzed the results and wrote the manuscript. All authors discussed the results and edited the manuscript.

simultaneous measurements of moulin and borehole hydraulic head and ice velocity in the Paakitsoq Region of western Greenland show that decreasing trends in ice velocity during the latter part of the melt season cannot be explained by changes in the ability of moulin-connected channels to convey supraglacial melt. Instead, these observations suggest that decreasing late-season ice velocity may be caused by changes in connectivity in unchannelized regions of the subglacial hydrologic system. Understanding this spatiotemporal variability in subglacial pressures is increasingly important as because melt-season dynamics affect ice velocity beyond the conclusion of the melt season [*Sole et al.*, 2013; *Tedstone et al.*, 2013; *Doyle et al.*, 2014].

3.2. MAIN TEXT

In the ablation zone of the Greenland Ice Sheet (GrIS), moulins deliver surface melt to the base of the ice sheet [*Catania and Neumann*, 2010], where fluctuations in meltwater supply modulate ice motion [*Hoffman et al.*, 2011; *Sundal et al.*, 2011; *Bartholomew et al.*, 2012]. The relationship between surface melting and ice velocity is thought to reflect the structure and evolution of the subglacial hydrologic system [*Bartholomew et al.*, 2010, 2012; *Hoffman et al.*, 2011; *Sundal et al.*, 2011]. Ice acceleration occurs when meltwater input exceeds the hydraulic capacity of the subglacial system, causing englacial and subglacial water storage and resulting in the widespread reduction in basal friction [*Bartholomaus et al.*, 2008; *Hoffman et al.*, 2011; *Bartholomew et al.*, 2012]. Subglacial water pressure and ice velocity of the GrIS are thought to remain elevated until a channelized drainage system develops, decreasing subglacial water pressure and ice velocity by efficiently routing surface meltwater to the glacier terminus via moulins [*Bartholomew et al.*, 2010; *Chandler et al.*, 2013; *Cowton et al.*, 2013]. Short-term increases in ice velocity can persist following channelization owing to temporary imbalances between the capacity of this efficient drainage system and the

magnitude of surface water input [*Bartholomaus et al.*, 2008; *Schoof*, 2010] from melt [*Bartholomew et al.*, 2012] and precipitation events [*Tedstone et al.*, 2013] or supraglacial lake drainage [*Das et al.*, 2008; *Hoffman et al.*, 2011]. In this paradigm, channelized system has been considered the key component governing ice-velocity sensitivity to supraglacial water input. Accordingly, moulin hydraulic head and ice velocity should both decrease seasonally as drainage efficiency increases.

Despite observations of decreasing minimum velocities during much of the melt season [*Bartholomew et al.*, 2010; *Hoffman et al.*, 2011; *Sole et al.*, 2013; *Tedstone et al.*, 2013], the role of channelization beneath some regions of the GrIS may be limited by shallow surface slopes and decreased basal conduit melt back [*Meierbachtol et al.*, 2013]. An extensive body of research on alpine glaciers highlights the central role of channelization in subglacial drainage evolution [*Hubbard et al.*, 1995; *Gordon et al.*, 1998; *Mair et al.*, 2003; *Bartholomaus et al.*, 2008], but also documents substantial complexity in the unchannelized regions of the bed [*Hubbard et al.*, 1995; *Murray and Clarke*, 1995; *Iken and Truffer*, 1997; *Gordon et al.*, 1998; *Mair et al.*, 2003; *Hoffman and Price*, 2014]. Borehole observations reveal that some portions of the unchannelized region transmit meltwater that is sourced from channels [*Hubbard et al.*, 1995; *Gordon et al.*, 1998], whereas other unchannelized regions of the bed are hydraulically isolated and receive little to no direct water input [*Murray and Clarke*, 1995; *Gordon et al.*, 1998; *Hoffman and Price*, 2014]. Basal pressure in these isolated regions respond to changes in the active drainage regions through transfer of mechanical support [*Murray and Clarke*, 1995; *Gordon et al.*, 1998; *Doyle et al.*, 2014] or as cavity volumes [*Iken and Truffer*, 1997] or pore volumes in subglacial sediment fluctuate in response to ice motion. While changing connectivity between active and isolated components of the subglacial drainage system has been directly observed [*Murray and Clarke*, 1995; *Gordon et al.*, 1998], it is

not believed to drive seasonal trends in ice velocity on alpine glaciers owing to the dominant control of channels [*Hubbard et al.*, 1995; *Iken and Truffer*, 1997; *Gordon et al.*, 1998].

Here we use borehole hydraulic heads to explore the response of the unchannelized region of the bed to channelized regions. Few direct measurements of water pressure have been made in channelized regions of the GrIS bed [*Cowton et al.*, 2013; *Meierbachtol et al.*, 2013], owing to the limited number of borehole studies [*Lüthi et al.*, 2002; *Meierbachtol et al.*, 2013; *Ryser et al.*, 2014b] and their inherently limited spatial extent. Consequently, we also measure water level in three different moulins to constrain hydraulic head in active regions of the subglacial drainage system. These borehole and moulin hydraulic heads are coupled with coincident measurements of surface ice velocity, bed separation, and air temperature to characterize relationships between ice dynamics and the subglacial hydrologic system during the 2011 and 2012 melt seasons.

At our primary field site in the ablation zone of Sermeq Avannarleq in western Greenland (Figure 3.1; Table 3.1; 69° 27′ N, 49° 53′ W), we drilled seven boreholes to the bed using a hot water drill and instrumented three of these with pressure transducers in 2011 (section 3.3.2) [*Ryser et al.*, 2014b]. The ice thickness in our instrumented boreholes was between 614 m and 624 m, and each borehole either drained slowly or did not drain before closure. The combination of gradual drainage following drilling and results from pump tests suggest borehole connection to unchannelized regions of the bed (section 3.3.2) [*Murray and Clarke*, 1995; *Gordon et al.*, 1998, 1998]. During 2011, we instrumented the FOXX moulin, about 0.3 km southwest of the boreholes, with a pressure transducer. In 2012, we instrumented moulins 3 and 4 with pressure transducers, 1.6 km and 1.9 km from the boreholes, respectively (sections 3.3.3 and 3.3.4). Because moulin

instrumentation could not proceed until the snowline had retreated past the field sites, these moulin measurements capture relationships between subglacial hydrology and ice motion after channelization is inferred to have begun [*Cowton et al.*, 2013]. We derive ice velocity and bed separation from Global Positioning System (GPS) installations at several locations (section 3.3.5). We use meteorological observations from a weather station co-located with the FOXX GPS to determine periods of increasing surface melt (section 3.3.6).

The magnitude and phase of moulin and borehole measurements differ substantially in their relationship to ice velocity (Figure 3.2; section 3.3.7), suggesting that each monitored a different component of the subglacial system. Moulin hydraulic heads were highly variable, with a mean diurnal fluctuation of approximately 95 ± 47 m (about 17% of overburden) during 2012 and minimum values (about 70% of overburden) well below the ice surface. In addition, hydraulic heads in moulins 3 and 4 are synchronous, despite being located in different supraglacial drainage basins and 1.5 km apart (Table 3.2). This similarity in hydraulic heads suggests pressure equalization within an efficient system [*Covington et al.*, 2012] that connects these moulins at the bed [*Chandler et al.*, 2013; *Cowton et al.*, 2013]. Further, numerical analysis supports the existence of subglacial channels in our study area (Figure 3.6; section 3.3.8). During periods of steady supraglacial input channel development via meltback may be limited; however, observed melt-event perturbations temporarily increase channel volume, allowing greater transmission of water. From these observations, we infer that moulin head reflects subglacial water pressure within a moulin-connected channel system [*Hubbard et al.*, 1995; *Gordon et al.*, 1998; *Cowton et al.*, 2013], which appears to increase in efficiency only over short timescales.

In contrast, our boreholes display high mean hydraulic head (close to or above overburden) and low-amplitude diurnal variability (less than 25 m or <5% of overburden). Borehole heads are anti-correlated with ice velocity (Figures 3.3A and 3.3B; Table 3.2). These systematic differences between moulins and boreholes further suggest that moulins connect to a channelized component of the drainage system, while boreholes monitor an isolated region of the bed unconnected to the channelized system (sections 3.3.9 and 3.3.10) [*Hubbard et al.*, 1995; *Murray and Clarke*, 1995; *Iken and Truffer*, 1997; *Gordon et al.*, 1998].

Strong correlations between diurnal peaks in moulin water level and ice velocity suggest that pressure variability in the channelized drainage system reduces basal friction in an adjacent active but unchannelized component of the hydraulic system and drives diurnal ice acceleration, as observed in alpine glaciers [*Bartholomaus et al.*, 2008]. However, on longer timescales the relationship between moulin head and ice velocity is characterized by hysteresis. In both 2011 and 2012, ice velocity decreases as the melt season progresses, despite relatively constant moulin heads (Figure 3.3C; section 3.3.11). Further, neither the minimum nor maximum daily moulin head decreases over the observation period, as would be expected with increasing efficiency, suggesting that pressure decreases in the efficient, channelized system do not control decreases in ice velocity during the latter portion of the melt season (Figure 3.3D). Therefore, while variability in moulin head appears to drive diurnal and multi-day velocity variations, longer-term decreases in ice velocity are potentially due to decreasing water pressure in the unchannelized regions of the subglacial hydrologic system.

As observed in alpine glaciers, isolated components of the subglacial hydrologic system may act to resist ice acceleration [*Iken and Truffer*, 1997]. Previous studies demonstrate that high (above overburden) water pressures out of phase with ice velocity

may be caused by transfer of mechanical support from channelized regions of the bed to isolated regions [*Murray and Clarke*, 1995; *Gordon et al.*, 1998; *Mair et al.*, 2003; *Ryser et al.*, 2014b]. However, the diurnal range of head in our boreholes is more strongly anti-correlated with the diurnal range of ice velocity than with the diurnal range of water pressure in nearby active regions of the bed (section 3.3.7), suggesting that borehole head variability is at least partly the result of non-locally generated sliding [*Iken and Truffer*, 1997]. In this proposed mechanism, pressurization of neighbouring regions of the bed that have an efficient connection to the channelized system induces sliding, which is transmitted to these unconnected areas by stress transfer laterally within the ice. In turn, water pressure in unconnected regions of the bed decreases as the volume of bedrock cavities increases through sliding [*Murray and Clarke*, 1995] or as basal sediments deform [*Dow et al.*, 2013; *Walter et al.*, 2014] without a commensurate water influx. A combination of these processes results in a dynamic water pressure environment, despite the apparent hydraulic isolation of these regions of the bed.

Negative feedback between increased ice velocity and decreased water pressure in unconnected regions can act to limit sliding [*Iken and Truffer*, 1997; *Hoffman and Price*, 2014] and potentially control minimum ice velocity. This resistance to sliding likely varies both spatially and temporally, owing to changes in connectivity within the isolated system [*Murray and Clarke*, 1995; *Gordon et al.*, 1998]. Although borehole heads are typically anti-correlated with ice velocity, some boreholes experienced infrequent periods when pressures are in phase with ice velocity following large melt events (e.g., on days 211–218 of 2011 in borehole 6, Figure 3.2A). These in-phase periods may indicate ephemeral connections to the unchannelized but interconnected parts of the drainage system, which occur when the hydraulic capacity of the subglacial drainage system is overwhelmed and water flows out of conduits into the surrounding unchannelized system

[*Bartholomaus et al.*, 2008; *Bartholomew et al.*, 2012; *Cowton et al.*, 2013; *Hewitt*, 2013].

While long-term decreases in ice velocity have previously been attributed to decreasing subglacial water pressure caused by increased channelization [*Bartholomew et al.*, 2010; *Sole et al.*, 2013; *Tedstone et al.*, 2013], our results suggest that during the latter part of the melt season, the spatial extent of the unchannelized system is a primary control on ice velocity. Basal traction is a function of both the interconnected and isolated regions of the unchannelized system [*Iken and Truffer*, 1997]. Therefore, increasing the spatial extent of the interconnected system, at the expense of the isolated system, should result in a larger fraction of the bed at lower water pressures. Gradually increasing the connectivity of the isolated system (that is, opening or enlargement of flow pathways) would have a similar result.

These processes could increase basal traction and decrease ice velocity without a change in the efficiency of the channelized system [*Hoffman and Price*, 2014]. Indeed, we observe a gradual decrease in water pressure in two of three boreholes (boreholes 4 and 6; Figures 3.3D and 3.4), implying increasing connectivity to active regions of the bed. This process is also observed at a second field site in 2011 (section 3.3.12). These reductions in subglacial pressure match well with velocity trends (Figure 3.3D), suggesting that systematically decreasing pressures within the isolated system are occurring. The observed decreases in water pressure may result in a higher spatially averaged basal traction at the end of the melt season that persists after meltwater inputs cease. Consequently, this mechanism could explain the winter mediation of summer acceleration [*Sole et al.*, 2013; *Tedstone et al.*, 2013].

Our results suggest that the subglacial drainage system consists of three components that exert varying control on ice velocity over different spatiotemporal

domains: a moulin-connected channelized system that transports the available meltwater efficiently; an active, interconnected unchannelized system strongly influenced by the channelized system; and an isolated system that responds passively to changes in bed separation because water flow is slow or absent. The spatiotemporal extents of these domains are probably highly variable, with the spatial extent of each component controlled by the spatial distribution of moulin locations [*Gulley et al.*, 2012], basal and surface topography [*Joughin et al.*, 2013] and the hydraulic conductivity of basal sediments [*Dow et al.*, 2013; *Walter et al.*, 2014].

Direct observations of multiple components of the subglacial hydrologic system illustrate how subglacial drainage efficiency modulates ice dynamics across multiple timescales. The degree of control that each component of the subglacial system exerts on ice velocity depends critically on the time period considered. Our data from a sector of the GrIS ablation zone indicate that the channelized system may only be sustained via frequent multi-day melt events and does not control long-term trends in ice velocity during the latter portion of the melt season. Thus, we caution against the application of channel-only models to explore the seasonal relationship between subglacial hydrology and the ice dynamics of the GrIS. Future work should consider the seasonal evolution of all observed components of the subglacial hydrologic system, including isolated regions of the bed. Such investigations are increasing in importance as new results suggest that the melt-season behaviour of the subglacial system affects ice dynamics in the ablation zone [*Sole et al.*, 2013; *Tedstone et al.*, 2013] and potentially farther inland [*Doyle et al.*, 2014] after the melt season.

3.3. EXTENDED METHODS

3.3.1. Seasonal Data Presentation

To clearly present diurnal variability in the measured parameters, the time series is shortened to the period of time over which moulin water pressures are measured (Figure 3.2). During 2011, velocity and bed separation were measured throughout the melt season; in 2012, all parameters except moulin pressures were recorded over the entire melt season (Figure 3.4).

3.3.2. Borehole Drilling and Instrumentation

During 2011, 13 boreholes were drilled at two sites, seven at FOXX (Figure 3.1; 69° 27′ N, 49° 53′ W) and six at GULL (69° 27′ N, 49° 43′ W) using hot water drilling techniques and equipment [*Iken et al.*, 1989; *Humphrey and Echelmeyer*, 1990; *Lüthi et al.*, 2002; *Ryser et al.*, 2014b]. Drill water had a consistent temperature and pressure of 80 °C and 8 MPa, respectively. At FOXX, three boreholes were instrumented with pressure transducers at depths between 614 m and 624 m (Table 3.1). In Greenland, thick cold ice results in rapid (less than a day) closure of boreholes, eliminating the influence of surface water input. Further, the volume of the boreholes is assumed to be small relative to the subglacial system. Therefore, we assume that these boreholes function as accurate manometers of the subglacial system.

Two boreholes (boreholes 4 and 6) were instrumented with the Swiss Federal Institute of Technology (ETH) designed digital borehole sensor system (DIBOSS) [*Ryser et al.*, 2014b]. Borehole 7 was instrumented with a Geokon 4500HD piezometer. All sensors were connected to the surface via cables able to accommodate an additional 20% strain before breaking (Cortland Cable Co.). Campbell Scientific CR1000 data loggers were used for switching power supply and recording sensor measurements via CFM100 storage modules. The sampling intervals ranged from 1 min to 15 min. Data were

decimated to 15-min intervals for analysis in this paper. All units remained powered between summer 2011 and spring 2013.

Several observations during and following the drilling process indicate that the boreholes connected to the ice–bed interface: (1) all boreholes reached similar depths of 614 to 624 m; these depths are similar to, though slightly deeper than, depths expected from a 2012 CReSIS depth-sounding radar track through the FOXX field site [*Gogineni*, 2012]; (2) drilling only ceased when pressures at the drill tip rapidly decreased; (3) boreholes 4 and 6 drained slowly over the course of several hours; and (4) pump tests were performed in boreholes 4 and 6, forcing a connection to the subglacial system. Changes associated with pump tests were ephemeral and boreholes gradually reverted to their pre-pump test state. Borehole 7 also connected to the bed because, even though it did not drain before closure, the diurnal lags and melt event pressure variations in borehole 7 are similar to those observed in boreholes 4 and 6 over the course of both melt seasons.

Borehole hydraulic heads were calculated from measured borehole pressure (from installed pressure transducer), surface elevation and borehole depth:

$$h = \frac{P_w}{\rho_w g} + z_{bed}, \tag{3.1}$$

where h is total hydraulic head. P_w is directly measured from borehole sensors, but is also equal to $\rho_w g h_w$. The density of water is ρ_w; g is the acceleration due to gravity and h_w is water height. z_{bed} is the bed elevation determined from GPS-derived elevation and borehole depth. Representing borehole data as hydraulic head allows us to determine water level absolutely, as measured from sea-level in different locations.

3.3.3. Moulin Instrumentation and Measurements

Moulins were instrumented in both the 2011 (FOXX moulin) and 2012 (moulins 3 and 4) melt seasons (Table 3.1). Water pressures were measured using the Geokon 4500 (2011) or 4500HD (2012) piezometers on armoured cables ranging from 400 m to 600 m in length. Campbell Scientific CR1000 data loggers were used for switching power supply and recording sensor measurements via CFM100 storage modules. Water pressures were corrected for local barometric pressure as measured at the FOXX GPS station (2011) and moulin 3 (2012). Sampling intervals were 5 min or 15 min. Data were decimated to 15 min for analysis except where noted.

Moulin instrumentation is complicated by moulin geometry and water-level fluctuations that occur during pressure sensor installation. To constrain the absolute elevation of the pressure sensor in each moulin several corrections to the measured moulin water level must be made. These corrections include adjustment for the rise of water levels during the sensor installation and the mean slope of the conduit.

During sensor installation, we periodically paused while lowering to observe the water-level rise with the sensor held in a static position. These pauses allowed us to constrain the total change in water level over the course of sensor installation. Once the water level was corrected to a static level, we corrected for the slope of the moulin. However, it is important to note that moulins in Greenland are generally nearly vertical [*Catania and Neumann*, 2010], so this correction is small. We subtracted the corrected sensor depth from the GPS-derived surface elevation at each site to constrain the vertical sensor location. Sensor elevation and measured water level provide hydraulic head without the need to use poorly constrained ice thicknesses and bed elevations at moulin sites.

Owing to the possibly complex geometry of moulins, the error in sensor location is higher than the error in borehole-sensor locations. We estimate the error in absolute head measurements to be approximately 20 m. Uncertainty related to absolute head measurements does not affect measurements of relative changes, such as diurnal amplitudes of hydraulic head. The sensor in moulin 3 is near the bed of the ice sheet, as indicated by the continual increase in water as the sensor was lowered and because the total cable length deployed was similar to the local ice thickness. The sensor in moulin 4 is approximately 175 m from the bed, on the basis of similar observations. The 2011 sensor in the FOXX moulin is much shallower, as indicated by the truncated pressure record. Owing to the deployment techniques, the absolute sensor location is not as well constrained in 2011 as in 2012. We estimate the FOXX sensor location to be 455 m above the bed.

Moulins connect directly to highly efficient components of the subglacial system [*Gulley et al.*, 2012] and have previously been used with varying levels of success to measure the water level of the channelized component of the subglacial system [*Iken*, 1972; *Holmlund and Hooke*, 1983; *Vieli et al.*, 2004; *Cowton et al.*, 2013]. Although moulins are not considered manometers, measured moulin pressures can be considered equivalent to subglacial water pressures within the channelized system, because pressure changes in multiple moulins are coincident (Table 3.2), despite drainage basins of differing sizes and discharges. The volume of water in a moulin is large relative to the volume of water being discharged at the bed, so water flow within the moulin is slow [*Werder et al.*, 2009]; we therefore neglect the velocity head.

In addition, to be considered effective measures of water pressure, the volume of water within the moulin must be small when compared to the volume of water in the channelized system. Considering that large portions of the channelized system are

connected [*Chandler et al.*, 2013; *Cowton et al.*, 2013], the total volume in a single moulin is probably small relative to the total water volume within the channelized system. With these assumptions, we consider the measured moulin pressures to be representative of subglacial pressures in the efficient component of the subglacial system.

3.3.4. Coincident Observations

Over the course of four days (approximately day 192.5 to day 196.5), we were able to monitor the water level in moulin 3 and 4 concurrently (Figure 3.2B). These observations suggest that the hydraulic heads of both moulins behave very similarly, with peaks, and even small perturbations, occurring in both moulins at the same time (Table 3.2). We did not calculate the hydraulic gradient between the two moulins because the length of the subglacial channel is unknown and channel paths may diverge from those predicted by hydraulic potential theory [*Gulley et al.*, 2012]. However, we do use the head difference as a proxy for the hydraulic gradient [*Gordon et al.*, 1998], assuming that the subglacial channel does not alter its path significantly over the course of the melt season.

3.3.5. Ice Velocity and Bed Separation

Kinematic GPS positions were determined using carrier-phase differential processing relative to a bedrock mounted reference station using Track 1.24 [*Chen*, 1998] and techniques described by *Hoffman et al.* [2011]. GPS observations at all stations were logged at 15-second intervals, and the relative position of each on-ice station was determined at this frequency. Each 15-second time series of on-ice station position was smoothed with a 6-hour moving average, applied to reduce spurious signals associated with GPS uncertainties, and then decimated to 15-min time series. Using the mean error generated during processing, the horizontal and vertical position errors for 2011 (and

2012) were ±9.9 cm (±8.8 cm) and ±1 cm (±1 cm) respectively, with a velocity uncertainty of ~8.8 m a^{-1} (~7.7 m a^{-1}).

During 2012, the antenna pole for the FOXX GPS station melted out owing to higher than expected ablation rates. The data become unreliable after day 208, and the station ceased recording by day 215. Owing to the similarity between FOXX and 25N1 data (Figures 3.2D and 3.4D), the 25N1 GPS data were used for 2012 analysis. Over the entire melt season, ice velocities at both stations display the characteristic decrease in daily minima (Figure 3.4) [*Hoffman et al.*, 2011].

Bed-separation calculations were performed incorporating additional observations from nearby GPS stations and following the procedures described in detail in previous work [*Hoffman et al.*, 2011]. Both longitudinal (along flow) and lateral (across flow) strain rates $\dot{\varepsilon}$ were calculated from GPS data as follows:

$$\dot{\varepsilon} = \frac{1}{l_0}\frac{\Delta l}{\Delta t}, \tag{3.2}$$

where Δl is the change in baseline distance between stations, Δt is the change in time between measurements and l_0 is the initial baseline distance. Longitudinal strain at our field location is generally compressional over the course of the season. During 2012, GPS malfunction prevented the collection of data from 19N1 and decreased the availability of data from the FOXX GPS; bed separation was therefore calculated between 25N1 and GULL and is presented as a proxy (Figures 3.2D and 3.4D). During 2012, malfunction of a GPS station used to determine lateral strain between 25N1 and GULL required that we assume a constant lateral strain for bed separation calculations after day 205.

We approximate the vertical strain rate $\dot{\varepsilon}$ with the continuity equation, assuming ice is incompressible:

$$\dot{\varepsilon}_{zz} = -(\dot{\varepsilon}_{xx} + \dot{\varepsilon}_{yy}), \tag{3.3}$$

where x, y and z represent the longitudinal, lateral and vertical directions, respectively.

Following accepted methodology [*Mair et al.*, 2002b; *Anderson et al.*, 2004; *Sugiyama and Gudmundsson*, 2004; *Harper et al.*, 2007; *Howat et al.*, 2008], we decompose the vertical motion w_s measured by the GPS as:

$$w_s = u_b \tan(\alpha) + \dot{\varepsilon}_{zz} H + \dot{c}, \tag{3.4}$$

where u is the horizontal velocity, α is the bed slope, H is the ice thickness at the GPS station, as measured by borehole depth, and $\dot{c}$ is rate of bed separation (cavity opening and/or till dilation). Subscripts 's' and 'b' refer to the surface and bed of the ice sheet, respectively. Equation (3.4) is solved for $\dot{c}$ using observations of the other parameters.

The length scale over which bed slope should be measured is difficult to estimate owing to the variability of bed roughness over several ice thicknesses in our study region [*Catania et al.*, 2008; *Bartholomew et al.*, 2012]. Therefore, we chose to derive the bed slope from calculations before the onset of summer melting and the associated increase in velocity. During this window, we assume that vertical strain and the rate of cavity opening are constant, yielding:

$$\alpha = \tan^{-1}\left(\frac{w_{s,bg} - \dot{\varepsilon}_{zz,bg} H}{u_{b,bg}}\right), \tag{3.5}$$

where the subscript 'bg' represents background conditions. We note that diurnal variations in bed separation are generally within the range of error. Our results suggest that vertical strain is a non-negligible component to vertical motion in regions of the GrIS (Figure 3.5); simply removing the bed-parallel component of bed separation while assuming that $\dot{\varepsilon}_{zz}$ is negligible may result in inaccurate estimates of bed separation.

3.3.6. Melt Events

During 2011 and 2012, an automatic weather station measured a wide range of atmospheric conditions every 5 min, including ablation, incoming and reflected short-

wave radiation, wind speed and direction, humidity and the air temperature at a height of 2 m above the ice surface. To quantitatively constrain melt events, we simply difference consecutive calculations of 24-hour average temperature (with noon Coordinated Universal Time (UTC) as the midpoint). A positive temperature differential (that is, an increase in the 24-hour average temperature) of 0.5°C is considered a melt event. To limit visual confusion, the start of the melt event is plotted as the minimum of the first day and the maximum of the last day of the melt event (Figure 3.2).

3.3.7. Cross-Correlation Analysis

To characterize the lead–lag relationship between borehole hydraulic head, moulin hydraulic head and ice velocity, we perform cross-correlation analyses. We use the maximum cross-correlation coefficients and associated lags to examine the temporal relationship between various time series (Table 3.2) [*Gordon et al.*, 1998].

The ice velocities used for cross-correlation analysis have a 1-hour moving average applied to reduce spurious noise [*Hoffman et al.*, 2011], but still maintain independence between velocity measurements used in this analysis. We then decimate ice velocity and hydraulic head measurements to a 1-hour sampling interval. For moulins 3 and 4, we use a 5-min sampling interval to determine more closely a potential lagged relationship. We detrended all data using a 24-hour moving window mean and recorded measurements as standardized residuals [*Gordon et al.*, 1998]. Data gaps, which primarily occur in velocity data (~3% during both years), are filled using linear interpolation. Less than 1% (and generally 0%) of borehole and moulin data were linearly interpolated in either year; the exception being the FOXX moulin data, with 6% in 2011. All re-expressed time series, except the FOXX moulin, approximate a Gaussian distribution with a mean centred at zero. Because the FOXX moulin does not

approximate a Gaussian distribution, we do not present cross-correlation analysis that includes the FOXX moulin.

Borehole hydraulic head and ice velocity exhibit the strongest inverse correlation with a lag of ~4 hours. As 1-hour averaged ice velocities have inherently higher errors than 6-hour averaged ice velocities, correlation coefficients with ice velocity are low but still significant (Table 3.2). Moulins 3 and 4 are strongly correlated at zero lag, despite having differing supraglacial inputs and geometries, suggesting pressure equalization within the channelized subglacial system [*Covington et al.*, 2012].

3.3.8. Subglacial Channel Geometry

Recent evidence suggests that characteristics of the GrIS ablation zone distal from the margin (low surface slope and limited conduit meltback) prevent the formation of an extensive channelized system [*Meierbachtol et al.*, 2013]. However, dye tracing suggests the presence of channelization through much of the ablation area [*Chandler et al.*, 2013]. Our moulin observations indicate a component of the subglacial system that is efficiently conducting the available melt water, though this may be the result of an efficient distributed pathway [*Meierbachtol et al.*, 2013]. To characterize the nature of the efficient system we performed a simple numerical analysis to explore the channel stability in our study area.

Using moulin 3 hydraulic head and supraglacial discharge estimated from ablation measurements at the FOXX weather station, we calculated the change in channel geometry over ~30 days in 2012, following previous work [*Schoof*, 2010; *Meierbachtol et al.*, 2013]:

$$\frac{dS}{dt} = c_1 Q\Psi + u_b h_b - c_2 N^2 S\,, \tag{3.6}$$

where subglacial discharge Q is calculated as a function of moulin head h_m and supraglacial input, Q_{sur}:

$$Q = Q_{sur} - \frac{dh_m}{dt} S_m, \tag{3.7}$$

and Ψ is the hydraulic gradient calculated as a function of downstream (indicated by subscript 'j') hydraulic head:

$$h_j = h_m + z_j - z_m - \frac{l_{m,j} c_3}{\rho_w g} Q^2 S_{m,j}^{-5/2}, \tag{3.8}$$

Effective pressure N was calculated at the point midway between h_m and h_j. Additional parameters are listed in Table 3.3.

For these calculations, we set $u_b h_b = 0$ to clarify the role of creep closure and channel melt-back in the maintenance of subglacial channels. This assumption is applicable for our data set because we measure pressures after the assumed onset of channelization [*Cowton et al.*, 2013]. Once channels are larger than bedrock bumps, cavity opening due to sliding probably plays a very limited part in continued channelization [*Schoof*, 2010]. Initial subglacial channel size is determined by initiating the model with a small channel and sinusoidal inputs approximating the daily average and range of moulin 3's head and supraglacial discharge into the modeled moulin until the channel size stabilizes. With this approach we cannot specifically address the timescale of channel development because we do not constrain supraglacial input and moulin hydraulic head at the beginning of the melt season. After determining the initial channel size, we forced the system with observations of supraglacial input and moulin 3 hydraulic head (Figure 3.7). Supraglacial input is calculated by scaling ablation measurements to half of the moulin 3 drainage basin area [*McGrath et al.*, 2011]. As moulin hydraulic head exceeds floatation only rarely, we assumed that all water entering the moulin enters and stays within the channelized system over the short distance

assessed here. This assumption is conservative with respect to maximum channel melt back.

Using distance (1.5 km), bed and surface slope similar to our study area, we were able to qualitatively reproduce the head difference between moulins 3 and 4 using this simple numerical analysis (Figure 3.7). This analysis suggests that with the observed supraglacial input and moulin hydraulic head, subglacial channels can be maintained in our study area. However, we do note that supraglacial melt perturbations may be required to sustain channels over long periods; so steady-state modelling may be insufficient to explore the spatial extent of subglacial channels under the GrIS. These calculations suggest that periods with elevated hydraulic gradients, probably during and shortly after melt events, allow for increased melting to effectively counter creep closure (Figure 3.7). This melting results in channel enlargement; however, during periods of normal diurnal variability, the available supraglacial melt and the associated hydraulic gradient are generally lower, resulting in rapid channel closure. Regular melt events may be essential in the maintenance of subglacial channels in this region of the GrIS.

Recent studies indicate that increased efficiency of subglacial channels during high melt years could result in the observed decline in late season ice velocities through more extensive drainage of the bed following the cessation of surface melting [*Sole et al.*, 2013; *Tedstone et al.*, 2013]. However, our results suggest that the rapid adjustment of subglacial channels to the available melt, and the need for melt events to open the conduits periodically, may preclude this possibility. Instead, the observed declines in ice velocity [*Bartholomew et al.*, 2010; *Hoffman et al.*, 2011; *Sole et al.*, 2013; *Tedstone et al.*, 2013], may be the result of changes in unchannelized regions of the subglacial system.

3.3.9. Potential Mechanisms for Borehole Diurnal Variability

Although the boreholes in this study connected to the bed, there are several lines of evidence that suggest borehole pressures are responding to pressure variations due to basal sliding rather than the direct propagation of water pressure pulses at the bed. First, during 2011 (and mostly during 2012), borehole hydraulic heads are always higher than those of the moulin that is only 300 m away, thus preventing the propagation of water from the channelized system to the borehole locations. Second, if pressure fluctuations in our boreholes resulted from propagation of diurnal pulses from channels to boreholes through till, we would expect boreholes further from the channel to exhibit smaller and more lagged peak diurnal water pressures. In contrast, we find that water-pressure maxima and minima in boreholes display no consistent pattern in lag times (Figure 3.2), and cross-correlation analysis indicates that lag does not increase as a function of distance from the moulin in 2011 (Table 3.2). Third, we computed the hydraulic diffusivity needed to produce the observed ~15-h phase lag between moulin and borehole pressure peaks following *Hubbard et al.*[1995]:

$$D = \frac{x^2}{2\omega t^2}, \tag{3.9}$$

where x and t are the distance and time lag, respectively, between the channel and the borehole sensor and w is the angular frequency of the periodic boundary condition ($2\pi t^{-1} = 7.27 \times 10^{-5} s^{-1}$ $2\pi/t = 7.27 \times 10^{-5}$ s^{-1} for a diurnal cycle). This calculation results in a diffusivity of approximately 10^{-1} m^2 s^{-1}, several orders of magnitude larger than expected hydraulic diffusivities for glacial till [*Cuffey and Paterson*, 2010] and in the range of the hydraulic diffusivity for rock [*Li*, 1985] and yet there is evidence of thick sediments beneath our field area [*Walter et al*., 2014]. Fourth, borehole minima are more closely correlated to moulin and velocity maxima (Table 3.2). As a result, we do not believe that the pressure lag observed in the borehole record results from diffusion of the

moulin-generated pressure wave through subglacial sediments. These observations and recent modeling results [*Ryser et al*., 2014a] lead us to conclude that borehole-pressure fluctuations result from non-locally forced ice motion. In this case, we expect and observe the pressure fluctuations in the boreholes to scale with diurnal velocity variability (Figure 3.3).

3.3.10. Flow Coupling and Mechanical Support Transfer

To constrain the mechanism driving changing pressures measured via boreholes, we examine the relationship between the diurnal range in borehole hydraulic head and the diurnal ranges in both ice velocity and moulin hydraulic head. Borehole water levels are anti-correlated with horizontal ice velocity and moulin water level (Figures 3.3A and 3.3B). Such anti-correlated behaviour has been observed on alpine glaciers and is generally hypothesized to occur through the transfer of mechanical support between the efficient and weakly connected regions of the bed [*Hubbard et al.*, 1995; *Murray and Clarke*, 1995; *Gordon et al.*, 1998; *Mair et al.*, 2003]. In our study, the two components are represented by the moulin and borehole water levels, respectively. However, if load transfer is the only mechanism controlling borehole water pressure, diurnal changes in borehole water level should be most strongly anti-correlated with diurnal changes in moulin water level. Instead, the diurnal magnitude of borehole head is more strongly anti-correlated with the diurnal magnitude of ice velocity, as follows. For moulin 3, (~day 192–240), borehole 4 $r^2 = 0.68$ ($p < 0.05$; $n = 89$), borehole 6 $r^2 = 0.70$ ($p < 0.05$; $n = 88$), borehole 7 $r^2 = 0.72$ ($p < 0.05$; $n = 85$). For ice velocity, (~day 192–240), borehole 4 $r^2 = 0.75$ ($p < 0.05$; $n = 80$), borehole 6 $r^2 = 0.80$ ($p < 0.05$; $n = 79$), borehole 7 $r^2 = 0.81$ ($p < 0.05$; $n = 75$)). Local load transfer would also result in moulin water levels and borehole pressures to be directly out of phase [*Murray and Clarke*, 1995]. We observe that minimum daily borehole pressures consistently lag daily maximum ice velocity and

moulin water level by about 4 hours (Table 3.2), further suggesting that flow coupling may be important in controlling unchannelized regions of the bed [*Iken and Truffer*, 1997].

3.3.11. Moulin–Velocity Hysteresis

During 2011 and 2012, the relationship between moulin hydraulic head and ice velocity changes, showing a decreasing trend in velocity without a similar change in moulin hydraulic head. Diurnal hysteresis is evident in both years (Figure 3.7).

3.3.12. GULL Borehole Observations

During the 2011 field season, a series of boreholes were also drilled and instrumented at GULL (69° 27′ N, 49° 43′ W), a site approximately 5 km up the flow line from FOXX. These boreholes were less than 500 m downstream of a moulin slowly draining a supraglacial lake. As at FOXX, pressure transducers were installed in three boreholes; however, owing to a highly deformable layer of ice, sensor cables sheared before the start of the 2012 melt season [*Ryser et al.*, 2014b]. Borehole head at GULL demonstrates small diurnal variations that are out of phase with velocity. Yet, despite a temporally limited water pressure record, we observe similar trends in decreasing daily minimum velocity values and borehole head as observed at FOXX during the 2012 melt season (Figure 3.8). Although these are observations are limited by the borehole spatial distribution, this trend suggests that these long-term dynamic changes may be widespread.

3.4. Acknowledgements

This project was supported by United States National Science Foundation grants OPP-0908156 and OPP-0909454, Swiss National Science Foundation grant 200021_127197, and National Geographic Society grant 9067-12. L. C. Andrews was

also supported by UTIG Ewing-Worzel and Gale White Graduate Student Fellowships. M. J. Hoffman was also supported by NASA Cryospheric Sciences and Climate Modeling Programs within the US Department of Energy, Office of Science. J. D. Gulley was also supported by an NSF Postdoctoral Fellowship (EAR-0946767). Logistical support was provided by CH2MHill Polar Services. The GPS base station and several on-ice GPS units were provided by the UNAVCO facility with support from the NSF and NASA under cooperative agreement EAR-0735156. The University of Minnesota Polar Geospatial Center, funded under NSF OPP collaborative agreement ANT-1043681, provided WorldView imagery. Figure 1 utilizes radar depth sounder data products from CReSIS generated with support from NSF grant ANT-0424589 and NASA Operation IceBridge grant NNX13AD53A. We thank K. M. Schild, J. D. Nowinski, J. A. MacGregor, and B. F. Morriss for assistance in the field.

3.5. Author Contributions

G. A. Catania, J. D. Gulley, M. P. Lüthi, R. L. Hawley and T. A. Neumann designed this study. L. C. Andrews, R. L. Hawley, M. J. Hoffman, M. P. Lüthi, C. Ryser and J. D. Gulley performed the fieldwork. L. C. Andrews analyzed the results and wrote the manuscript. All authors discussed the results and edited the manuscript.

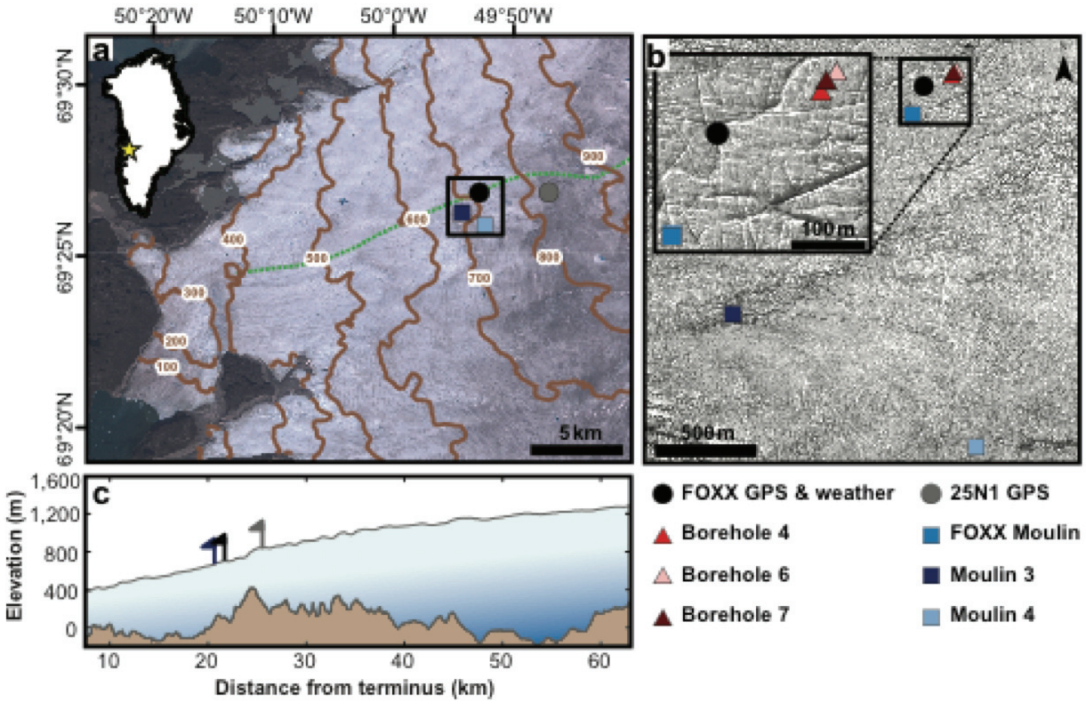

Figure 3.1. Study area in the western ablation zone of the Greenland Ice Sheet. A) Landsat-7 image of Sermeq Avannarleq. Ice-surface contours (meters; brown) derived from GIMP surface DEM [Howat et al., 2014] and site locations are indicated. The black box indicates the area in B. The 2012 CReSIS flight line (marked in green) provides the bed (brown) and surface (blue) elevations shown in C. B, 2009 Worldview-2 image of the study area; locations as indicated. C) Bed and surface elevations from CReSIS [Gogineni, 2012]. Moulin 3, FOXX and 25N1 are projected onto the flight line (colors as indicated). Moulin 4 projects onto the FOXX location.

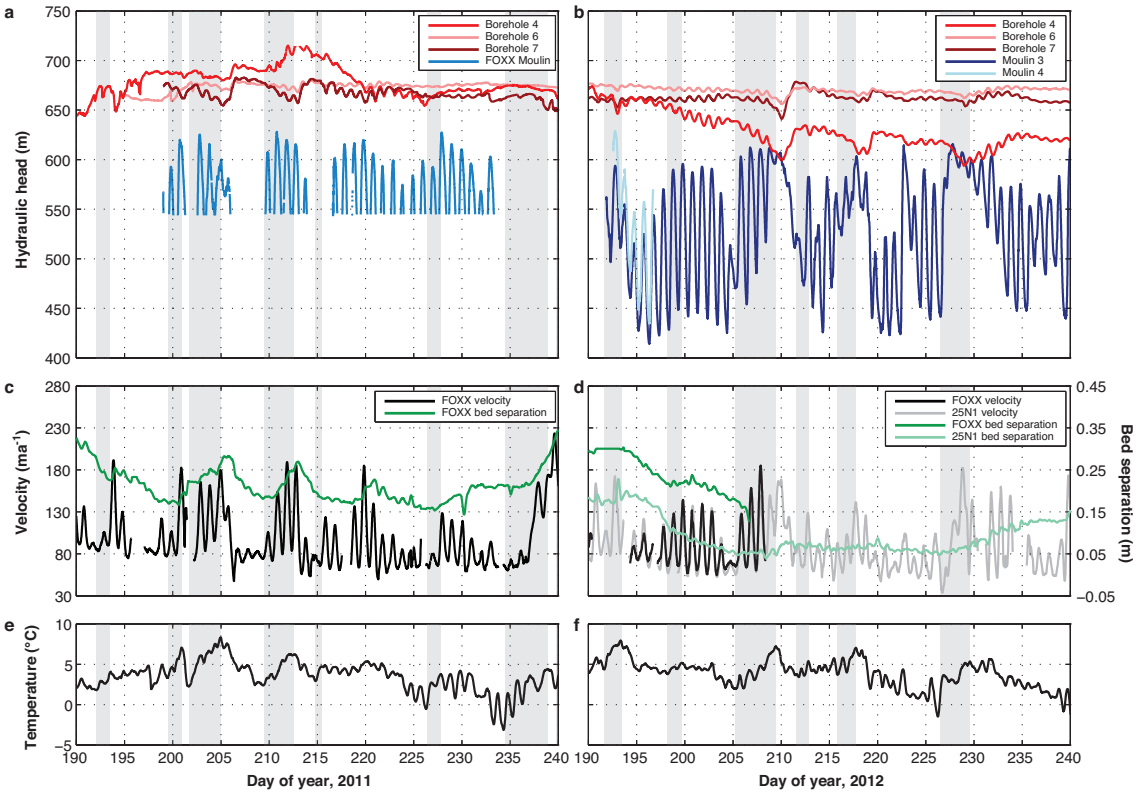

Figure 3.2. Borehole and moulin head and ice-surface velocity during 2011 and 2012. A) 2011 hydraulic head measurements from the FOXX moulin (blue), borehole 4 (red), borehole 6 (pink) and borehole 7 (dark red). B) 2012 data from moulin 3 (navy) and moulin 4 (light blue). Borehole colors are as in 2011. C) 2011 GPS-derived surface velocity (black) and bed separation (green) for FOXX. D) 2012 GPS-derived surface velocity for FOXX and 25N1 (grey) and bed separation for FOXX and 25N1 (light green). E, F) 6-hour averaged 2-m air temperature for 2011 and 2012. Grey bars in all panels indicate periods identified as melt events.

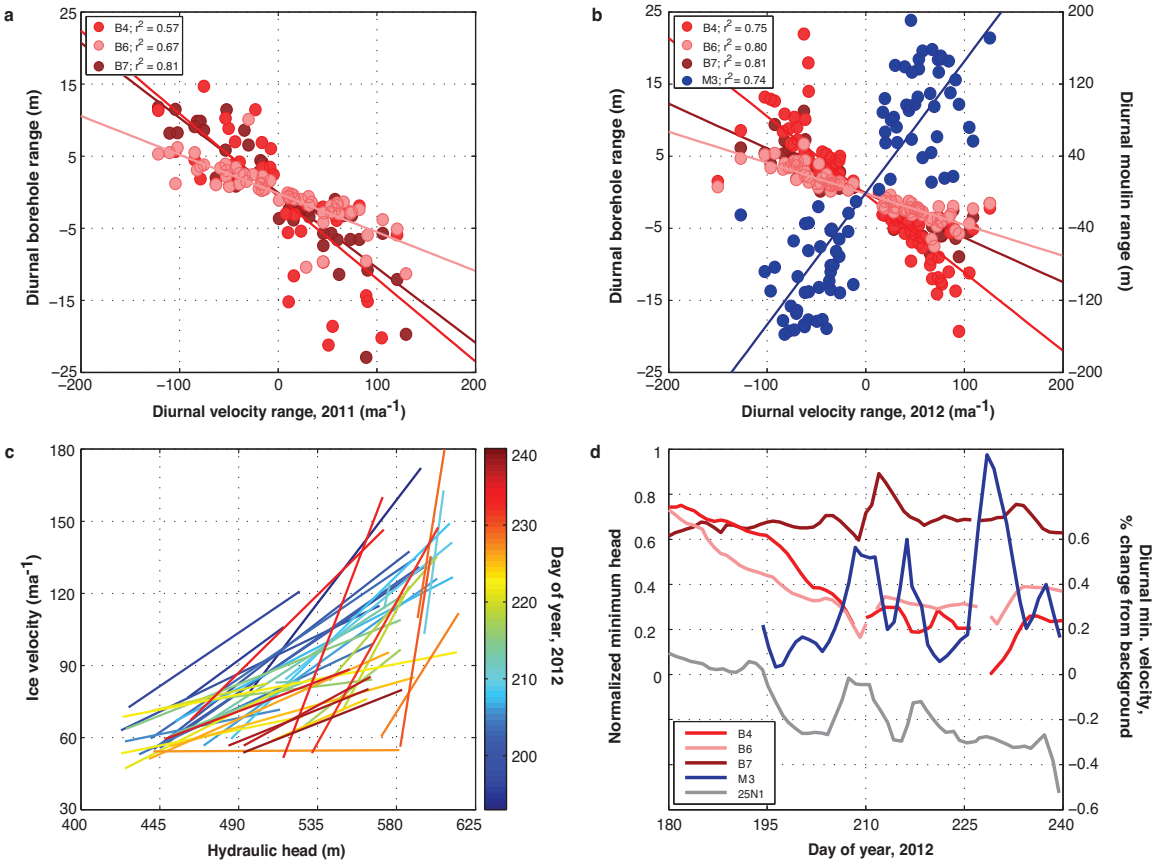

Figure 3.3. Relationships between hydraulic head and ice-surface velocity. A) Linear regression between the magnitude of diurnal changes in ice velocity and borehole and moulin head for 2011 ($p < 0.05$; borehole 4 $n = 48$, borehole 6 $n = 59$, borehole 7 $n = 50$). B) Linear regression between the magnitude of diurnal changes in ice velocity and borehole and moulin head between day 192 and 240 in 2012 ($p < 0.05$; borehole 4 $n = 80$, borehole 6 $n = 79$, borehole 7 $n = 75$, M3 $n = 85$). Days when borehole head and ice velocity are in phase are excluded. C) Daily maximum and minimum moulin head plotted against associated ice velocity for 2012. D) Normalized daily minimum hydraulic heads and ice velocity as a percentage of winter background for 2012. The minimum values are smoothed over 5 days to minimize daily effects.

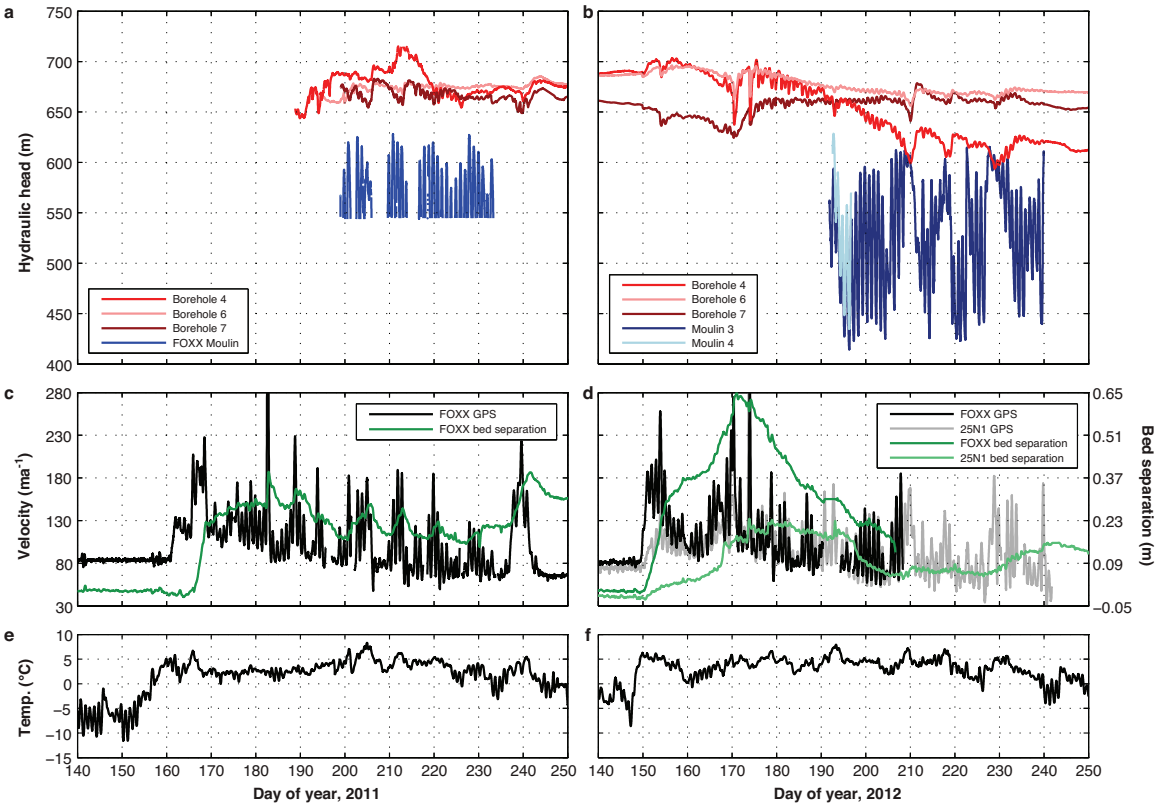

Figure 3.4. Borehole and moulin head and ice-surface velocity over two melt seasons. A) 2011 measurements from FOXX moulin (blue), borehole 7 (dark red), borehole 6 (pink) and borehole 4 (red). B) 2012 measurements from moulin 3 (navy) and moulin 4 (light blue). C) 2011 ice velocity (black) and bed separation (green) for FOXX. Peak velocity on day 182 is 402.3 m a^{-1} (exceeding the *y*-axis limit). D) 2012 ice velocity and bed separation for FOXX and 25N1 (grey, light green). Peak velocity for FOXX and 25N1 (312 m a^{-1} and 337 m a^{-1}) occurred on day 173. E, F) 6-h averaged air temperature for 2011 and 2012. Grey bars are melt events.

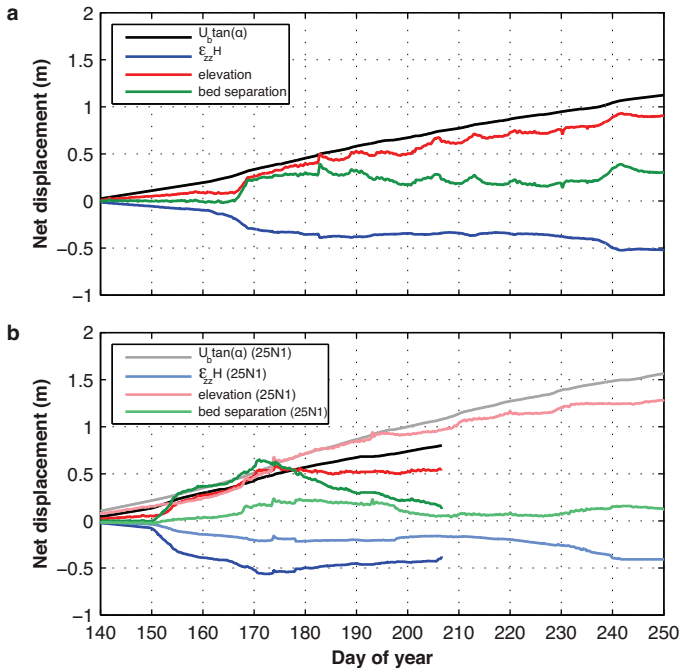

Figure 3.5. Components of vertical motion 2011 and 2012. A) Components of vertical motion for 2011 at FOXX. Bed parallel motion ($u_b \tan(\alpha)$; black), strain thickening and thinning ($\dot{\varepsilon}_{zz} H$; blue), elevation with measured winter elevation removed (red), and calculated bed separation (green). B) Components of vertical motion for 2012. Colors as in A for FOXX. Lighter colors correspond to components of vertical motion from 25N1.

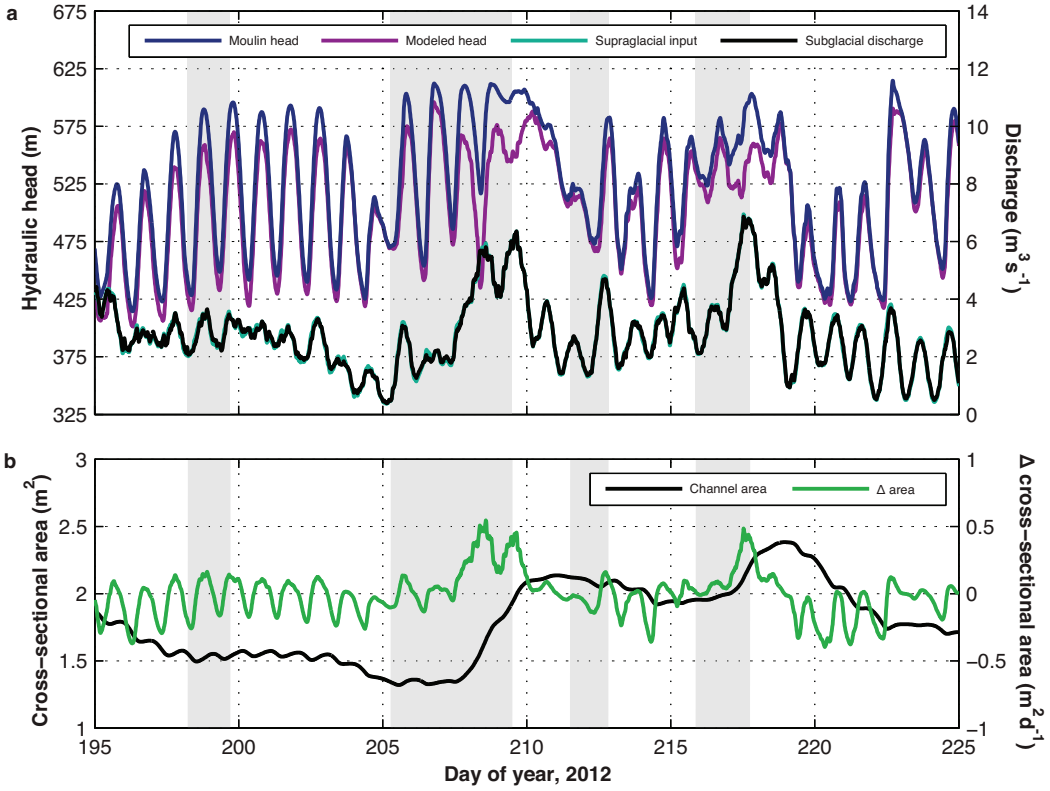

Figure 3.6. Modeled hydraulic head and conduit geometry. A) Moulin 3 head (blue) and supraglacial input (teal) are model inputs. Predicted downstream head is calculated from Equation (3.8) (purple). Subglacial discharge (black) is calculated as a function of head change and supraglacial inputs. It does not vary significantly from supraglacial input even when a large moulin geometry is used. B) Modeled subglacial channel cross-sectional area (green) changes rapidly (black) during and shortly after expected melt events (grey bars).

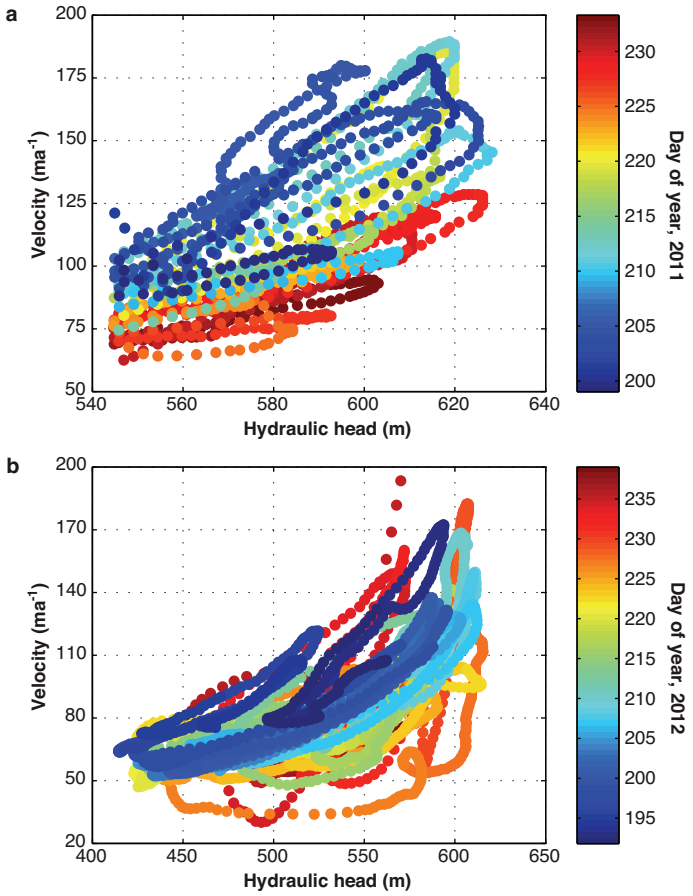

Figure 3.7. Long-term relationship between moulin head and ice velocity for 2012 and 2011. Moulin hydraulic head and associated ice velocity data plotted every 15 min over the course of the measurement periods for 2011 (A) and 2012 (B). 2011 data are truncated below 543 m by the high elevation of the moulin sensor.

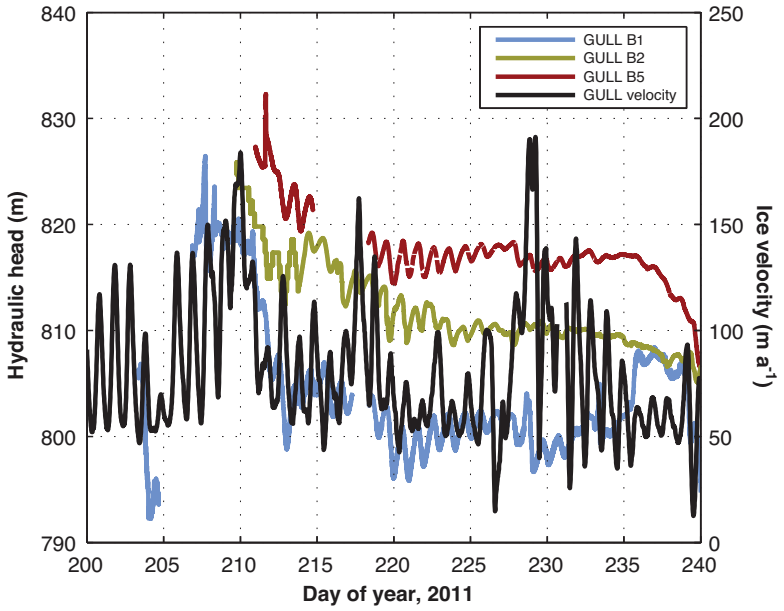

Figure 3.8. Borehole hydraulic heads and ice velocity at GULL during 2011. Three hydraulic head records (red, yellow, blue) from boreholes located ~0.5 km from a moulin. Ice velocity from GULL GPS (black), ~0.75 km south of GULL boreholes.

Field Site	Latitude	Longitude	Elevation (m)	Ice thickness (m)	Surface characteristics
FOXX GPS & weather station	69.4458	-49.8847	716	602*	uncrevassed, on small ridge
25N1 GPS	69.4454	-49.7890	851	608*	local crevasses
Borehole 4	69.4465	-49.8802	716	624	uncrevassed, near large supraglacial stream
Borehole 6	69.4463	-49.8807	716	614	uncrevassed, near large supraglacial stream
Borehole 7	69.4464	-49.8805	716	623	uncrevassed, near large supraglacial stream
FOXX moulin	69.4446	-49.8859	714	620*	supraglacial stream entering from northeast
Moulin 3	69.4358	-49.9092	657	564*	supraglacial streams entering from east & west
Moulin 4	69.4296	-49.8785	709	540*	supraglacial stream entering from east

Table 3.1. Site coordinates and characteristics. Location and surface elevations determined from GPS. Ice thicknesses at borehole locations determined during drilling. Additional ice thicknesses interpolated from CReSIS radar sounding data (indicated by asterisks) [*Gogineni*, 2012].

	2011		2012			
	Observation period (195 to 235)		Melt season (150 to 240)		Moulin period (192 to 240)	
	Peak to minimum	Peak to peak	Peak to minimum	Peak to peak	Peak to minimum	Peak to peak
Borehole 4/ velocity	-0.15 (7)	0.16 (18)	-0.45 (5)	0.38 (16)	-0.49 (4)	0.46 (16)
Borehole 6/ velocity	-0.21 (1)	0.23 (17)	-0.34 (5)	0.34 (16)	-0.49 (3)	0.46 (15)
Borehole 7/ velocity	-0.39 (4)	0.39 (15)	-0.42 (5)	0.39 (16)	-0.44 (4)	0.43 (16)
Moulin 3/ velocity	--	--	--	--	-0.45 (-13)	0.48 (0)
Borehole 4/ moulin 3	--	--	--	--	-0.83 (4)	0.75 (16)
Borehole 6/ moulin 3	--	--	--	--	-0.80 (2)	0.74 (14)
Borehole 7/ moulin 3	--	--	--	--	-0.76 (3)	0.69 (16)
Moulin 4/ moulin 3	--	--	--	--	0.80 (11.5)	1.0 (0)

Table 3.2. Cross-correlation analysis for boreholes, moulins, and ice velocity. Maximum positive and negative correlation coefficient between indicated data sets; lag times are noted in parentheses. In 2011, sample sizes for borehole 4, borehole 6 and borehole 7 cross-correlations are $n = 1{,}105$, 981 and 839, respectively. For the 2012 melt season, $n = 2{,}159$. Between days 192 to 240, 2012, $n = 1{,}155$. The moulin 4 to moulin 3 cross-correlation sample size is $n = 901$. The 99% confidence interval for all cross-correlation coefficients is less than 0 ± 0.1. Negative lags indicate that the first series leads the second series.

Symbol	Value	Parameter
ρ_i	910 kg m^{-3}	Density of ice
ρ_w	1000 kg m^{-3}	Density of water
n	3	Glen's flow law exponent
N	$\rho_i g h_i - \rho_w g h_w$	Effective pressure
A	$5.3e^{-24}$	Glen's flow law coefficient
L	$3.35e^{5}$ J kg^{-1}	Latent heat of fusion
f	0.18	Friction factor
Ψ	Pa m^{-1}	Hydraulic gradient
S	m^2	Conduit cross-sectional area
S_m	m^2	Moulin cross-sectional area
z	m	Bed elevation
u_b	m a^{-1}	Ice sliding velocity
h_b	m	Bedrock bump height
c_1	$1/\rho_i L$	Melting parameter
c_2	An^{-n}	Closing parameter
c_3	$(\pi + 2)\rho_w f / 2^{5/2} \pi^{1/2}$	

Table 3.3. Parameters used in conduit-geometry calculations.

Chapter 4. Modeled and observed seasonal evolution of drainage efficiency in the Paakitsoq Region of western Greenland

4.1. ABSTRACT

The configuration and seasonal evolution of the subglacial hydrologic system beneath the ablation zone of the Greenland Ice Sheet modulates seasonal perturbations in its velocity, as forced by surface melting. Both channelized (efficient drainage) and distributed (inefficient drainage and storage) components have been identified, but recent observations suggest that their roles in the seasonal evolution of the subglacial hydrologic system evolution are not yet fully understood. Here we explore the seasonal evolution of this system using a model of subglacial drainage. We force this model using realistic estimates of surface melting during the 2011 and 2012 summer melt seasons for the Paakitsoq Region of western Greenland, where we have contemporaneous observations of moulin hydraulic head and GPS-derived ice surface velocities. This model successfully predicts melt-induced ice acceleration and multi-day to multi-week trends in moulin head during the latter half of both melt seasons, but not the observed complexity of the seasonal onset of ice acceleration and the transition to efficient drainage. Hence, while the model suggests a gradual transition between inefficient and efficient drainage, observations of GPS-derived ice velocity indicate that this transition occurs both more rapidly and uniformly than modeled. We conclude that careful consideration of subglacial conditions is needed to accurately reproduce seasonal evolution of the subglacial hydrologic system in ice-sheet ablation zones.

4.2. INTRODUCTION

The Greenland Ice Sheet (GrIS) is losing mass at an accelerating rate [e.g., *Vaughan et al*., 2013; *Velicogna et al*., 2014]. Dynamic mass loss of the GrIS due to increased ice motion and outlet glacier calving accounts for approximately half of the

annual mass loss, with surface mass loss accounting for the remainder [*Csatho et al*., 2014]. Though dynamic thinning is concentrated at marine-terminating outlet glaciers [*van den Broeke et al*., 2009; *Csatho et al*., 2014], the ice flow of land-terminating regions undergoes an annual dynamic response due to changes in surface meltwater supply [e.g., *Zwally et al*., 2002; *van de Wal et al*., 2008; *Hoffman et al*., 2011]. This ice acceleration occurs as surface meltwater is routed through the supraglacial hydrologic system and to the bed of the ice sheet via crevasses and moulins, which can form in regions of extensional strain [*Catania et al*., 2008] and through hydrofracture associated with supraglacial lake drainage [*Das et al*., 2008; *Stevens et al*., 2015]. The introduction of meltwater to the ice–bed interface acts to decrease basal friction, thereby increasing basal sliding [e.g., *Iken and Bindschadler*, 1986]. However, observations indicate that over the course of the melt season, variability in the supply of supraglacial meltwater encourages the development of a drainage network that can readily accommodate available meltwater [*Schoof*, 2010; *Bartholomew et al*., 2012]. This evolution results in a decline in ice velocity that can mitigate early season ice acceleration [*Sole et al*., 2013; *Tedstone et al*., 2013] and results in a non-linear relationship between ice motion and surface melting.

Predictive models that parameterize the impact of increased basal lubrication on ice dynamics suggest that this process exerts in a negligible impact on long-term GrIS mass loss [*Shannon et al*., 2013; *Fürst et al*., 2015]. However, the validity of simple parameterizations of this feedback is not yet well established. Recent studies have placed limits on subglacial drainage evolution due to low ice surface slopes and high subglacial pressures [*Meierbachtol et al*., 2013; *Dow et al*., 2014], established the importance of flow coupling in controlling ice motion [*Price et al*., 2008; *Doyle et al*., 2014] and demonstrated that the state and evolution of the subglacial hydrologic system can

influence local variability in outlet glacier response to regional forcings [*Moon et al*., 2014].

The relationship between melt supply and ice velocity evolves over the course of the melt season [e.g., *Bartholomew et al*., 2010]. During the winter, the lack of meltwater from surface melting results in a quiescent period for the subglacial hydrologic system. The onset of surface melting between May and June, and its rapid delivery to the ice-bed interface initially overwhelms the subglacial system. The inability of the winter subglacial system to efficiently conduct this meltwater to glacier termini results in increasing subglacial water pressure and storage, which allows for increased ice motion [e.g., *Bartholomew et al.*, 2010; *Hoffman et al.*, 2011; *Cowton et al.*, 2013]. Subglacial flow of this meltwater allows for the formation of efficient subglacial pathways (subglacial channels) when melt (driven by the dissipation of turbulent energy) exceeds creep closure. It is widely assumed that, once subglacial channels can readily accommodate the available meltwater, subglacial storage of meltwater and ice velocities decline [*Bartholomew et al.*, 2010; *Hoffman et al.*, 2011; *Sundal et al.*, 2011].

This non-linear relationship between meltwater input and ice velocity is further complicated by spatiotemporal variations in melt supply and delivery. The seasonal evolution of the subglacial system is interrupted by a series of short lived increases in melt supply, including diurnal and anomalously warm periods [*Shepherd et al.*, 2009; *Hoffman et al.*, 2011; *Andrews et al.*, 2014], as well as supraglacial lake drainages [*Das et al.*, 2008; *Morriss et al.*, 2013]. The duration and magnitude of the ice velocity response to these regional and local increases in melt supply depends on the current state of the subglacial hydrologic system [*Anderson et al.*, 2004; *Bartholomew et al.*, 2010; *Hoffman et al.*, 2011]. Significant spatial heterogeneity in ice velocity is caused by the pattern of

supraglacial melt flow and englacial features [*Palmer et al.*, 2011] as well basal [*Joughin et al.*, 2013] and ice surface topography [*Meierbachtol et al.*, 2013].

Despite extensive study of the subglacial hydrologic system, questions remain regarding its spatiotemporal evolution in response to increasing melt intensity [*van Angelen et al.*, 2013] and melt extent [*McGrath et al.*, 2013; *van de Wal et al.*, 2015] giving ongoing anthropogenic climate change. In particular, the extent to which channelization drives the seasonal pattern of ice velocities is in question. Further, modeling suggests that drainage efficiency can increase within the distributed system without requiring extensive channelization [*Hoffman and Price*, 2014]. Together, these results suggest that evolving drainage efficiency outside of the channelized system may be the primary driver of seasonal patterns in ice velocity [*Andrews et al.*, 2014].

Numerous studies have modeled the subglacial hydrologic system in the ablation region of the GrIS, with the primary aim of understanding seasonal and multi-year trends in subglacial evolution and subglacial water storage with comparisons to proglacial discharge [*Banwell et al*., 2013] or multiday mean ice [*Colgan et al*., 2012; *Hewitt*, 2013]. Most models focus on channelization [e.g., *Bartholomew et al.*, 2012; *Meierbachtol et al.*, 2013; *Dow et al.*, 2014], although recent work has included significantly improved representation of subglacial drainage outside of the channelized area [*Hewitt*, 2013; *Werder et al.*, 2013]. In all cases, model comparison to measured ice velocity and subglacial pressure is limited, due to the scarcity of coincident observational data such as borehole [e.g., *Lüthi et al.*, 2002; *Meierbachtol et al.*, 2013; *Ryser et al.*, 2014a, 2014b] and moulin measurements [*Cowton et al.*, 2013; *Andrews et al.*, 2014].

Here we develop a one-dimensional (1D) model of channelization and subglacial water storage to explore the subglacial processes that are necessary to better match the pattern of GPS-derived ice velocities and observed moulin water pressures during the 2011

and 2012 melt seasons. This model is forced by realistic time series of supraglacial melt input and its moulin distribution is based on observations within the Paakitsoq Region of western Greenland. This model is simple, in that it does not constrain evolution outside of the channelized system, but it permits straightforward investigation of the hypothesis that the evolution of subglacial channels is the main driver of the seasonal deceleration of the ice sheet as summer melting progresses.

4.3. Data and Methods

Our model is configured to simulate the subglacial water-pressure response to seasonal surface melting during the 2011 and 2012 summer melt seasons. It is forced using approximations for melt input calibrated from on-ice weather stations (section 4.3.1.2) and results are compared to GPS-derived ice velocities (section 4.3.1.4) and water levels in two moulins (section 4.3.1.4). The model domain, supraglacial input locations and subglacial water routing are constrained by subglacial and supraglacial topography (section 4.3.1.1).

4.3.1. Remote-Sensing and Field Observations

Our study area encompasses a ~1300 km^2 region of Sermeq Avannarleq in the Paakitsoq Region of western Greenland (Figure 4.1A). This study area exhibits annual ice velocities of ~100 m a^{-1} and is located north of Jakobshavn Isbræ, but is largely out of its direct dynamic influence. The local equilibrium line elevation (ELA), at ~1,600 m, has migrated inland over the past two decades [*Mernild et al*., 2010; *McGrath et al*., 2013]. Seasonal supraglacial melting is substantial (~6 m a^{-1}) within the drainage basin [*Ryser et al*., 2014b] and supraglacial lake drainage occurs irregularly [*Morriss et al*., 2013].

4.3.1.1. Drainage Basin Delineation

We delineate subglacial drainage using the subglacial hydrologic potential, ϕ [*Shreve*, 1972]:

$$\phi = k\rho_i g(h - z) + \rho_w g z \,, \tag{4.1}$$

where ϕ is the sum of the pressure and elevation potentials, g is the acceleration due to gravity, ρ_i and ρ_w, the densities of ice and fresh water, respectively, k is the fraction of overburden and h and z are surface and bed elevations, respectively. Bed elevations in this region are adequately determined by a mass-conservation algorithm, which combines radar-measured ice thickness with satellite-derived ice flow velocities to determine an ice thickness that is physically consistent with both observations [*Morlighem et al.*, 2011, 2014]. Surface elevations come from a high resolution (10-m) surface digital elevation model (DEM) constructed from WorldView-2 (WV-2) imagery [*Noh and Howat*, 2015] that is resampled to the bed DEM resolution (150 m) using bilinear interpolation.

The fraction of flotation, k, is the ratio of water pressure to the ice-overburden pressure. This ratio is known to be spatiotemporally variable [*Cowton et al.*, 2013; *Meierbachtol et al.*, 2013; *Andrews et al.*, 2014; *Ryser et al.*, 2014b, 2014b]. However, subglacial drainage pathways initiate at the beginning of the melt season, when water pressures are high, so we use $k = 0.91$ to determine ϕ.

We determine subglacial flow pathways using gradients in ϕ and observed moulin locations identified in WV-2 imagery [*Andrews and Catania*, in prep.]. Flow pathways are determined using the number of cells 'draining' into a downstream cell [*Jenson and Domingue*, 1988]. Because a large fraction of, if not all, supraglacial water drains via moulins [*Smith et al.*, 2015], we modify this algorithm by assigning cells with moulins a higher cell value, scaled to the average discharge of the moulin's drainage basin. Non-moulin cells are assigned a uniform discharge of 20 mm a^{-1} based on modeled

regional basal melt rates [*Aschwanden et al*., 2012]. This approach results in the subglacial flow pathways and drainage basin shown in Figure 4.1. Our defined drainage basin differs from previous modeling efforts due to differences in the resolution of the surface and bed topography and significant changes in surface topography due to melting [*Banwell et al*., 2013; *Mayaud et al*., 2014] resulting in the study area switching from land to ocean terminating. Our chosen basin also differs from the model space used by *Colgan et al*. [2011b, 2012], who delineate the model space using the ice flowline derived from the steepest ice surface slope originating from the terminus of Sermeq Avannarleq.

For surface melting to be relevant to our model, it must be directed into a nearby moulin. We employ a routing algorithm (similar to that described for subglacial hydrology) based on surface topography and moulin locations. Moulin locations are manually identified in 2011 WV-2 imagery with a resolution of ~50 cm and supraglacial drainage basins are delineated following *Andrews and Catania* [in prep.], using the WV-2 surface DEM [*Noh and Howat*, 2015].

4.3.1.2. Supraglacial Drainage

Estimates of the spatiotemporal variability in surface melt supply are necessary to provide a realistic supraglacial forcing. Daily degree-index, or degree-day, models are well correlated with surface melting on the GrIS [*Braithwaite and Olesen*, 1989; *Braithwaite*, 1995], allowing for their widespread use in predicting surface melting [e.g., *Bartholomew et al*., 2011; *Hoffman et al*., 2011; *Clason et al*., 2015]. However, modeling diurnal changes in the subglacial system requires sub-daily estimates of supraglacial discharge. Therefore, we use a modified degree-index model [*Pellicciotti et al*., 2005] to calculate surface melt for each surface raster cell at sub-daily time intervals and then sum this melt over the supraglacial drainage basin for any particular moulin. Because these

sub-daily estimates of melt benefit from the incorporation of additional parameters, including surface albedo and incoming shortwave radiation and have only been calibrated on alpine glaciers [*Hock*, 2003; *Pellicciotti et al*., 2005], we utilize observations of surface ablation and energy balance modeling at three locations within the study area to calibrate the modified degree index model.

Between May 2011 and September 2011, weather conditions (air temperature and pressure, humidity, precipitation, wind speed and direction) were monitored using Vaisala WTX520 weather stations at FOXX, GULL and HARE. These data are augmented with data from full weather stations in our region, one each at FOXX and GULL installed in July 2011 and one at JAR-2 (Figure 4.1A) [*Steffen et al*., 1996]. These weather stations provide measurements of incoming and reflected shortwave and long-wave radiation, surface ablation and temperature data that allow us to develop a full energy balance model at FOXX, GULL and JAR-2. Because sub-daily measurements of ablation are noisy and often within the measurement error of the instrumentation, we fit the energy balance model to the long-term observations of surface ablation and then compare hourly energy balance derived surface ablation to surface ablation estimated using a modified degree-index model. Following *Pellicciotti et al*. [2005], we calculate hourly surface melt rate S_m as:

$$S_m = \begin{cases} B_T T + B_{SW}(1-\alpha)SW, & T > T_m \\ 0, & T \leq T_m \end{cases}, \tag{4.1}$$

where T is air temperature, T_m is the freezing temperature, α is surface albedo, SW is incoming solar radiation and B_T and B_{SW} are empirical coefficients for the melt sensitivity to T and SW, respectively. We use hourly energy balance calculations of surface ablation at FOXX, GULL and JAR-2 to calibrate these empirical coefficients, using a nonlinear regression analysis to find the best-fit values for B_T and B_{SW}, 0.3353

and 0.0073, respectively because These coefficient values result in a goodness-of-fit of $r^2 = 0.71$, $p < 0.01$, for combined hourly energy balance at FOXX, GULL and JAR-2.

In order to expand these estimates to the entire study area, we calculate the hourly lapse rate between FOXX and HARE in 2011 and JAR-2 and GULL in 2012; the different spatial intervals arises from availability of data in each year. The incoming solar radiation is similar at JAR-2, FOXX and GULL; therefore, we apply a spatially uniform incoming shortwave radiation forcing for the entire study area. Surface albedo is constrained using the daily Moderate-Resolution Imaging Spectroradiometer (MODIS) MOD10A1 surface-albedo product, which has a resolution of 500 m [*Hall et al*., 2006] and is resampled to 150 m using bilinear interpolation. With suitable processing, MOD10A1 provides reasonable surface albedo estimates for our study area [*Stroeve et al*., 2006]. Where data is unavailable due to cloud cover or satellite angle, we interpolate surface albedo between previous and future time steps with the assumption that surface albedo will change linearly over short time windows.

Surface routing of supraglacial water impacts the timing of meltwater delivery to the subglacial hydrologic system in a number of ways, including storage and flow retardation within the remnant snow during melt onset, along with the routing across the ice surface, which can change substantially over the course of a melt season [*Jansson et al*., 2003]. Although it is possible to use a linear reservoir model to route surface flow [*Banwell et al*., 2012; *Liston and Mernild*, 2012], necessary ice-surface characteristics, such as snow density and ice surface roughness are poorly constrained.

Field observations indicate that snow cover in our field area was limited below ~700 m, likely due to wind removal, a pattern that is similar to observations of other low-elevation areas of the GrIS ablation zone [*van den Broeke et al*., 2008, 2010]. Above this elevation, snow depths ranged from patchy to ~1.1 m in both years. In 2012, the weather

station at GULL, which had ~1.0 m of snow cover, records ice surface ablation began on day 154. Therefore, we expect snow to influence supraglacial discharge at high-elevation areas during the beginning of the melt season only. As a result, we assume that supraglacial discharge corresponds directly to the sum of surface melt within a drainage basin and our prescribed supraglacial discharge curves may not accurately reflect the true curves during the onset of melting. Additionally, within the FOXX supraglacial basin, we observe a lag of 3 hours between peak melt intensity (observed by air temperature) and peak meltwater delivery to the bed (observed by supraglacial discharge). For simplicity, we forgo any physically based parameterization of lag times and instead apply a 3-h low-pass filter to reduce high-frequency noise in our modeled supraglacial melt input.

4.3.1.3. Moulin Hydraulic Head

During 2011 and 2012, water levels in three moulins were monitored during the latter part of the melt season, two of which are presented here (FOXX, Moulin 3; Figure 4.1A) [*Andrews et al*., 2014]. During 2011, the pressure sensor installed at a moulin near the FOXX GPS station was too shallow; therefore, moulin water levels were only recorded during part of the day. In 2012, we were able to capture the entire record over ~50 days. Using GPS-recorded ice surface elevation and a record of the length of cable deployed from the surface, we convert measured water levels to hydraulic heads. See *Andrews et al*. [2014] for further details.

4.3.1.4. Ice Velocity

In 2011 and 2012, we deployed 11 on-ice GPS stations, roughly along the Sermeq Avannarleq flow line, with four stations placed off-axis to detect transverse-to-flow variations in ice velocity (Figure 4.1A). Eight of 11 GPS stations fall within the bounds

of the delineated drainage basin. We include an additional GPS station (HARE) from outside the drainage basin in our analysis due to its proximity and relation to the model domain (Figure 4.1B). With the exception of FOXX, GULL and HARE, GPS station names refer to the along-flow distance (note that this is different than the model domain) from the terminus and their north/south offset from the flowline. GPS antennas were attached to poles installed ~6 m below the ice surface and powered using 12-V batteries recharged by solar panels. GPS receivers logged positions continuously at 15-s intervals, with occasional data gaps associated with receiver power loss, which were more common in 2012.

Kinematic GPS positions were determined using carrier-phase differential processing relative to a bedrock-mounted reference station (QING) using Track 1.24 [*Chen*, 1998], following techniques in *Hoffman et al.* [2011] and *Andrews et al.* [2014]. Each 15-s time series of on-ice station position was smoothed with either a 6-h moving average to suppress spurious signals due to positional uncertainties while preserving diurnal signals or a 24-h moving average to examine seasonal trends. Each ice velocity record is then normalized against its spring (pre-melt) ice speed.

4.3.2. Subglacial Drainage Model

Subglacial drainage models are generally composed of elements representing efficient and inefficient water flow, with the capacity of these components dependent on available subglacial water and the effective water pressure in the subglacial system [*Fountain and Walder*, 1998]. The morphology and conductivity of the inefficient component of the subglacial hydrologic system varies, based on the nature of the ice–bed interface. It is most commonly modeled as cavities that form on the lee side of bed obstacles [e.g., *Schoof*, 2010; *Hewitt*, 2013; *Hoffman and Price*, 2014], but it is has also been characterized as till or a porous medium [e.g., *Bougamont et al*., 2005, 2014; *de*

Fleurian et al., 2014] and as sheet flow [e.g., *Flowers*, 2008; *Pimentel and Flowers*, 2011; *Dow et al*., 2015] All of these systems allow for the inefficient system to act as one that both stores and slowly transports water to the glacier terminus. The capacity of the inefficient system evolves due to imbalances in the physical processes that drive growth (including, but not limited to sliding over bed bumps, erosion of sediment, uplift due to over pressurization and ice melting) and collapse (including, but not limited to, viscous creep of ice and sediments, and sediment deposition) of its prescribed morphology. During much of the year, steady state basal melting is the primary source of available water in the inefficient system and this system exhibits a positive relation between pressure and discharge [*Kamb*, 1987; *Fountain and Walder*, 1998].

The model used here is composed of elements representing the englacial (moulins), channelized (efficient), and subglacial storage components of the subglacial hydrologic system. The storage component is formulated similarly to an inefficient system; however, water can only flow into and out of this component along the channel boundary. No flow is allowed between the storage components, although the capacity of the storage components can evolve individually based on a constant sliding opening and creep closure.

4.3.2.1. Channelized Drainage

We prescribe water flow in the efficient system to occur via ice-incised, semi-circular R-channels that, under steady-state conditions, exhibit an inverse relationship between subglacial pressure and discharge [*Röthlisberger*, 1972; *Nye*, 1976]. Following *Hewitt* [2011] and *Hoffman and Price* [2014], the mass balance within a channel is defined as:

$$\frac{\partial S}{\partial t} + \frac{\partial Q}{\partial x} = \frac{M}{\rho_w} + \gamma \Delta x \quad , \tag{4.3}$$

where S is the channel cross-sectional area, Q is the channel discharge and M is the channel melt rate, ρ_w is the density of water and x is the along channel direction (Table 4.1). The water flux from storage is γ, which is determined from the hydraulic gradient between the channel and storage and described below (equation 4.15).

The channel cross-sectional area is determined by

$$\frac{\partial S}{\partial t} = \frac{M}{\rho_i} - 2An^{-n}N^n S + u_b h_r \ , \tag{4.4}$$

following *Schoof* [2010] and *Hewitt* [2013], where the rate of channel enlargement, $\frac{\partial S}{\partial t}$ depends on melting due to the turbulent dissipation of energy, $\frac{M}{\rho_i}$, and creep closure of overlying ice, $2An^{-n}N^n S$. The final term, $u_b h_r$, is associated with opening due to sliding over bedrock aspersions and is only active when the subglacial channel radius is less than the height of bedrock aspersions. These terms are described in more detail below.

The channel melt rate is related to the turbulent discharge through the channel Q, the latent heat of fusion L and the hydraulic gradient within the channel $\frac{\partial \psi}{\partial x}$, such that:

$$M = \frac{Q}{L}\frac{\partial \psi}{\partial x} \ , \tag{4.5}$$

We parameterize Q using a Darcy-Weisbach law relating flow velocity in a semi-circular conduit to the hydraulic gradient [*Clarke*, 1996; *Schoof*, 2010]:

$$Q = c_c S^{5/4} \left| \frac{\partial \psi}{\partial x} \right|^{-1/2} \frac{\partial \psi}{\partial x} \ , \tag{4.6}$$

where $c_c = 2^{\frac{1}{4}}\sqrt{(\pi + 2)}/(\pi^{\frac{1}{4}}\sqrt{\rho_w f})$. Note that c_c depends on the relative roughness of the subglacial channel through the friction factor f. Subglacial conduit roughness is poorly constrained due to the difficulty of obtaining direct visual observations of the ice-bed interface; therefore, we set f = 0.2, within the range of values used for similar studies [*Gulley et al.*, 2014].

Creep closure depends on the ice flow law exponent, n, relating the deviatoric shear stress and strain rate, which is taken to be 3, and the rate factor, A, which depends on ice temperature and fabric [*Cuffey and Paterson*, 2010]. The value of A used here corresponds approximately to ice at the pressure melting point at FOXX (Table 4.1). While ice temperature varies both vertically and spatially in the ablation zone of the GrIS, the bed is consistently at the pressure melting [*Lüthi et al.*, 2015]. Creep closure also depends on the effective pressure N within the subglacial system, which is related to both the ice thickness H and subglacial water pressure:

$$N = \rho_i g H - \rho_w g h_m = \rho_w g z + \rho_i g H - \psi \quad , \tag{4.7}$$

where h_m is the height of the water column (the subscript m refers to 'moulin'). N can also be alternatively defined as the elevation potential (with z as the bed elevation) plus the potential of the ice minus the hydraulic potential ψ, which allows for the calculation of effective pressure without a prescribed water column height.

The final term in Equation 4.4 is sliding opening due to cavity growth, where u_b is the basal sliding speed (75 m a^{-1}, based on *Ryser et al.* [2014b]) and h_r is the average height of bedrock aspersions. This term allows for the spontaneous transition between siding-dominated and melt-dominated conduit growth [*Schoof*, 2010; *Hewitt*, 2013]. Most channel-only models neglect this term and instead prescribe an initial early-season channel geometry [e.g., *Bartholomew et al.*, 2012; *Chandler et al.*, 2013; *Meierbachtol et al.*, 2013; *Dow et al.*, 2014b]. The choice of the initial channel geometry impacts channel growth rates, particularly if there is an initial period of no melt input at high elevation locations. Here we allow sliding opening when the subglacial channel radius is smaller than the bedrock aspersion height (h_r = 0.2 m).

Returning to Equation 4.3, the change in subglacial discharge over a given channel length depends on the change in discharge capacity between two model nodes, as well as the supraglacial discharge added to the system through moulins. Thus,

$$\frac{\partial Q}{\partial x} \approx \frac{Q_i - Q_j + Q_{in}}{\Delta x} \ , \tag{4.8}$$

where the subscripts *i* and *j* represent consecutive nodes, with *j* representing the upstream discharge, and Q_{in} is the supraglacial discharge added to the system. Any change in Q results in a change in moulin water level, given by

$$\frac{\partial h_m}{\partial t} = \frac{Q_i - Q_j + Q_{in}}{S_m} \ , \tag{4.9}$$

where S_m is the cross-sectional area of the moulin and is prescribed to be 12 m^2. These equations are combined to solve for moulin water level and subglacial channel geometry numerically using a forward Euler time step. This time evolution requires time steps to remain small to prevent numerical instability.

4.3.2.2. Subglacial Storage

We characterize storage within the subglacial system as a macroporous sheet [e.g., *Flowers et al.*, 2004; *Hewitt*, 2011; *Pimentel and Flowers*, 2011; *Hoffman and Price*, 2014] with a prescribed hydraulic transmissivity between the storage and channelized components and a uniform water depth h_{st}. Over a sufficiently large area, h_{st} is representative of the volume of water within a number of inefficient drainage features, including subglacial till, cavities or sediment-incised canals [e.g., *Flowers and Clarke*, 2002; *Flowers et al.*, 2004; *Hewitt*, 2011; *Hoffman and Price*, 2014]. Within the distributed system, mass is conserved following:

$$\frac{\partial h_{st}}{\partial t} + \nabla \cdot \vec{q} = \frac{M_{st}}{\rho_w} - \gamma \ , \tag{4.10}$$

where q is the areal discharge of the sheet and M_{st} is the melt rate within the distributed system. Growth and collapse of the distributed system is caused by cavity opening due to ice motion over a rough bed and closure due to ice creep, so the evolution of the distributed system volume is represented following *Hewitt* [2013] as:

$$\frac{\partial h_{st}}{\partial t} = u_b\left(\frac{h_r - h_{st}}{l_r}\right) - 2An^{-n}N_{st}^{n}h_{st} \quad , \tag{4.11}$$

where h_r and l_r, represent the height and wavelength of the bed roughness, respectively, N_{st} is the effective pressure of the subglacial storage. The last term is creep closure.

The discharge between the sheet and channel is determined from a Darcy-style relation as

$$\vec{q} = \frac{kh_{st}^{3}}{\eta_w}\nabla\psi \quad , \tag{4.12}$$

where kh_{st}^{3} is the transmissivity of the distributed system and k is a transmissivity coefficient. Here, we set $k = 0.01$, which allows for relatively efficient exchange between the channelized and storage components of our model (Table 4.1). Because we are only modeling water movement into and out of the channelized system, there is no flow in the along-flow direction.

Following *Hewitt* [2013], melt within the distributed system is expressed as

$$M_{st} = \frac{1}{L}(G - u_b \cdot \tau_b) \quad , \tag{4.14}$$

where G is the geothermal heat flux (Table 4.1) and the product of basal sliding and shear stress, τ_b, produces frictional melting. We assume that τ_b and u_b are constant (Table 4.1). Fixing these two parameters greatly simplifies our calculations and eliminates the need to choose from a wide range of sliding laws, but it decouples the model from ice dynamics. However, we recognize that neither basal condition is truly steady nor uniform in our study area [*Ryser et al.*, 2014b].

The channelized and distributed systems are linked through movement of water into and out of the channelized system. Because the distributed system acts uniformly on either side of the channel, channel discharge is defined as

$$\gamma = 2\frac{kh_{st}^3}{\eta_w}\frac{\partial \psi}{\partial y} \quad . \tag{4.15}$$

4.3.2.3. Subglacial Overpressurization

Water pressures above overburden are commonly observed in boreholes in both Greenland and alpine glaciers [e.g., *Murray and Clarke*, 1995; *Meierbachtol et al*., 2013; *Andrews et al*., 2014; *Ryser et al*., 2014b] and suggests that supraglacial water is being supplied at a rate that cannot be accommodated by any component of the subglacial system. Within the subglacial hydrologic system, these periods of 'overpressurization' occur when the available water supply fluctuates significantly [e.g., *Murray and Clarke*, 1995] or during supraglacial lake drainages [e.g., *Das et al*., 2008; *Morriss et al*., 2013]. Although overpressurization is physically possible, our model does not directly consider this phenomenon. Instead, we treat overpressurization as an instantaneous addition to the distributed sheet thickness and ignore creep closure when negative effective pressures would result in unstable sheet growth. Recent work demonstrates that overpressurization can be more effectively treated as a free boundary problem [e.g., *Hewitt et al*., 2012; *Schoof et al*., 2012], but such an implementation is complex and still lacks the ability to treat other physical processes, such as hydraulic jacking [e.g., *Das et al*., 2008]. In such instances, ice–bed separation may be better treated using elastic beam theory [*Pimentel and Flowers*, 2011] or linear elastic fracture mechanics [*Tsai and Rice*, 2010]. Both our treatment and other more complex treatments of overpressurization are also limited by poorly constrained boundary conditions. For example, hydraulic jacking has the potential to allow significant water flow to unconnected regions of the bed [*Murray and Clarke*,

1995]. Therefore, during periods of overpressurization, the physics of our model are not necessarily correct.

4.4. Results and Analysis

4.4.1. Supraglacial Hydrology

Supraglacial discharge hydrographs for individual moulins, calculated from modeled supraglacial melt, are used to drive the subglacial models presented below. Based on our formulation, significant supraglacial melting begins on approximately day 156 in 2011 and day 148 in 2012 (Figure 4.2). The onset of melting in 2012 is both early and abrupt, especially at lower elevations. It was also regional and resulted in a large increase in melt duration [*Tedesco et al*., 2013a]. At most locations, peak temperatures correspond to peak melting. In both study years, nearly continuous surface melting occurs throughout the drainage basin until about day 240, after which surface melting is more sporadic.

4.4.2. GPS Observations

The onset of summer ice motion and the transition between multi-day ice acceleration and deceleration can provide insight into the ability of the subglacial system to accommodate surface meltwater [*van de Wal et al*., 2008; *Bartholomew et al*., 2010; *Hoffman et al*., 2011]. The initial pulse of water overwhelms the subglacial hydrologic system and initiates channel formation, while peak ice velocity signals the onset of ice deceleration associated with ability of the channelized system to readily accommodate available supraglacial meltwater [e.g., *Banwell et al*., 2013; *van de Wal et al*., 2015]. Therefore, we identify the onset of ice acceleration and deceleration in the GPS data using 24-h mean ice velocities (Figures 4.3 and 4.4).

Eight of 11 GPS stations fall within the bounds of the delineated drainage basin. We include an addition GPS station (HARE) from outside the drainage basin in our analysis due to its proximity and relation to the model domain (Figure 4.1). All GPS stations exhibit similar seasonal patterns of motion (Figures 4.3 and 4.4) [e.g., *Bartholomew et al*., 2010; *Hoffman et al*., 2011] that consist of an initial early-season acceleration trailing the onset of melting (days 159–166 in 2011; 149–152 in 2012) followed by peak ice velocity (days 166–188 in 2011; 170–173 in 2012) and then a gradual deceleration to below springtime values. The onset of sliding occurs 1–11 days after the onset of surface melting in the study area, with the shortest lags occurring closest to the terminus, falling within the range of previously reported values [*Zwally et al*., 2002; *Hoffman et al*., 2011]. Near the end of the melt season, diurnal minima in velocity generally fall below spring velocity values (Figures 4.5 and 4.6). The seasonal pattern is overlain by significant diurnal variability and additional distinct acceleration events most likely related to lake drainages. Following the cessation of diurnal variability the cessation of diurnal variability (~day 240) velocity remains low (Figures 4.5 and 4.6).

While similar ice-velocity observations have been noted by multiple authors [*Bartholomew et al*., 2010; *Hoffman et al*., 2011; *van de Wal et al*., 2015], there are clear spatial differences in ice motion, which likely depend on both the supply of supraglacial melt and SHS capacity. In both years, the downstream stations and one mid-elevation station (19N1, FOXX, 22N4, 25N1) all experience an abrupt onset of ice acceleration (130–240% of the spring background velocity) over the course of 1–5 days. This acceleration is more gradual at higher elevations until peak velocity is reached.

Peak ice velocity occurs 7–24 days after the onset of summer ice acceleration (Figures 4.3 and 4.4). In 2011, this transition occurs on day 160 at 19N1. Additional low elevation GPS stations and 28N4 experience peak velocity on day 182. The remaining

stations experience peak velocity between days 188–189. During 2012, the GPS records are sparse, but we still observed the onset of ice deceleration, at the available stations. Ice deceleration occurs at low elevation stations and 28N4 occurs on day 170, while mid- and high-elevation stations transition on day 173. These observed times are plotted in Figure 4.7, along with model results.

4.4.3. Model Results

Model outputs include moulin hydraulic head and subglacial channel geometry. Subglacial water pressure within the channelized system is also presented and referred to as either hydraulic head or fraction of overburden pressure (subglacial water pressure divided by ice overburden pressure) to ease regional comparisons. We discuss these results in three parts. First, we discuss the model results generally, focusing on the growth and collapse of the subglacial channel system. Although the model outputs are sub-daily, we examine daily mean values in order to examine the seasonal evolution. Next, we compare GPS-derived onset and termination of ice acceleration to modeled results to characterize the ability of our model to capture observed patterns in ice velocity. Finally, we compare observed and modeled moulin hydraulic head, focusing on late-season trends and diurnal variability.

4.4.3.1 Modeled Subglacial Characteristics

Both in 2011 and 2012, small pulses of melt result in elevated pressures before the onset of sustained melt (days 140–155; Figure 4.7A and days 140–148; Figure 4.7B). However, the sudden and sustained onset of elevated water pressures (i.e. high fraction of flotation) progresses rapidly upstream during the initiation of persistent summer melting (Figures 4.7A-D). Because these high water pressures result from the meltwater supply

exceeding the capacity of the existing system, this behavior is mirrored in the rapid increase in subglacial water storage and effective pressure.

Subsequent to the onset of melt, we model a rapid decline in the fraction of overburden that roughly corresponds to the development of large subglacial channels (Figures 4.7E and 4.7F), marking the transition from inefficient to efficient drainage. During 2011, this transition to lower pressures progresses upstream at ~0.75 km day^{-1}, while in 2012, it is slightly faster at ~0.84 km day^{-1}. The increase in this rate is not driven by an increase in the total melt, but rather by an increase in melt variability [*Schoof*, 2010; *Bartholomew et al*., 2012].

There is a reasonable correspondence between the transition to efficient drainage and the development of subglacial channels (Figures 4.7E and 4.7F). However, the decline in subglacial water pressure does not necessarily correspond to a particular channel size as drainage efficiency is related to the ability of the channel geometry to accommodate the available meltwater. We note that, across the model domain, drainage efficiency within the channelized system is attained after the channel expands beyond the height of the prescribed bedrock aspersions (Figures 4.7A and 4.7B). At high elevations, the period of time when sliding opening is active is substantially longer than near the terminus, suggesting that the development and presence of secondary drainage efficiency is important for subglacial water flow at higher elevations.

While the transition between inefficient and efficient subglacial drainage progresses relatively uniformly upstream over much of the model domain, there is discontinuity between km 30–37 in the model domain. There, channelization initiates earlier than downstream locations, resulting in a local reduction in subglacial pressure (Figure 4.7). This region has steep subglacial hydraulic gradients and relatively thin ice, as it is located on the lee side of a large bedrock high (Figure 4.1). Steeper hydraulic

gradients accelerate subglacial water flow, while thinner ice reduces the rate of creep closure within the subglacial channel. The combination of these two processes results in faster channel growth in this region. Faster channelization and increased drainage efficiency upstream results in a large supply of meltwater that cannot be readily accommodated by downstream channels, resulting in prolonged period of high subglacial pressures downstream (30 to 37 km; Figures 4.7A and 4.7B).

4.4.3.2 Comparison of Modeled Subglacial Characteristics and Observed Ice Velocity

We compare our model results to GPS observations by assuming that the onset of high fraction of flotation in the early season should correlate to the onset of ice acceleration (white circles; Figure 4.7). We find that GPS stations do not record the onset of ice acceleration until several days after the onset of sustained high pressures (Figures 4.7A and 4.7B). This effect is more pronounced in 2011 than 2012, likely due to differences in winter accumulation (2012 having greater accumulation and thus more remnant snow in the spring retarding overland flow of meltwater).

We also test the assumption that the transition to lower fraction of overburden should correlate with the onset of seasonal ice deceleration owing to the development and growth of subglacial channels [e.g., *Bartholomew et al*., 2010; *Sundal et al*., 2011; *Banwell et al*., 2013; *Cowton et al*., 2013]. We find no uniform relationship between the observed onset of ice deceleration and modeled subglacial channelization (magenta diamonds; Figure 4.7). Where subglacial hydraulic gradients are relatively high (km 30 to 37; Figure 4.1), the transition from inefficient to efficient drainage is reasonably represented, particularly in 2011. However, above and below this region, where subglacial hydraulic gradients are lower, GPS observations suggest a more rapid transition from inefficient to efficient drainage than we modeled (Figures 4.7A and 4.7B).

Both the observed onset of ice acceleration and the modeled subglacial pressures indicate that the onset of subglacial activity advances upstream rapidly. However, the observed onset of ice deceleration and modeled subglacial pressures are not as uniform. Between km 30–37, there is a reasonable match between the onset of GPS-derived deceleration and the onset of diurnal variability of channelized subglacial pressures, as well as the overall duration of time between early season and midseason changes. Regions above and below this location display a significant mismatch between observed and modeled characteristics. In those regions, the observed deceleration occurs earlier than suggested by modeled subglacial pressures by ~1–3 weeks. Because regional ice deceleration should indicate when subglacial channels can accommodate the available meltwater [e.g., *Bartholomew et al*., 2010], these disparities suggest that our model is not capturing an important physical phenomenon.

4.4.3.3. Modeled and Observed Moulin Hydraulic Head

Comparison of observed and modeled moulin heads can provide important information regarding modeled and observed efficiency within the subglacial system. Observed moulin hydraulic head displays large diurnal amplitude variations (Figures 4.8A and 4.8B) and is strongly correlated with ice velocity [*Andrews et al*., 2014]. However, the modeled amplitude of diurnal variability is substantially higher than observed, suggesting that the modeled system is more efficient than the natural system and is lacking additional storage within the englacial or subglacial systems. However, modeled 3-day trends in moulin hydraulic head reasonably match observed moulin hydraulic head in 2012 (Figure 4.8C).

4.5. DISCUSSION

4.5.1. Seasonal Evolution of the Subglacial Hydrologic System

4.5.1.1 Onset of Summer Ice Motion

The delay between the observed onset of surface melt and the onset of summer ice acceleration has been attributed to characteristics of the englacial and supraglacial hydrologic systems, including snow cover, ice surface roughness and the timing of hydrofracture associated with supraglacial lake drainage [*Banwell et al*., 2012; *Clason et al*., 2015; *Mernild et al*., 2015]. The observed onset of ice acceleration is better correlated with the modeled onset of high subglacial water pressure during 2012 than in 2011 (Figure 4.7). This inter-annual difference is likely due to differing ice-surface characteristics at the beginning of each melt season. A negative snowfall anomaly in the winter of 2011 and an early, large-scale melt event in 2012 resulted in the rapid removal of snow cover in 2012 as compared to 2011 and increasing supraglacial runoff [*Tedesco et al*., 2013a]. Combined, these processes reduce the lag time between modeled subglacial pressure and observed ice acceleration. Although the timing between observed ice acceleration and onset of elevated modeled pressures is improved in 2012, we note that the relative magnitude of the ice-velocity response is still dampened at higher elevations in both years (Figures 4.5 and 4.6). This pattern is likely due to unconsidered supraglacial meltwater retention and refreezing, which are stronger at higher elevations [*Clason et al*., 2015].

As with many models of the subglacial hydrologic system [e.g., *Meierbachtol et al*., 2013; *Werder et al*., 2013], we did not consider moulin development as a factor in delaying the introduction of water to the ice-sheet bed. It is generally assumed that supraglacial meltwater reaches the bed instantaneously via open moulins. Indeed, we find a reasonable match between the onset of ice acceleration and modeled subglacial pressure

in 2012 (Figure 4.7B), and moulins can be persistent features that can remain water-filled over winter [*Catania and Neumann*, 2010]. Our approach thus reasonably represents the reopening of moulins each year, instead of requiring this englacial connection to be formed through the drainage of supraglacial lakes [*Banwell et al*., 2013].

4.5.1.2 Transition to Efficient Subglacial Drainage

Although our GPS array did not cover the entirety of the model domain, our observations suggest that the ability of modeled subglacial pressures to represent the observed ice deceleration and inferred transition to efficient drainage is spatially variable (Figure 4.7). Our relatively simple conceptualization displays reasonable agreement between km 30–37 km of the model domain, in a region with relatively thin ice and steep surface and bed slopes (Figure 4.1). Outside of this region, modeled channelization and observed ice deceleration does not match as well, with observations suggesting a faster transition to an efficient subglacial drainage than modeled. Mismatched regions generally have low surface slopes and low or even inverse bed slopes, producing low subglacial hydraulic gradients and reductions in channel growth through melt (Equation 4.4) [e.g., *Clarke*, 1996]. Our observed mismatch between observation-inferred and modeled efficiency supports results suggesting that changes in subglacial drainage efficiency are not limited to channelized regions of the bed [*Meierbachtol et al*., 2013; *Andrews et al*., 2014; *Hoffman and Price*, 2014], with the added complication that these processes do not act uniformly in regions with variable bed topography.

We modeled channelization with a storage component whose capacity depends on a constant rate of basal motion and creep closure. While evolving water storage influences ice velocity [*Bartholomaus et al*., 2008], the capacity of the storage system is also important, as regional subglacial water pressures and basal traction are though to be the primary driver of ice motion [e.g., *Iken and Truffer*, 1997]. Increased basal motion

encourages the expansion of subglacial cavities, resulting in a reduction in regional subglacial pressure which can act to truncate periods of rapid ice motion [*Iken and Truffer*, 1997; *Bartholomaus et al*., 2011]. This negative feedback can result in the decay of ice acceleration even in the absence of a subglacial channel [*Hoffman and Price*, 2014]. Thus, not including this mechanism in our model may explain the discrepancies we observe in regions of low subglacial hydraulic potential.

Observations suggest that, within the ablation zone of the GrIS, changes in subglacial drainage efficiency propagate gradually upstream as melt supply increases and then gradually recede as the melt season terminates [*Cowton et al*., 2012; *Chandler et al*., 2013]. However, those observations focused on regions of the ice sheet where the bed is relatively flat and the ice-surface profile is uniform [e.g., *Meierbachtol et al*., 2013]. In our study area, and likely in many other regions of the ablation zone, the bed and surface topography undulate with typical horizontal length scales of ~5 km [*Ryser et al*., 2014a]. Because the development of efficient subglacial channels depends strongly on both the variability in meltwater supply and the local gradient in the subglacial hydrologic potential, undulating basal topography and variable ice thickness can result in non-uniform channel growth, as we infer here (Figures 4.7E-F).

Non-uniform channel development and storage may also influence the diurnal range of observed ice velocity, as this diurnal range is tied closely to moulin hydraulic head [*Andrews et al*., 2014]. We test this hypothesis by examining the ratio of diurnal range of ice velocity at 19N1 (downstream; km 25–30) and 25N1 (upstream; km 30–37) and the associated range of storage pressure and moulin hydraulic heads (Figure 4.9). In our study area, the downstream capacity of the channelized system is lower than that upstream, due to differences in channel melting associated with turbulent flow, leading to higher subglacial drainage efficiency upstream. A more efficient subglacial channel will

experience larger diurnal variability, which results in a shorter period of water retention [*Chandler et al*., 2013]. A stronger diurnal exchange of water between efficient and inefficient components should result in a larger diurnal range in basal traction [*Iken and Truffer*, 1997] and thus a stronger diurnal variability in ice velocity. Comparison of observed ice velocity and modeled storage pressure ranges and moulin hydraulic head demonstrates a general agreement, although a better representation of the inefficient system is needed to more fully explore this relationship. Relative differences in diurnal ice velocity and spatially heterogeneous subglacial pressures can result in complex patterns of ice motion that depend on both local and non-local controls [*Ryser et al*., 2014a]. This flow coupling may also be important in understanding the regional ice velocity response to supraglacial meltwater delivery to the bed [*Price et al*., 2008; *Hoffman et al*., 2011; *Doyle et al*., 2014].

4.5.2. Modeled and Observed Moulin Hydraulic Head

The diurnal amplitude of observed moulin hydraulic head, when compared to modeled moulin hydraulic head, can be used to infer characteristics of the englacial system not included in our model or other models. Overall, the reduced lag and larger diurnal range in our modeled system indicates that we may lack storage capacity (Figure 4.8B). Englacial storage volume is related to moulin geometry and evolution, as well as additional storage associated with microscopic or macroscopic void space connected either to moulins or the subglacial system [*Fountain and Walder*, 1998; *Bartholomaus et al*., 2011]. Microscopic englacial storage is likely limited by cold ice temperatures [*Gulley et al*., 2012; *Lüthi et al*., 2015], while macroscopic storage in likely to be in the form of basal crevasses [*Harper et al*., 2010] and/or moulin-connected surface crevasses and englacial fractures [*Fountain and Walder*, 1998]. Unfortunately, the volume and spatial extent of englacial water storage on the GrIS is unknown and partitioning

englacial water volume into void space and moulin geometry is difficult. Therefore, instead of attempting to match modeled and observed moulin head, we examine their differences.

Much like subglacial channels, moulin geometry is controlled by creep closure and melting due to the dissipation of turbulent energy; however, creep closure will be more variable due to vertical changes in ice and water pressure and depth-dependent ice rheology (mainly temperature). Further complications arise when considering the transfer of thermal energy associated with temperature differences between meltwater and the surrounding ice. Therefore, moulin geometry is generally represented as fixed in models of the subglacial system though its potential to impact on diurnal variability is noted [e.g., *Bartholomew et al*., 2012; *Hewitt*, 2013; *Meierbachtol et al*., 2013; *Werder et al*., 2013]. Nevertheless, by examining changes in the relationship between modeled and observed moulin hydraulic head, we can infer how moulin geometry, and hence water storage within moulins, can change over time.

Differences between modeled and observed moulin hydraulic head are particularly noticeable during and after changes in melt supply, when moulin geometry is most likely to experience significant changes (Figure 4.8B). During periods of low melt, modeled moulin hydraulic head experiences large drops in pressure unobserved in the natural system (i.e. days 204, 219, 226 and 239, Figure 4.8B). With a fixed and vertically constant moulin geometry, this pattern is expected; however, in the natural system we expect both active creep closure in the moulin and variations in moulin shape to dampen these pressure drops by reducing moulin volume. The opposite effect can be inferred during periods of increased melt. An increase in supraglacial melt supply will increase moulin volume as elevated hydraulic head counteracts creep closure and melts channel walls as water flows through the moulin. Continued growth during a period of high melt

can reestablish diurnal variability more rapidly than we modeled (e.g., days 227–234; Figure 4.8B) and will dampen diurnal variability following melt events when the englacial storage volume is large (e.g., days 207–212 and 234–240 in 2012; Figure 4.8B).

Limiting evolution within the glacial hydrologic system to only occurring within the subglacial channel does result in a reasonable long-term match between observed and modeled moulin hydraulic head (Figure 4.8C). However, discrepancies in observed and modeled hydraulic head during periods of variable supraglacial melt supply suggest that variability in moulin geometry can act to influence subglacial pressures. The relative impact of changing moulin geometry is likely to be more important in regions with higher moulin density as the relative volume within the englacial and subglacial systems change.

4.6. CONCLUSIONS

We develop a 1D model of the subglacial hydrologic system to explore the relationship between channelized subglacial water pressure and GPS-derived ice velocity. Using realistic supraglacial inputs, moulin locations and bed and surface geometry, we find that, while the model does evolve over the course of the melt season, its ability to reproduce the timing of GPS-inferred changes in efficiency depends on the local gradient in subglacial hydraulic potential. In regions of high bed and surface slope, modeled and inferred changes in efficiency are reasonably matched, while in regions of low subglacial hydraulic gradients, channelization alone cannot explain observed ice velocity. This result supports previous observations that, in regions of low subglacial hydraulic gradients, seasonal evolution of ice velocity is more strongly controlled by changes outside of the channelized subglacial system [*Meierbachtol et al*., 2013; *Andrews et al*., 2014]. This pattern may explain the spatial variability in observed diurnal ranges of ice velocity. Thus, non-uniform development of the subglacial hydrologic system influences how ice velocity responds to available supraglacial melt.

We also compared modeled and observed moulin hydraulic head. Model outputs reasonably capture the long-term trend in observed moulin hydraulic head. However, our inability to match diurnal variability suggests that the modeled system is too efficient. An evolving relationship between modeled and observed diurnal ranges indicates that evolution of moulin geometry in response to meltwater supply contributes to this discrepancy. This finding indicates that better constraints on englacial storage and its spatiotemporal variability are needed to fully assess the development of the subglacial hydrologic system.

4.7. Acknowledgements

This project was supported by United States National Science Foundation grants OPP-0908156 and OPP-0909454, Swiss National Science Foundation grant 200021_127197, and National Geographic Society grant 9067-12. L. C. Andrews was also supported by UTIG Ewing-Worzel and Gale White Graduate Student Fellowships. Logistical support was provided by CH2MHill Polar Services. The GPS base station and several on-ice GPS units were provided by the UNAVCO facility with support from the NSF and NASA under cooperative agreement EAR-0735156. We thank K. M. Schild, J. D. Nowinski and B. F. Morriss for assistance in the field.

4.8. Author Contributions

G. A. Catania, J. D. Gulley, M. P. Lüthi, R. L. Hawley and T. A. Neumann designed this study. L. C. Andrews, R. L. Hawley, M. J. Hoffman, M. P. Lüthi, C. Ryser and J.D. Gulley performed the fieldwork. L.C. Andrews processed the GPS data, implemented the supraglacial runoff calculations, developed the subglacial model and wrote the manuscript.

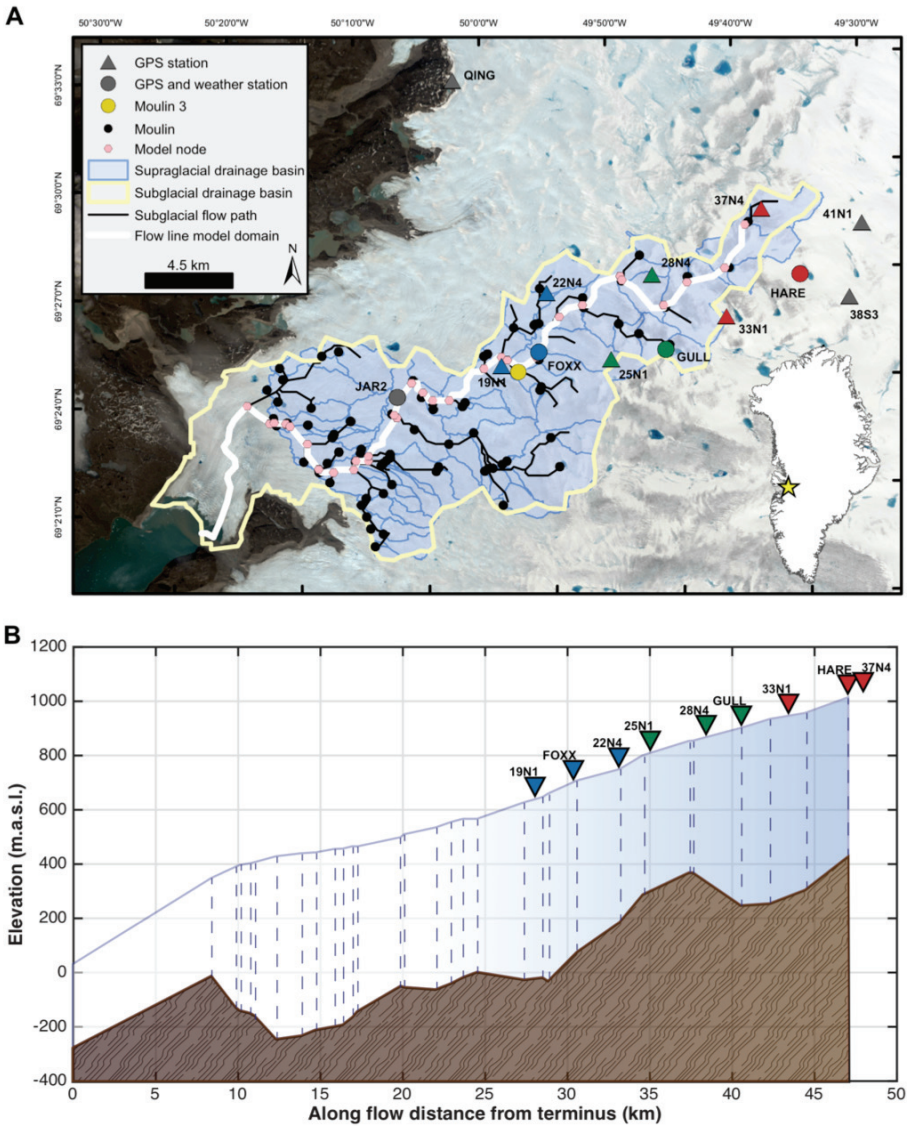

Figure 4.1. Study area in the Paakitsoq Region of western Greenland. A) Features are as indicated in the legend. GPS stations are colored according to their elevation grouping low (blue), mid (green), and high (red). Station names are indicated in black. B) Model domain. Vertical dashed lines correspond to locations of pink hexagons in A. GPS locations are labeled are colored according to their elevation grouping.

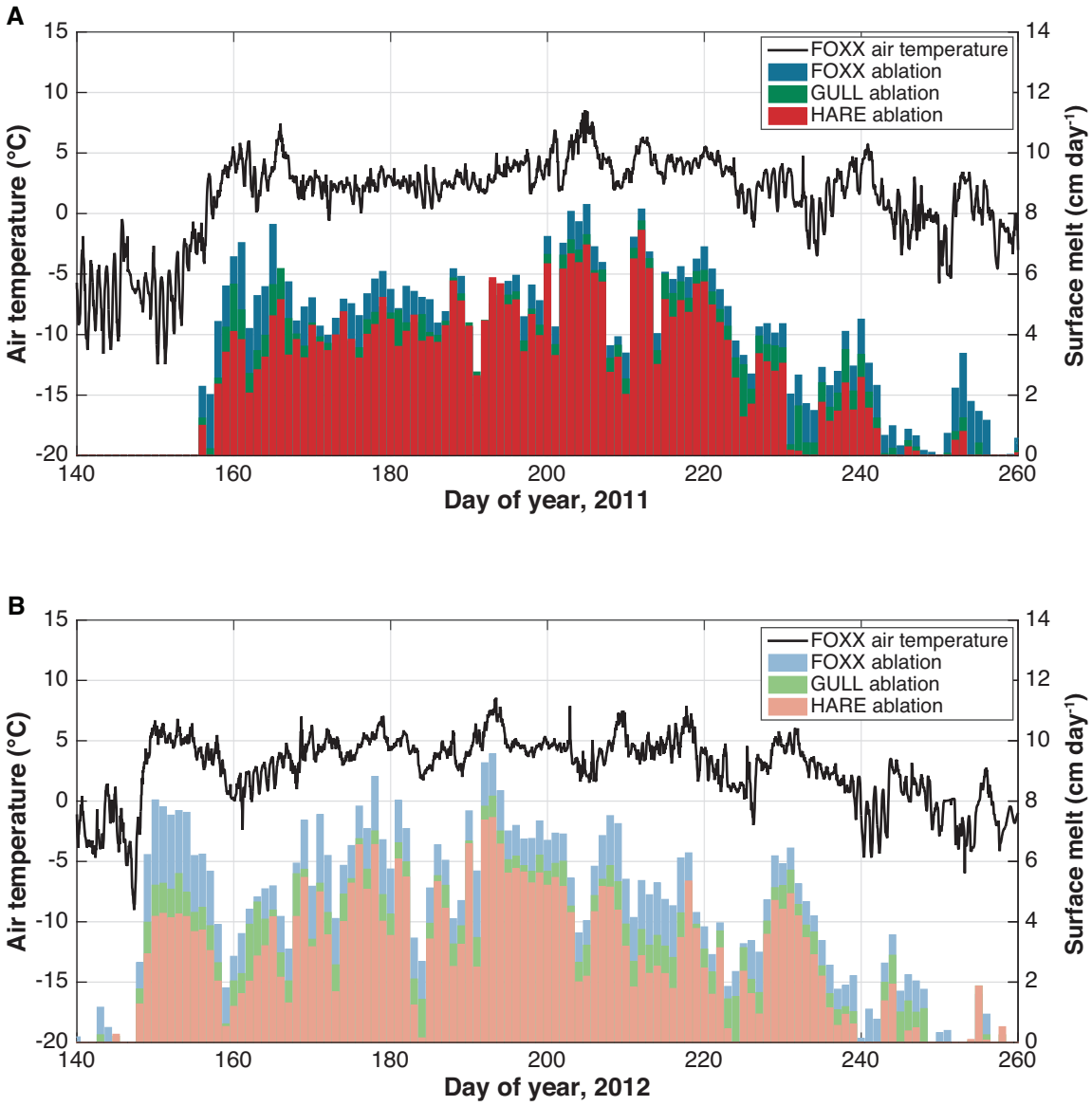

Figure 4.2. Modeled daily ablation for three locations in the study domain. A) Air temperature at FOXX (black) and modeled daily ablation (bars) at FOXX (blue), GULL (green) and HARE (red) for 2011. B) Air temperature at FOXX (black) and modeled daily ablation (bars) at FOXX (light blue), GULL (light green) and HARE (light red) for 2012.

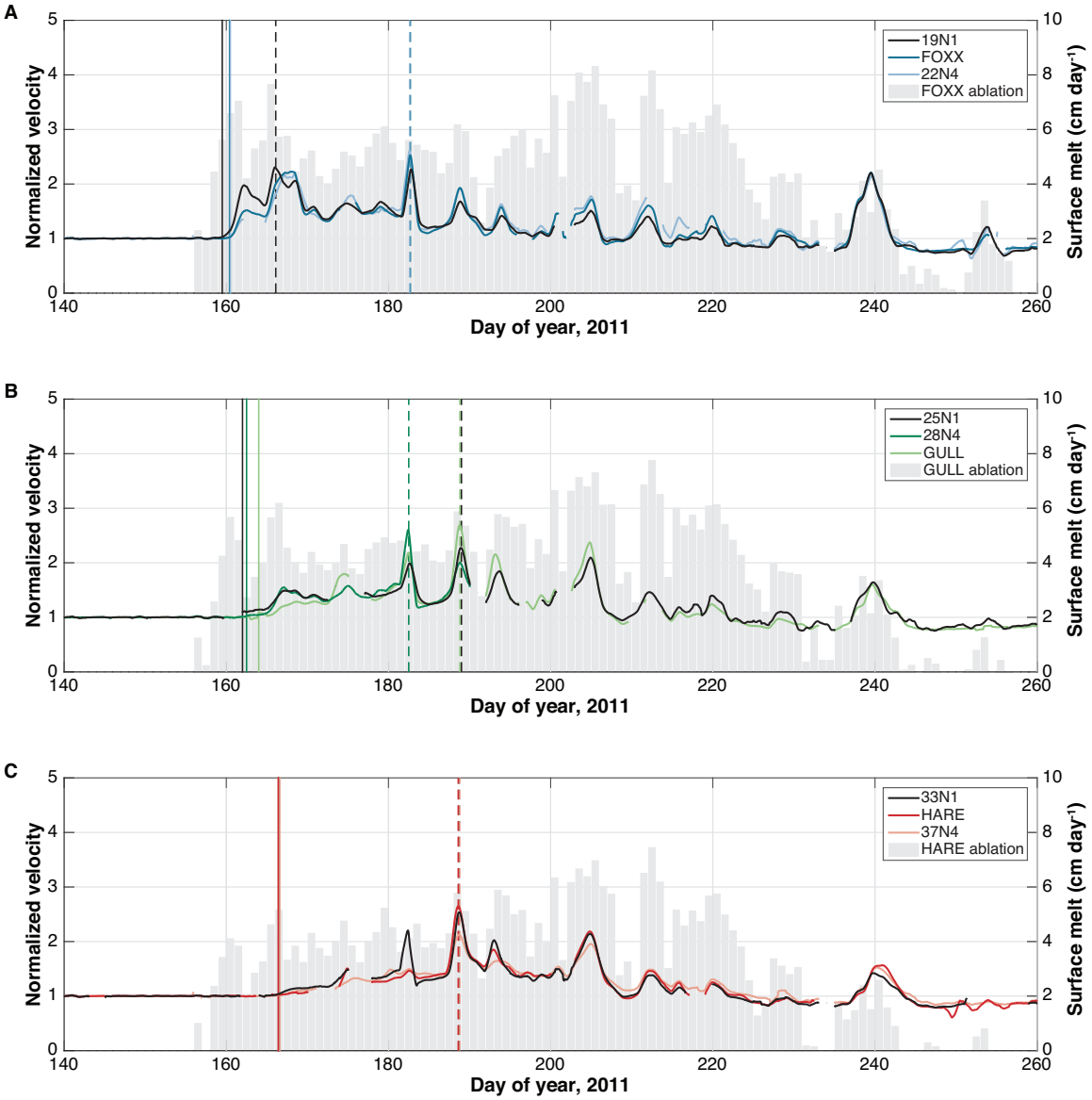

Figure 4.3. 24-h GPS-derived ice surface velocities and surface melt rates for 2011, normalized to background value. A) Low elevation stations: 19N1 (black), FOXX (blue), and 22N4 (light blue) and surface ablation at FOXX (grey bars). B) Mid-elevation stations: 25N1 (black), GULL (green), and 28N4 (light green) and surface ablation at GULL (grey bars). C) High elevation stations: 33N1 (black), HARE (red), and 37N4 (pink) and surface ablation at HARE (grey bars). The onset of summer ice motion and ice deceleration are marked with solid and dashed vertical lines, respectively.

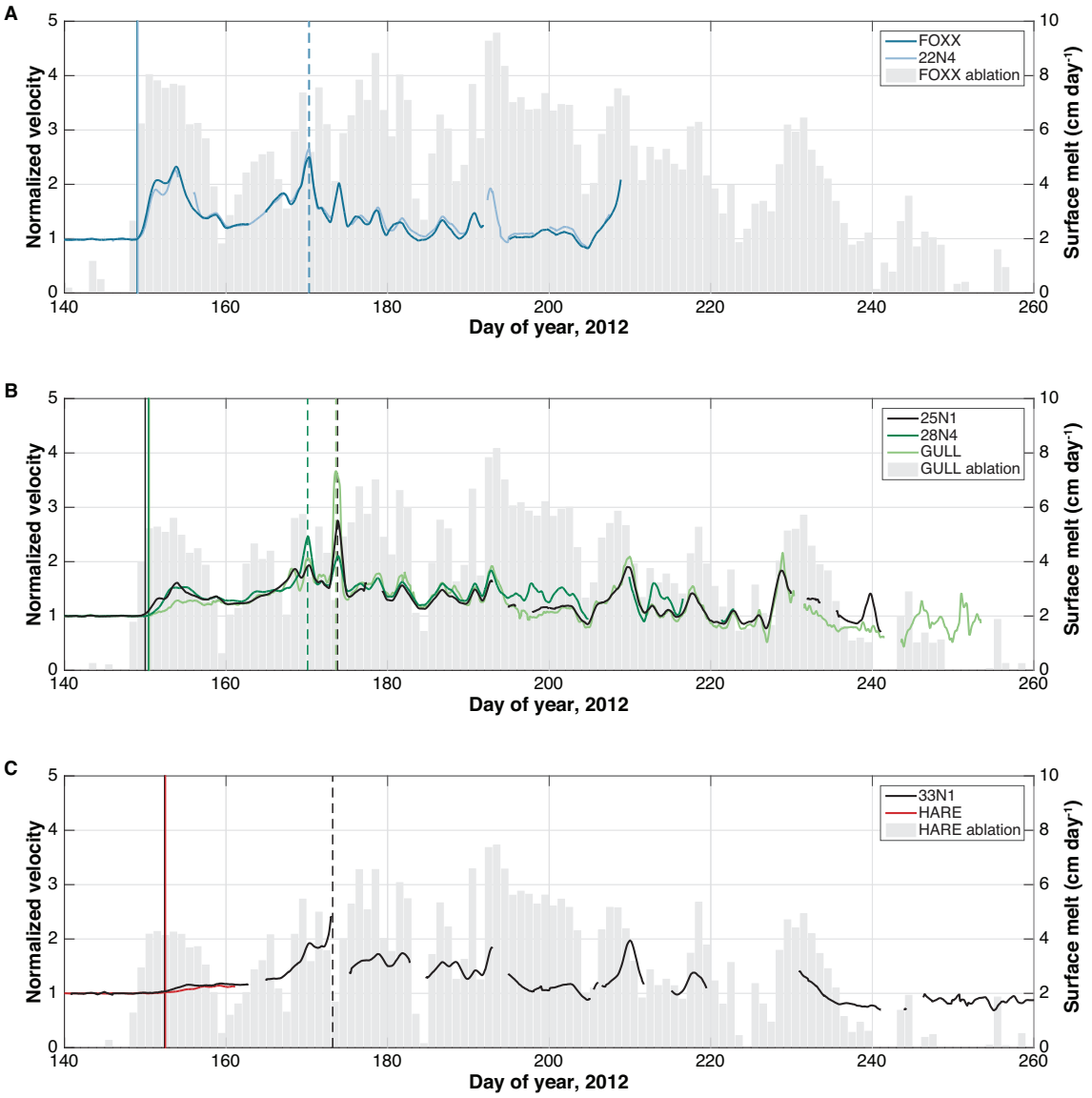

Figure 4.4. 24-h GPS-derived ice surface velocities and surface melt rates for 2012, normalized to background value. Same as Figure 4.3 but for 2012.

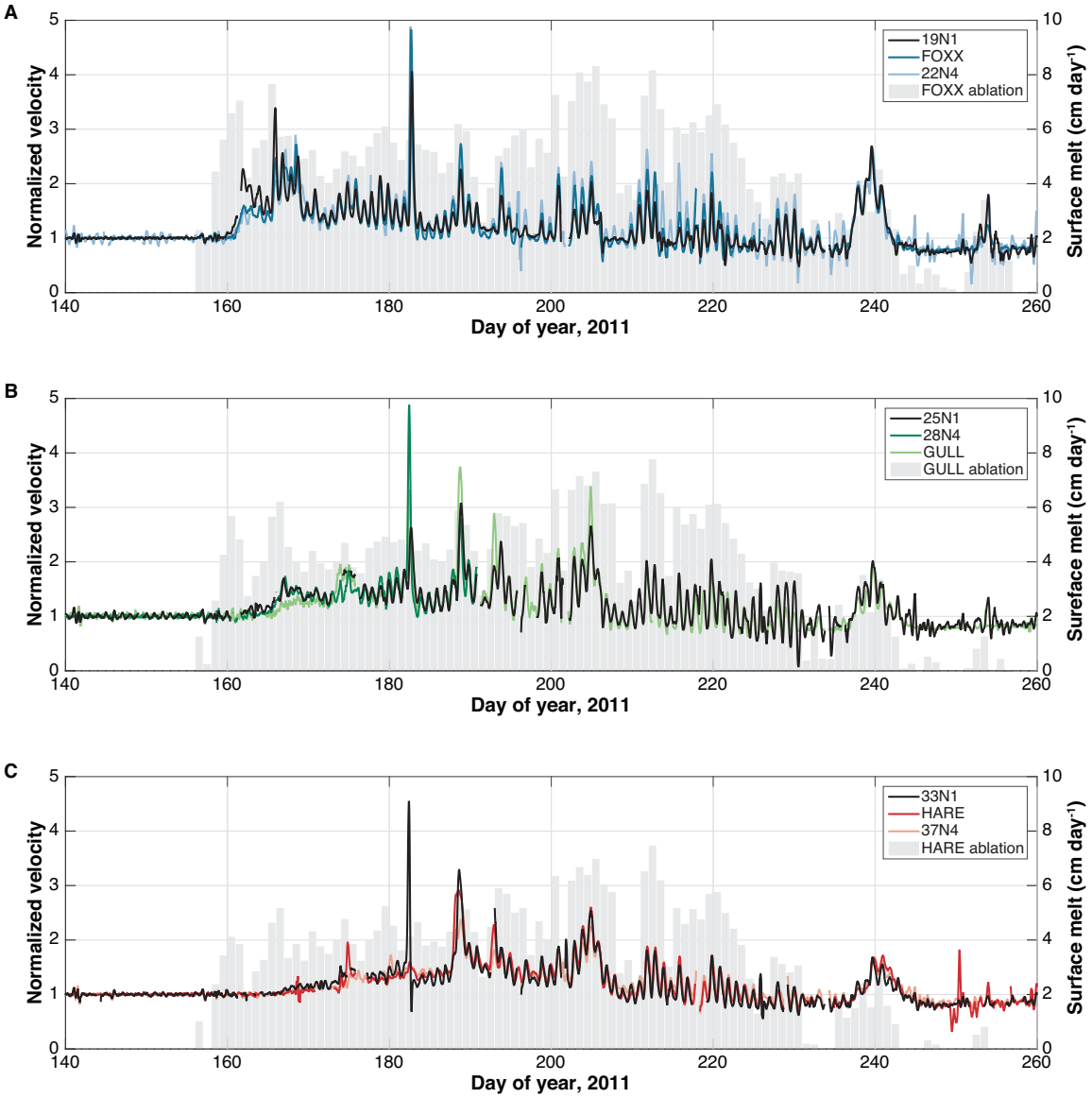

Figure 4.5. 6-h GPS-derived ice surface velocities and surface melt rates for 2011, normalized to background value. A) Low elevation stations: 19N1 (black), FOXX (blue), and 22N4 (light blue) and surface ablation at FOXX (grey bars). B) Mid-elevation stations: 25N1 (black), GULL (green), and 28N4 (light green) and surface ablation at GULL (grey bars). C) High elevation stations: 33N1 (black), HARE (red), and 37N4 (pink) and surface ablation at HARE (grey bars).

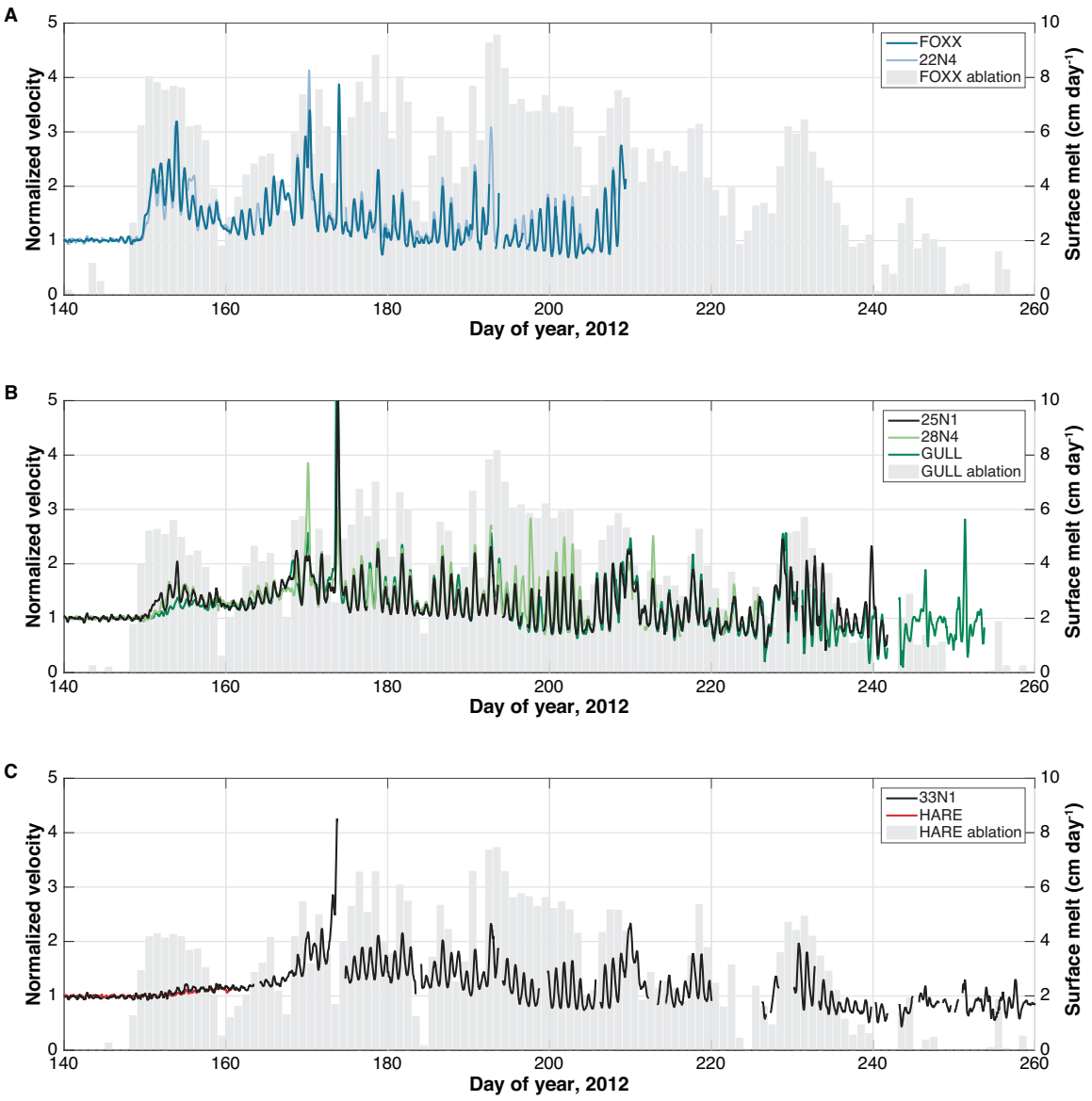

Figure 4.6. 6-h GPS-derived ice surface velocities and surface melt rates for 2012, normalized to background value. Same as Figure 4.5 but for 2012.

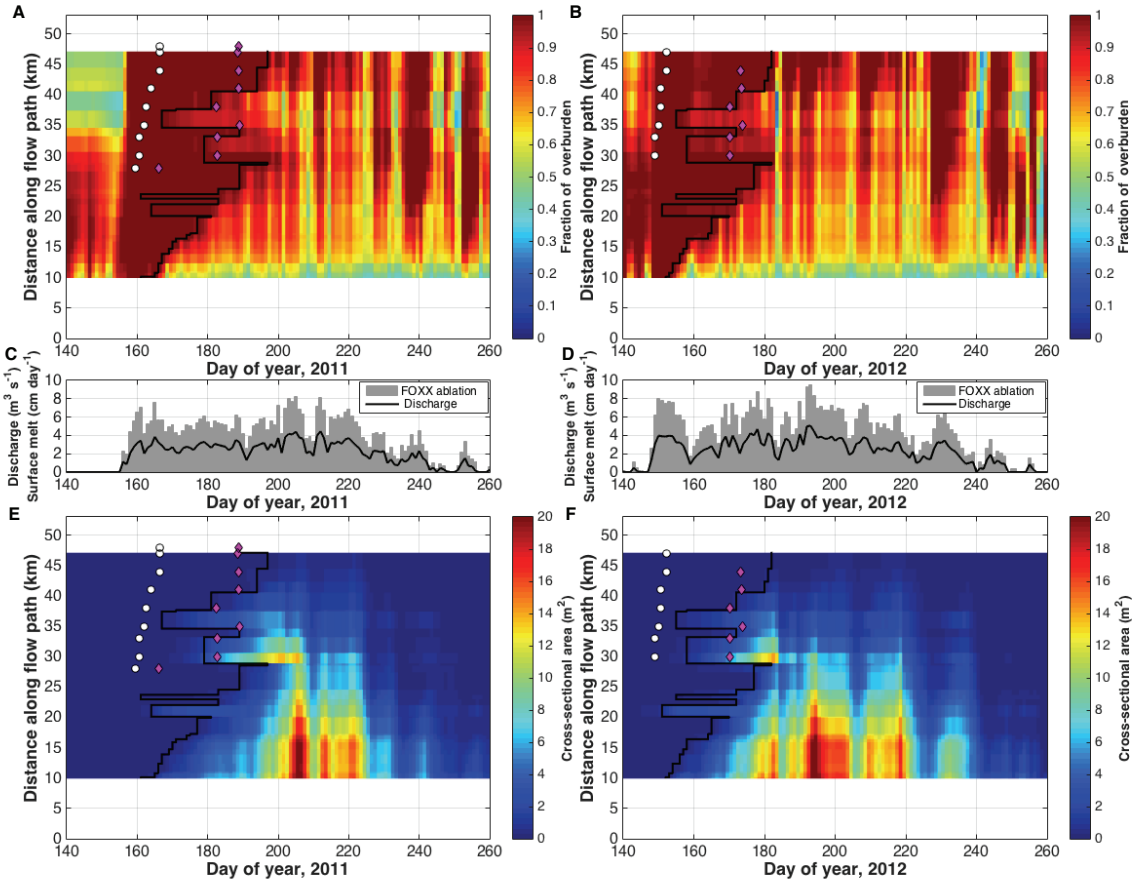

Figure 4.7. Modeled fraction of overburden and subglacial channel geometry for 2011 (left column) and 2012 (right column). Note that the modeled terminus is at 0 km for A, B, E, and D. A-B) Daily mean fraction of overburden (P_w/P_i). C-D) Supraglacial discharge into moulin 22.0 (each moulin in the model domain is identified by its distance in kilometers from the terminus) and daily melt at FOXX. E-F) Subglacial channel geometry for the model domain. The GPS-identified onset of summer acceleration (white circles) and deceleration (magenta diamonds) are marked in A, B, E and F. Fraction of overburden below one following the onset of significant melt is indicated with black line in A, B, E and F.

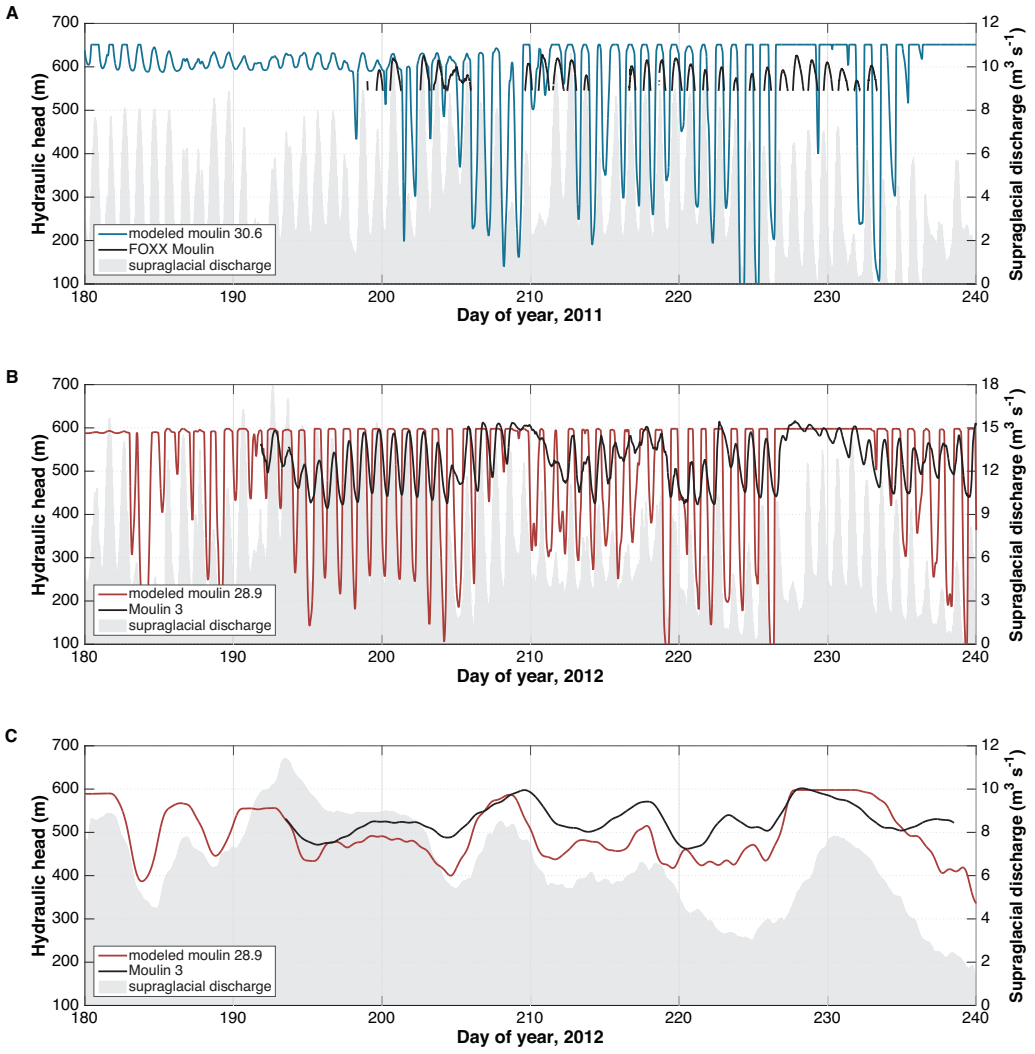

Figure 4.8. Observed and modeled moulin hydraulic head in 2011 and 2012. A-B) Observed moulin hydraulic head from *Andrews et al*. [2014] (black) and modeled moulin head from 2011 (blue) and 2012 (red). Supraglacial discharge into modeled moulins is marked with grey bars. C) 3-day moving average of 2012 modeled (red) and observed (black) moulin head and modeled supraglacial discharge (grey). Note that the depth uncertainty of the moulin pressure sensors is ± 20 m, and that Moulin 3 is approximately 1.25 km upstream of moulin 28.9 (Figure 4.1A).

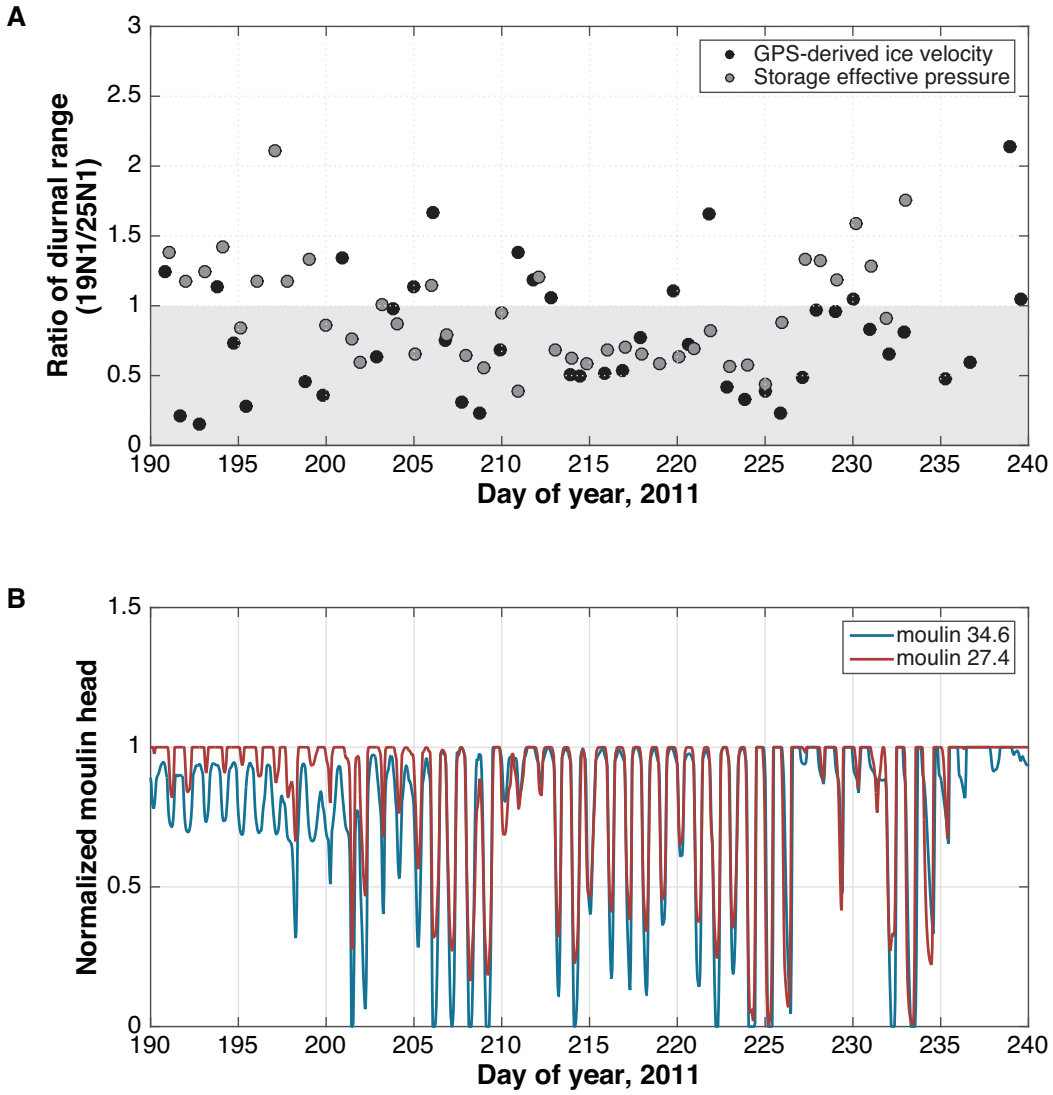

Figure 4.9. Non-uniform channel development and diurnal ice velocity. A) Ratios of the diurnal range of velocity and modeled effective pressure within the distributed system between GPS stations 19N1 and 25N1. Values less than one indicate that the diurnal range of 25N1 (upstream and on the lee side of a bed bump) is greater than that of 19N1 (upstream and in a bed overdeepening). B) Normalized moulin hydraulic head for upstream (blue) and (red) moulins in overdeepenings.

Symbol	Value	Parameter
	Physical Constants	
ρ_i	910 kg m^{-3}	Density of ice
ρ_w	1000 kg m^{-3}	Density of water
g	9.8 m^2 s^{-1}	Gravitational acceleration
L	3.35 * 10^5 J kg^{-1}	Latent heat of fusion
η_w	10^{-3} Pa s	Viscosity of water
	Model Parameters	
S_m	12 m^2	Mean moulin area
y	1000 m	Storage width
f	0.2	Darcy-Weisbach friction factor
A	5.3 * 10^{-24} s^{-1} Pa^{-3}	Ice creep parameter
n	3	Ice flow law exponent
h_r	0.2 m	Bedrock aspersion height
l_r	1 m	Wavelength of bed roughness
G	6.5 * 10^{-2} W m^{-2}	Geothermal heat flux
τ_b	120 kPa	Basal shear stress
u_b	75 m a^{-1}	Ice sliding velocity
k	0.01	Transmissivity coefficient

Table 4.1. Parameters used in 1D subglacial model.

Chapter 5. Conclusions

5.1. Synthesis

All components of the glacio-hydrologic system play an important role in the seasonal acceleration of the GrIS. The distribution and characteristics of surface features can alter the spatiotemporal pattern of meltwater delivery to the ice–bed interface, while the ever-evolving state of the subglacial hydrologic system influences the magnitude and duration of the ice sheet's velocity response. In this dissertation, I demonstrate that careful consideration of all aspects of the glacio-hydrologic system, including both surface and bed conditions, is necessary to explain the seasonal evolution of ice motion within the ablation zone of the GrIS. Further, individual subglacial hydrologic system components are not independent entities. Rather, they fall on a continuum and evolve that depends on local bed characteristics and each other. The seasonal formation of subglacial channels does not preclude continued evolution within the distributed, or even unconnected regions of the ice-sheet bed. Thus, parameterizations of basal lubrication for large-scale ice-sheet models should not rely on either a solely positive nor a solely negative feedback between surface melting and basal sliding [*Shannon et al.*, 2013].

5.2. Summary of this Dissertation

The spatial distribution of moulins does not change significantly with increasing surface melt. Instead, their locations can be spatially fixed over multi-decadal periods and, moulin spatial densities do not change unless there are substantial changes in local ice dynamics or significant thinning that allows for an increase in surface crevassing. The identification of numerous matched moulins over a 26-year period indicates that, for large portions of our study area, supraglacial water is reaching the bed at similar locations over long time periods.

I also demonstrate that, when considering modern ice velocity and the spacing between matched moulins, the median occupation time of any given moulin is longer than a single year. This interval is critical, because it demonstrates that moulins in the ablation zone of the GrIS are not reformed every year by hydrofracture and supraglacial lake drainage, which reduces the temporal lag between the onset of melting and subglacial water delivery to the ice–bed interface. In fact, long-term persistence of moulins may actually be necessary for the rapid drainage of nearby supraglacial lakes [*Stevens et al*., 2015]. Further, as moulins drain the majority of supraglacial melt [*Smith et al*., 2015], their long-term stability has implications for the development of subglacial drainage efficiency. In particular, consistent high-velocity water flow can result in increased bedrock erosion or the winnowing of basal sediments, neither of which are currently represented in state of the art models of subglacial water flow.

Moulins are directly connected to efficient components of the subglacial hydrologic system. Therefore, understanding pressure variations within moulins provides substantial insight into the development and form of this portion of the subglacial hydrologic system. I find that, while moulin hydraulic heads are diurnally correlated with local ice velocity, there is a long-term hysteresis in this relationship. This late-season hysteresis indicates that, while the ice sheet decelerates over the course of the melt season, high water pressures are maintained within the efficient portion of the subglacial hydrologic system. The observed pattern suggests that ice velocity is, at least in part, responding to evolution outside of subglacial channels. Low connectivity between a moulin and nearby boreholes suggests that the spatial extent of the distributed system is limited. However, declining pressure in a borehole previously unconnected to the active subglacial hydrologic system suggests that ice motion acts to gradually increase the extent of the distributed system, allowing yet higher pressure unconnected regions of the bed to

gradually connect. This transition can result in an areal increase in basal traction, causing ice velocity to decline below its winter background value and potentially limiting the impact of surface melt-induced ice acceleration.

While these direct observations were primarily made during the latter part of the melt season, the GPS-derived ice velocity records I collected span both the 2011 and 2012 melt seasons. I use these observations in conjunction with a simple model of subglacial hydrology to explore the role of the subglacial hydrologic system in controlling the onset and gradual termination of melt-induced ice acceleration. In particular, I investigate whether the formation of efficient subglacial channels can explain the observed ice-velocity patterns.

These results indicate that the development of subglacial channels alone cannot explain the observed timing between the onset of summer acceleration and mid-season deceleration, unless hydraulic roughness is assumed to be significantly lower than observed values. As such, both channelization and the dynamic feedback between basal ice motion and regional effective pressures are necessary to explain seasonal patterns in ice velocity. Together, these studies indicate that, while channelization occurs, the evolution of the entire subglacial hydrologic system is truly that. It cannot be represented accurately by a single component. Instead, it is best explained as the interaction of multiple parts.

5.3. Direction of Future Work

Modeling of the subglacial hydrologic system has advanced substantially in recent years, with the development of two-dimensional models coupled to ice flow [e.g., *Hewitt*, 2013; *Hoffman and Price*, 2014]. Yet, despite these advances these models as well as the simpler model developed here, are hampered by our ability to obtain information on the nature of the ice–bed interface.

The mechanism by which subglacial channels initiate is poorly characterized. Models often circumvent this issue by assigning an initial channel geometry [e.g., *Colgan et al*., 2012; *Banwell et al*., 2013; *Meierbachtol et al*., 2013; *Dow et al*., 2014]. However, the timing of channel development is critically sensitive to initial conditions. We allow for drainage efficiency to be maintained through a small cavity-opening term when subglacial channel height is smaller than the prescribed bed roughness. In both instances, these choices idealize the onset of channelization. However, my observation that moulin locations can be stationary over long periods strongly supports the idea that the development of high connectivity pathways via subglacial erosion can precondition the bed for channel development, especially where subglacial sediment is present (Chapter 2) [*Dow et al*., 2013; *Walter et al*., 2014]. This information can be used to better characterize how channelization within the subglacial system can be initiated on reasonable timescales.

Our understanding of subglacial channels is also hampered by limited constraints on local bed roughness, all of which are from small alpine glaciers [e.g., *Willis et al*., 2012; *Gulley et al*., 2014]. During incipient channel formation, high bed roughness and channel geometry can inhibit flow and limit channel growth through viscous dissipation. However, basal characteristics are so poorly constrained that subglacial hydrologic system models often use a fixed roughness parameterization, as I did in Chapters 3 and 4. Both factors suggest that better characterization of the onset of summer acceleration and channel development can be gained through further investigation of subglacial bedrock and till heterogeneity and an improved treatment of basal conditions within subglacial models. Further, without better constraints on subglacial properties, characterizing spatiotemporal extent of channelization may be premature.

When modeling the englacial system, I choose to represent moulin geometry as cylindrical. This is a common first-order assumption [e.g., *Hewitt*, 2013; *Meierbachtol et al*., 2013; *Werder et al*., 2013], but observations [e.g., *Holmlund*, 1988; *Gulley et al*., 2009] indicate that differing creep-closure rates, the alternating presence and absence of water, dissipation of thermal and turbulent energy, and ice motion all contribute to a non-uniform shape and spatial variability in moulin capacity. Spatial variation due to changing ice thickness may result in larger moulins in thinner ice where creep closure is limited. This phenomenon could result in larger hydraulic gradients than are currently modeled, because similar supraglacial inputs would be accommodated within moulins at different rates. The impact of this effect would of course depend on the relative capacity and connectivity of additional englacial and subglacial hydrologic systems. Therefore, increased efforts to model changes in englacial storage could provide critical controls on subglacial hydrologic system development.

Direct observations of the subglacial hydrologic system are both logistically and instrumentally challenging. Boreholes are often used to measure subglacial water pressure on both the GrIS and on alpine glaciers; however, boreholes frequently intersect regions of the bed unconnected to the active subglacial hydrologic system [e.g., *Murray and Clarke*, 1995; *Gordon et al*., 1998; *Andrews et al*., 2014; *Ryser et al*., 2014]. When combined with measurements of the active subglacial hydrologic system either via moulins [*Cowton et al*., 2013; *Andrews et al*., 2014] or well-connected boreholes [*Murray and Clarke*, 1995; *Gordon et al*., 1998], substantial information can be gained about subglacial behavior. Indeed, this implied vast and changing expanse of the bed unconnected to the active subglacial hydrologic system (Chapter 3) warrants its inclusion in future models. Additional borehole-based studies are necessary to explore regions of the bed with transitioning characteristic

References

Ahn, Y., and I. M. Howat (2011), Efficient automated glacier surface velocity measurement from repeat images using multi-image/multichip and null exclusion feature tracking, *IEEE Trans. Geosci. Remote Sens.*, *49*(8), 2838–2846, doi:10.1109/TGRS.2011.2114891.

Alley, R. B., and I. M. Whillans (1984), Response of the East Antarctica Ice Sheet to sea-level rise, *J. Geophys. Res.*, *89*(C4), 6487–6493.

Amundson, J. M., M. Truffer, and M. P. Lüthi (2006), Time-dependent basal stress conditions beneath Black Rapids Glacier, Alaska, USA, inferred from measurements of ice deformation and surface motion, *J. Glaciol.*, *52*(178), 347–357, doi:10.3189/172756506781828593.

Anderson, R. S., B. Hallet, J. Walder, and B. F. Aubry (1982), Observations in a cavity beneath Grinnell Glacier, *Earth Surf. Process. Landf.*, *7*(1), 63–70, doi:10.1002/esp.3290070108.

Anderson, R. S., S. P. Anderson, K. R. MacGregor, E. D. Waddington, S. O'Neel, C. A. Riihimaki, and M. G. Loso (2004), Strong feedbacks between hydrology and sliding of a small alpine glacier, *J. Geophys. Res. Earth Surf.*, *109*(F3), F03005, doi:10.1029/2004JF000120.

Andrews, L. C., and G. A. Catania (in prep.), Multi-decadal moulin variability and implications for subglacial drainage of the Greenland Ice Sheet.

Andrews, L. C., G. A. Catania, M. J. Hoffman, J. D. Gulley, M. P. Lüthi, C. Ryser, R. L. Hawley, and T. A. Neumann (2014), Direct observations of evolving subglacial drainage beneath the Greenland Ice Sheet, *Nature*, *514*(7520), 80–83, doi:10.1038/nature13796.

van Angelen, J. H., M. R. van den Broeke, B. Wouters, and J. T. M. Lenaerts (2013), Contemporary (1960–2012) evolution of the climate and surface mass balance of the Greenland Ice Sheet, *Surv. Geophys.*, *35*(5), 1155–1174, doi:10.1007/s10712-013-9261-z.

Arnold, N. S., A. F. Banwell, and I. C. Willis (2014), High-resolution modelling of the seasonal evolution of surface water storage on the Greenland Ice Sheet, *The Cryosphere*, *8*(4), 1149–1160, doi:10.5194/tc-8-1149-2014.

Aschwanden, A., E. Bueler, C. Khroulev, and H. Blatter (2012), An enthalpy formulation for glaciers and ice sheets, *J. Glaciol.*, *58*(209), 441–457, doi:10.3189/2012JoG11J088.

Banwell, A. F., N. S. Arnold, I. C. Willis, M. Tedesco, and A. P. Ahlstrøm (2012), Modeling supraglacial water routing and lake filling on the Greenland Ice Sheet, *J. Geophys. Res.*, *117*(F4), doi:10.1029/2012JF002393.

Banwell, A. F., I. C. Willis, and N. S. Arnold (2013), Modeling subglacial water routing at Paakitsoq, W Greenland, *J. Geophys. Res. Earth Surf.*, *118*(3), 1282–1295, doi:10.1002/jgrf.20093.

Bartholomaus, T. C., R. S. Anderson, and S. P. Anderson (2008), Response of glacier basal motion to transient water storage, *Nat. Geosci.*, *1*(1), 33–37, doi:10.1038/ngeo.2007.52.

Bartholomaus, T. C., R. S. Anderson, and S. P. Anderson (2011), Growth and collapse of the distributed subglacial hydrologic system of Kennicott Glacier, Alaska, USA, and its effects on basal motion, *J. Glaciol.*, *57*(206), 985–1002, doi:10.3189/002214311798843269.

Bartholomew, I., P. Nienow, D. Mair, A. Hubbard, M. A. King, and A. Sole (2010), Seasonal evolution of subglacial drainage and acceleration in a Greenland outlet glacier, *Nat. Geosci.*, *3*(6), 408–411, doi:10.1038/ngeo863.

Bartholomew, I., P. Nienow, A. Sole, D. Mair, T. Cowton, and M. A. King (2012), Short-term variability in Greenland Ice Sheet motion forced by time-varying meltwater drainage: Implications for the relationship between subglacial drainage system behavior and ice velocity, *J. Geophys. Res. Earth Surf.*, *117*(F3), F03002, doi:10.1029/2011JF002220.

Bartholomew, I. D., P. Nienow, A. Sole, D. Mair, T. Cowton, M. A. King, and S. Palmer (2011), Seasonal variations in Greenland Ice Sheet motion: Inland extent and behaviour at higher elevations, *Earth Planet. Sci. Lett.*, *307*(3–4), 271–278, doi:10.1016/j.epsl.2011.04.014.

Bell, R. E. (2008), The role of subglacial water in ice-sheet mass balance, *Nat. Geosci.*, *1*(5), 297–304, doi:10.1038/ngeo186.

Bindschadler, R. A. (1983), The importance of pressurized subglacial water in separation and sliding at the glacier bed, *J. Glaciol.*, *29*(101), 3–19.

Bougamont, M., J. L. Bamber, and W. Greuell (2005), A surface mass balance model for the Greenland Ice Sheet, *J. Geophys. Res.*, *110*(F4), doi:10.1029/2005JF000348.

Bougamont, M., P. Christoffersen, H. A. L, A. A. Fitzpatrick, S. H. Doyle, and S. P. Carter (2014), Sensitive response of the Greenland Ice Sheet to surface melt drainage over a soft bed, *Nat. Commun.*, *5*, doi:10.1038/ncomms6052.

Boulton, G. S., and A. S. Jones (1979), Stability of temperate ice caps and ice sheets resting on beds of deformable sediment, *J. Glaciol.*, *24*(90), 29–43.

Box, J. E., X. Fettweis, J. C. Stroeve, M. Tedesco, D. K. Hall, and K. Steffen (2012), Greenland ice sheet albedo feedback: thermodynamics and atmospheric drivers, *The Cryosphere*, *6*(4), 821–839, doi:10.5194/tc-6-821-2012.

Braithwaite, R. J. (1995), Positive degree-day factors for ablation on the Greenland ice sheet studied by energy-balance modelling, *J. Glaciol.*, *41*(137), 153–160.

Braithwaite, R. J., and O. B. Olesen (1989), Calculation of Glacier Ablation from Air Temperature, West Greenland, in *Glacier Fluctuation and Climatic Change*, Kluwer Academic Publishers, Dordrect, Netherlands.

van den Broeke, M., P. Smeets, J. Ettema, C. van der Veen, R. van de Wal, and J. Oerlemans (2008), Partitioning of melt energy and meltwater fluxes in the ablation zone of the west Greenland Ice Sheet, *The Cryosphere*, *2*(2), 179–189, doi:10.5194/tc-2-179-2008.

van den Broeke, M., C. Bus, J. Ettema, and P. Smeets (2010), Temperature thresholds for degree-day modelling of Greenland ice sheet melt rates, *Geophys. Res. Lett.*, *37*(18), L18501, doi:10.1029/2010GL044123.

van den Broeke, M. van den, J. Bamber, J. Ettema, E. Rignot, E. Schrama, W. J. van de Berg, E. van Meijgaard, I. Velicogna, and B. Wouters (2009), Partitioning recent Greenland Mass Loss, *Science*, *326*(5955), 984–986, doi:10.1126/science.1178176.

Budd, W. F., P. L. Keage, and N. A. Blundy (1979), Empirical studies of ice sliding, *J. Glaciol.*, *23*, 157–170.

Carver, S., D. Sear, and E. Valentine (1994), An observation of roll waves in a supraglacial meltwater channel, Harlech Gletscher, East Greenland, *J. Glaciol.*, *40*(134), 76–78.

Catania, G. A., and T. A. Neumann (2010), Persistent englacial drainage features in the Greenland Ice Sheet, *Geophys. Res. Lett.*, *37*(2), L02501, doi:10.1029/2009GL041108.

Catania, G. A., T. A. Neumann, and S. F. Price (2008), Characterizing englacial drainage in the ablation zone of the Greenland Ice Sheet, *J. Glaciol.*, *54*(187), 567–578, doi:10.3189/002214308786570854.

Chandler, D. M. et al. (2013), Evolution of the subglacial drainage system beneath the Greenland Ice Sheet revealed by tracers, *Nat. Geosci.*, *6*(3), 195–198, doi:10.1038/ngeo1737.

Chen, G. (1998), GPS kinematic positioning for airborne laser altimetry at Long Valley, California, Massachusetts Institute of Technology, Cambridge, MA.

Cheung, C. K., and W. Shi (2004), Estimation of the positional uncertainty in line simplification in GIS, *Cartogr. J.*, *41*(1), 37–45, doi:10.1179/000870404225019990.

Chu, V. W. (2014), Greenland Ice Sheet hydrology: A review, *Prog. Phys. Geogr.*, *38*(1), 19–54, doi:10.1177/0309133313507075.

Chu, V. W., L. C. Smith, A. K. Rennermalm, R. R. Forster, J. E. Box, and N. Reeh (2009), Sediment plume response to surface melting and supraglacial lake drainages on the Greenland ice sheet, *J. Glaciol.*, *55*(194), 1072–1082, doi:10.3189/002214309790794904.

Clarke, G. K. C. (1996), Lumped-element analysis of subglacial hydraulic circuits, *J. Geophys. Res. Solid Earth*, *101*(B8), 17547–17559, doi:10.1029/96JB01508.

Clason, C. C., D. W. F. Mair, P. W. Nienow, I. D. Bartholomew, A. Sole, S. Palmer, and W. Schwanghart (2015), Modelling the transfer of supraglacial meltwater to the bed of Leverett Glacier, Southwest Greenland, *The Cryosphere*, *9*(1), 123–138, doi:10.5194/tc-9-123-2015.

Colgan, W., K. Steffen, W. S. McLamb, W. Abdalati, H. Rajaram, R. Motyka, T. Phillips, and R. Anderson (2011a), An increase in crevasse extent, West Greenland: Hydrologic implications, *Geophys. Res. Lett.*, *38*(18), L18502, doi:10.1029/2011GL048491.

Colgan, W., H. Rajaram, R. Anderson, K. Steffen, T. Phillips, I. Joughin, H. J. Zwally, and W. Abdalati (2011b), The annual glaciohydrology cycle in the ablation zone of the Greenland ice sheet: Part 1. Hydrology model, *J. Glaciol.*, *57*(204), 697–709, doi:10.3189/002214311797409668.

Colgan, W., H. Rajaram, R. S. Anderson, K. Steffen, H. J. Zwally, T. Phillips, and W. Abdalati (2012), The annual glaciohydrology cycle in the ablation zone of the Greenland ice sheet: Part 2. Observed and modeled ice flow, *J. Glaciol.*, *58*(207), 51–64, doi:10.3189/2012JoG11J081.

Covington, M. D., A. F. Banwell, J. Gulley, M. O. Saar, I. Willis, and C. M. Wicks (2012), Quantifying the effects of glacier conduit geometry and recharge on

proglacial hydrograph form, *J. Hydrol.*, *414–415*, 59–71, doi:10.1016/j.jhydrol.2011.10.027.

Cowton, T., P. Nienow, I. Bartholomew, A. Sole, and D. Mair (2012), Rapid erosion beneath the Greenland ice sheet, *Geology*, *40*(4), 343–346, doi:10.1130/G32687.1.

Cowton, T., P. Nienow, A. Sole, J. Wadham, G. Lis, I. Bartholomew, D. Mair, and D. Chandler (2013), Evolution of drainage system morphology at a land-terminating Greenlandic outlet glacier, *J. Geophys. Res. Earth Surf.*, *118*(1), 29–41, doi:10.1029/2012JF002540.

Csatho, B. M., A. F. Schenk, C. J. van der Veen, G. Babonis, K. Duncan, S. Rezvanbehbahani, M. R. van den Broeke, S. B. Simonsen, S. Nagarajan, and J. H. van Angelen (2014), Laser altimetry reveals complex pattern of Greenland Ice Sheet dynamics, *Proc. Natl. Acad. Sci.*, *111*(52), 18478–18483, doi:10.1073/pnas.1411680112.

Cuffey, K. M., and S. J. Marshall (2000), Substantial contribution to sea-level rise during the last interglacial from the Greenland ice sheet, *Nature*, *404*(6778), 591–594, doi:10.1038/35007053.

Cuffey, K. M., and W. S. B. Paterson (2010), *The Physics of Glaciers*, Fourth Edition, Elsevier, Boston, MA.

Das, S. B., I. Joughin, M. D. Behn, I. M. Howat, M. A. King, D. Lizarralde, and M. P. Bhatia (2008), Fracture Propagation to the base of the Greenland Ice Sheet during supraglacial lake drainage, *Science*, *320*(5877), 778–781, doi:10.1126/science.1153360.

Dow, C. F., A. Hubbard, A. D. Booth, S. H. Doyle, A. Gusmeroli, and Y. B. Kulessa (2013), Seismic evidence of mechanically weak sediments underlying Russell Glacier, West Greenland, *Ann. Glaciol.*, *54*(64), 135–141, doi:10.3189/2013AoG64A032.

Dow, C. F., B. Kulessa, I. C. Rutt, S. H. Doyle, and A. Hubbard (2014), Upper bounds on subglacial channel development for interior regions of the Greenland ice sheet, *J. Glaciol.*, *60*(224), 1044–1052, doi:10.3189/2014JoG14J093.

Dow, C. F. et al. (2015), Modeling of subglacial hydrological development following rapid supraglacial lake drainage, *J. Geophys. Res. Earth Surf.*, *120*(6), 2014JF003333, doi:10.1002/2014JF003333.

Doyle, S. H., A. Hubbard, A. A. W. Fitzpatrick, D. van As, A. B. Mikkelsen, R. Pettersson, and B. Hubbard (2014), Persistent flow acceleration within the interior

of the Greenland ice sheet, *Geophys. Res. Lett.*, *41*(3), 2013GL058933, doi:10.1002/2013GL058933.

Doyle, S. H. et al. (2015), Amplified melt and flow of the Greenland ice sheet driven by late-summer cyclonic rainfall, *Nat. Geosci.*, *8*(8), 647–653, doi:10.1038/ngeo2482.

Echelmeyer, K., and W. Harrison (1990), Jakobshavns Isbræ, West Greenland: Seasonal variations in velocity-or lack thereof, *J. Glaciol.*, *36*.

Engelhardt, H. F., W. D. Harrison, and B. Kamb (1978), Basal sliding and conditions at the glacier bed as revealed by bore-hole photography, *J. Glaciol.*, *20*(84), 469–508.

ESRI (2014), *ArcGIS Desktop: Release 10.1*, Environmental Systems Research Institute, Redlands, CA.

de Fleurian, B., O. Gagliardini, T. Zwinger, G. Durand, E. Le Meur, D. Mair, and P. Råback (2014), A double continuum hydrological model for glacier applications, *The Cryosphere*, *8*(1), 137–153, doi:10.5194/tc-8-137-2014.

Flowers, G. E. (2008), Subglacial modulation of the hydrograph from glacierized basins, *Hydrol. Process.*, *22*(19), 3903–3918, doi:10.1002/hyp.7095.

Flowers, G. E. (2015), Modelling water flow under glaciers and ice sheets, *Proc. R. Soc. Math. Phys. Eng. Sci.*, *471*(2176), 20140907–20140907, doi:10.1098/rspa.2014.0907.

Flowers, G. E., and G. K. C. Clarke (2002), A multicomponent coupled model of glacier hydrology 1. Theory and synthetic examples, *J. Geophys. Res. Solid Earth*, *107*(B11), 2287, doi:10.1029/2001JB001122.

Flowers, G. E., H. Björnsson, F. Pálsson, and G. K. C. Clarke (2004), A coupled sheet-conduit mechanism for jökulhlaup propagation, *Geophys. Res. Lett.*, *31*(5), L05401, doi:10.1029/2003GL019088.

Forbes, J. (1859), Fourth Letter on Glaciers, in *Occasional Papers on the Theory of Glaciers*, pp. 26 – 35, Adam and Charles Black, Edinburgh, Scotland.

Forster, R. R. et al. (2014), Extensive liquid meltwater storage in firn within the Greenland ice sheet, *Nat. Geosci.*, *7*(2), 95–98, doi:10.1038/ngeo2043.

Fountain, A. G., and J. S. Walder (1998), Water flow through temperate glaciers, *Rev. Geophys.*, *36*(3), 299–328, doi:10.1029/97RG03579.

Fowler, A. C. (1981), A theoretical treatment of the sliding of glaciers in the absence of cavitation, *Philos. Trans. R. Soc. Lond. Math. Phys. Eng. Sci.*, *298*(1445), 637–681, doi:10.1098/rsta.1981.0003.

Fürst, J. J., H. Goelzer, and P. Huybrechts (2015), Ice-dynamic projections of the Greenland ice sheet in response to atmospheric and oceanic warming, *The Cryosphere*, *9*(3), 1039–1062, doi:10.5194/tc-9-1039-2015.

Gagliardini, O., D. Cohen, P. Råback, and T. Zwinger (2007), Finite-element modeling of subglacial cavities and related friction law, *J. Geophys. Res.*, *112*(F2), doi:10.1029/2006JF000576.

Getis, A., and J. K. Ord (1992), The analysis of spatial association by use of distance statistics, *Geogr. Anal.*, *24*(3), 189–206, doi:10.1111/j.1538-4632.1992.tb00261.x.

Gogineni, P. (2012), *CReSIS Radar Depth Sounder Data*, Digital Media, Lawrence, Kansas, USA.

Gordon, S., M. Sharp, B. Hubbard, C. Smart, B. Ketterling, and I. Willis (1998), Seasonal reorganization of subglacial drainage inferred from measurements in boreholes, *Hydrol. Process.*, *12*(1), 105–133, doi:10.1002/(SICI)1099-1085(199801)12:1<105::AID-HYP566>3.0.CO;2-#.

Greuell, W. (2000), Melt–water accumulation on the surface of the Greenland Ice Sheet: Effect on albedo and mass balance, *Geogr. Ann. Ser. Phys. Geogr.*, *82*(4), 489–498, doi:10.1111/j.0435-3676.2000.00136.x.

Gudmundsson, G. H. (2003), Transmission of basal variability to a glacier surface, *J. Geophys. Res.*, *108*(B5), doi:10.1029/2002JB002107.

Gulley, J. D., D. I. Benn, E. Screaton, and J. Martin (2009), Mechanisms of englacial conduit formation and their implications for subglacial recharge, *Quat. Sci. Rev.*, *28*(19–20), 1984–1999, doi:10.1016/j.quascirev.2009.04.002.

Gulley, J. D., M. Grabiec, J. B. Martin, J. Jania, G. Catania, and P. Glowacki (2012), The effect of discrete recharge by moulins and heterogeneity in flow-path efficiency at glacier beds on subglacial hydrology, *J. Glaciol.*, *58*(211), 926–940, doi:10.3189/2012JoG11J189.

Gulley, J. D., P. D. Spellman, M. D. Covington, J. B. Martin, D. I. Benn, and G. Catania (2014), Large values of hydraulic roughness in subglacial conduits during conduit enlargement: implications for modeling conduit evolution, *Earth Surf. Process. Landf.*, *39*(3), 296–310, doi:10.1002/esp.3447.

Hall, D. K., V. V. Salomonson, and G. A. Riggs (2006), *MODIS/Terra Snow Cover Daily L3 Global 500m Grid. Version 5. [May 2011 - September 2012]*, NASA National Snow and Ice Data Distributed Active Archive Center, Boulder, Colorado USA.

Hanna, E., S. H. Mernild, J. Cappelen, and K. Steffen (2012), Recent warming in Greenland in a long-term instrumental (1881–2012) climatic context: I. Evaluation of surface air temperature records, *Environ. Res. Lett.*, *7*(4), 045404, doi:10.1088/1748-9326/7/4/045404.

Harbor, J., M. Sharp, L. Copland, B. Hubbard, P. Nienow, and D. Mair (1997), Influence of subglacial drainage conditions on the velocity distribution within a glacier cross section, *Geology*, *25*(8), 739–742, doi:10.1130/0091-7613(1997)025<0739:IOSDCO>2.3.CO;2.

Harper, J. T., and N. F. Humphrey (1995), Borehole video analysis of a temperate glacier' englacial and subglacial structure: Implications for glacier flow models, *Geology*, *23*(10), 901–904, doi:10.1130/0091-7613(1995)023<0901:BVAOAT>2.3.CO;2.

Harper, J. T., N. F. Humphrey, W. T. Pfeffer, and B. Lazar (2007), Two modes of accelerated glacier sliding related to water, *Geophys. Res. Lett.*, *34*(12), L12503, doi:10.1029/2007GL030233.

Harper, J. T., J. H. Bradford, N. F. Humphrey, and T. W. Meierbachtol (2010), Vertical extension of the subglacial drainage system into basal crevasses, *Nature*, *467*(7315), 579–582, doi:10.1038/nature09398.

Harrington, J. A., N. F. Humphrey, and J. T. Harper (2015), Temperature distribution and thermal anomalies along a flowline of the Greenland ice sheet, *Ann. Glaciol.*, *56*(70), 98–104, doi:10.3189/2015AoG70A945.

Hart, J. K., K. C. Rose, A. Clayton, and K. Martinez (2015), Englacial and subglacial water flow at Skálafellsjökull, Iceland derived from ground penetrating radar, in situ Glacsweb probe and borehole water level measurements, *Earth Surf. Process. Landf.*, doi:10.1002/esp.3783.

Hewitt, I. J. (2011), Modelling distributed and channelized subglacial drainage: the spacing of channels, *J. Glaciol.*, *57*(202), 302–314, doi:10.3189/002214311796405951.

Hewitt, I. J. (2013), Seasonal changes in ice sheet motion due to melt water lubrication, *Earth Planet. Sci. Lett.*, *371–372*, 16–25, doi:10.1016/j.epsl.2013.04.022.

Hewitt, I. J., C. Schoof, and M. A. Werder (2012), Flotation and free surface flow in a model for subglacial drainage. Part 2. Channel flow, *J. Fluid Mech.*, *702*, 157–187, doi:10.1017/jfm.2012.166.

Hock, R. (2003), Temperature index melt modelling in mountain areas, *J. Hydrol.*, *282*(1-4), 104–115, doi:10.1016/S0022-1694(03)00257-9.

Hoffman, M., and S. Price (2014), Feedbacks between coupled subglacial hydrology and glacier dynamics, *J. Geophys. Res. Earth Surf.*, *119*(3), 414–436, doi:10.1002/2013JF002943.

Hoffman, M. J., G. A. Catania, T. A. Neumann, L. C. Andrews, and J. A. Rumrill (2011), Links between acceleration, melting, and supraglacial lake drainage of the western Greenland Ice Sheet, *J. Geophys. Res. Earth Surf.*, *116*(F4), F04035, doi:10.1029/2010JF001934.

Hollander, M., and D. A. Wolfe (1999), *Nonparametric Statistical Methods*, 2nd ed., John Wiley and Sons, New York.

Holmlund, P. (1988), Internal geometry and evolution of moulins, *J. Glaciol.*, *34*(117), 242–248.

Holmlund, P., and R. L. Hooke (1983), High water-pressure events in moulins, Storglaciären, Sweden, *Geogr. Ann. Ser. Phys. Geogr.*, *65*(1/2), 19–25.

Hooke, R. L. B. (1984), On the role of mechanical energy in maintaining subglacial water conduits at atmospheric pressure, *J. Glaciol.*, *30*(105), 180–187.

Howat, I. M., S. Tulaczyk, E. Waddington, and H. Björnsson (2008), Dynamic controls on glacier basal motion inferred from surface ice motion, *J. Geophys. Res. Earth Surf.*, *113*(F3), F03015, doi:10.1029/2007JF000925.

Howat, I. M., A. Negrete, and B. E. Smith (2014), The Greenland Ice Mapping Project (GIMP) land classification and surface elevation data sets, *The Cryosphere*, *8*(4), 1509–1518, doi:10.5194/tc-8-1509-2014.

Hubbard, B., and P. Nienow (1997), Alpine subglacial hydrology, *Quat. Sci. Rev.*, *16*, 939–955.

Hubbard, B. P., M. J. Sharp, I. C. Willis, M. K. Nielsen, and C. C. Smart (1995), Borehole water-level variations and the structure of the subglacial hydrological system of Haut Glacier d'Arolla, Valais, Switzerland, *J. Glaciol.*, *41*(139), 572–583.

Humphrey, N., and K. Echelmeyer (1990), Hot-Water drilling and bore-hole closure in cold ice, *J. Glaciol.*, *36*(124), 287–298, doi:10.3189/002214390793701354.

Iken, A. (1972), Measurements of water pressure in moulins as part of a movement study of the White Glacier, Axel Heiberg Island, Northwest Territories, Canada, *J. Glaciol.*, *11*(61), 53–58.

Iken, A. (1981), *The effect of the subglacial water pressure on the sliding velocity of a glacier in an idealized numerical model*, Versuchsanst. für Wasserbau, Hydrologie u. Glaziologie an d. Eidg. Techn. Hochsch.

Iken, A., and R. Bindschadler (1986), Combined measurements of subglacial water pressure and surface velocity of Findelengletscher, Switzerland: conclusions about drainage system and sliding mechanism, *J. Glaciol.*, *32*(110), 101–119.

Iken, A., and M. Truffer (1997), The relationship between subglacial water pressure and velocity of Findelengletscher, Switzerland, during its advance and retreat, *J. Glaciol.*, *43*(144), 328–338.

Iken, A., H. Röthlisberger, A. Flotron, and W. Haeberli (1983), The uplift of Unteraargletscher at the beginning of the melt season - A consequence of water storage at the bed?, *J. Glaciol.*, *29*(101), 28–47.

Iken, A., K. Echelmeyer, and W. D. Harrison (1989), A light-weight hot water drill for large depth: experiences with drilling on Jakobshavns glacier, Greenland, in *Ice core drilling*, pp. 1123–136, Grenoble, Centre National de la Recherche Scientifique. Laboratoire de Glaciologie et Géophysique de'Environment.

James, L. A., M. E. Hodgson, S. Ghoshal, and M. M. Latiolais (2012), Geomorphic change detection using historic maps and DEM differencing: The temporal dimension of geospatial analysis, *Geomorphology*, *137*(1), 181–198, doi:10.1016/j.geomorph.2010.10.039.

Jansson, P., R. Hock, and T. Schneider (2003), The concept of glacier storage: a review, *J. Hydrol.*, *282*(1–4), 116–129, doi:10.1016/S0022-1694(03)00258-0.

Jenson, S. K., and J. O. Domingue (1988), Extracting topographic structure from digital elevation data for geographic information system analysis, *Photogramm. Eng. Remote Sens.*, *54*(11), 1593–1600.

Joughin, I., B. E. Smith, I. M. Howat, T. Scambos, and T. Moon (2010a), Greenland flow variability from ice-sheet-wide velocity mapping, *J. Glaciol.*, *56*(197), 415–430, doi:10.3189/002214310792447734.

Joughin, I., B. E. Smith, I. M. Howat, and T. A. Scambos (2010b), *MEaSUREs Greenland Ice Sheet Velocity Map from InSAR Data [2008-2009]*, NASA National Snow and Ice Data Distributed Active Archive Center, Boulder, Colorado USA.

Joughin, I., S. B. Das, G. E. Flowers, M. D. Behn, R. B. Alley, M. A. King, B. E. Smith, J. L. Bamber, M. R. van den Broeke, and J. H. van Angelen (2013), Influence of ice-sheet geometry and supraglacial lakes on seasonal ice-flow variability, *The Cryosphere*, *7*(4), 1185–1192, doi:10.5194/tc-7-1185-2013.

Kamb, B. (1970), Sliding motion of glaciers: Theory and observation, *Rev. Geophys.*, *8*(4), 673–728, doi:10.1029/RG008i004p00673.

Kamb, B. (1987), Glacier surge mechanism based on linked cavity configuration of the basal water conduit system, *J. Geophys. Res. B*, *92*(B9), 9083–9100.

Kamb, B. (2001), Basal Zone of the West Antarctic Ice Streams and its Role in Lubrication of Their Rapid Motion, in *The West Antarctic Ice Sheet: Behavior and Environment*, edited by R. B. Alley and R. A. Bindschadler, pp. 157–199, American Geophysical Union.

Kamb, B., H. Engelhardt, M. A. Fahnestock, N. Humphrey, M. Meier, and D. Stone (1994), Mechanical and hydrologic basis for the rapid motion of a large tidewater glacier: 2. Interpretation, *J. Geophys. Res. Solid Earth*, *99*(B8), 15231–15244, doi:10.1029/94JB00467.

Karlstrom, L., P. Gajjar, and M. Manga (2013), Meander formation in supraglacial streams, *J. Geophys. Res. Earth Surf.*, *118*(3), 1897–1907, doi:10.1002/jgrf.20135.

Kavanaugh, J. L., and G. K. C. Clarke (2001), Abrupt glacier motion and reorganization of basal shear stress following the establishment of a connected drainage system, *J. Glaciol.*, *47*(158), 472–480, doi:10.3189/172756501781831972.

Kjær, K. H. et al. (2012), Aerial Photographs Reveal Late–20th-Century Dynamic Ice Loss in Northwestern Greenland, *Science*, *337*(6094), 569–573, doi:10.1126/science.1220614.

Koenig, L. S. et al. (2015), Wintertime storage of water in buried supraglacial lakes across the Greenland Ice Sheet, *The Cryosphere*, *9*(4), 1333–1342, doi:10.5194/tc-9-1333-2015.

Lampkin, D. J., and J. VanderBerg (2011), A preliminary investigation of the influence of basal and surface topography on supraglacial lake distribution near Jakobshavn

Isbræ, western Greenland, *Hydrol. Process.*, *25*(21), 3347–3355, doi:10.1002/hyp.8170.

Lewis, S. M., and L. C. Smith (2009), Hydrologic drainage of the Greenland Ice Sheet, *Hydrol. Process.*, *23*(14), 2004–2011, doi:10.1002/hyp.7343.

Liston, G. E., and S. H. Mernild (2012), Greenland Freshwater Runoff. Part I: A Runoff Routing Model for Glaciated and Nonglaciated Landscapes (HydroFlow), *J. Clim.*, *25*(17), 5997–6014, doi:10.1175/JCLI-D-11-00591.1.

Li, V. C. (1985), Estimation of in-situ hydraulic diffusivity of rock masses, *Pure Appl. Geophys.*, *122*, 545–559.

Lliboutry, L. (1968), General theory of subglacial cavitation and sliding of temperate glaciers, *J. Glaciol.*, *7*(49), 21–58.

Lüthi, M. P., M. Funk, A. Iken, S. Gogineni, and M. Truffer (2002), Mechanisms of fast flow in Jakobshavn Isbræ, West Greenland: Part III. Measurements of ice deformation, temperature and cross-borehole conductivity in boreholes to the bedrock, *J. Glaciol.*, *48*(162), 369–385, doi:10.3189/172756502781831322.

Lüthi, M. P., C. Ryser, L. C. Andrews, G. A. Catania, M. Funk, R. L. Hawley, M. J. Hoffman, and T. A. Neumann (2015), Heat sources within the Greenland Ice Sheet: dissipation, temperate paleo-firn and cryo-hydrologic warming, *The Cryosphere*, *9*(1), 245–253, doi:10.5194/tc-9-245-2015.

Mair, D., P. Nienow, I. Willis, and M. Sharp (2001), Spatial patterns of glacier motion during a high-velocity event: Haut Glacier d'Arolla, Switzerland, *J. Glaciol.*, *47*(156), 9–20, doi:10.3189/172756501781832412.

Mair, D., P. W. Nienow, M. J. Sharp, T. Wohlleben, and I. Willis (2002a), Influence of subglacial drainage system evolution on glacier surface motion: Haut Glacier d'Arolla, Switzerland, *J. Geophys. Res.*, *107*(B8), doi:10.1029/2001JB000514.

Mair, D., I. Willis, U. H. Fischer, B. Hubbard, P. Nienow, and A. Hubbard (2003), Hydrological controls on patterns of surface, internal and basal motion during three spring events'': Haut Glacier d'Arolla, Switzerland, *J. Glaciol.*, *49*(167), 555–567, doi:10.3189/172756503781830467.

Mair, D. W., M. J. Sharp, and I. C. Willis (2002b), Evidence for basal cavity opening from analysis of surface uplift during a high-velocity event: Haut Glacier d'Arolla, Switzerland, *J. Glaciol.*, *48*(161), 208–216.

Marsden, L. E. (1960), How the National map accuracy standards were developed, *Surv. Mapp.*, *20*, 427–429.

Mayaud, J. R., A. F. Banwell, N. S. Arnold, and I. C. Willis (2014), Modeling the response of subglacial drainage at Paakitsoq, west Greenland, to 21st century climate change, *J. Geophys. Res. Earth Surf.*, *119*(12), 2014JF003271, doi:10.1002/2014JF003271.

McGrath, D., W. Colgan, K. Steffen, P. Lauffenburger, and J. Balog (2011), Assessing the summer water budget of a moulin basin in the Sermeq Avannarleq ablation region, Greenland ice sheet, *J. Glaciol.*, *57*(205), 954–964, doi:10.3189/002214311798043735.

McGrath, D., W. Colgan, N. Bayou, A. Muto, and K. Steffen (2013), Recent warming at Summit, Greenland: Global context and implications, *Geophys. Res. Lett.*, *40*(10), 2091–2096, doi:10.1002/grl.50456.

Meierbachtol, T., J. Harper, and N. Humphrey (2013), Basal Drainage System Response to Increasing Surface Melt on the Greenland Ice Sheet, *Science*, *341*(6147), 777–779, doi:10.1126/science.1235905.

Mernild, S. H., G. E. Liston, C. A. Hiemstra, and J. H. Christensen (2010), Greenland Ice Sheet Surface Mass-Balance Modeling in a 131-Yr Perspective, 1950–2080, *J. Hydrometeorol.*, *11*(1), 3–25, doi:10.1175/2009JHM1140.1.

Mernild, S. H., D. M. Holland, D. Holland, A. Rosing-Asvid, J. C. Yde, G. E. Liston, and K. Steffen (2015), Freshwater flux and spatiotemporal simulated runoff variability into Ilulissat Icefjord, West Greenland, linked to salinity and temperature observations near tidewater glacier margins obtained using instrumented Ringed Seals, *J. Phys. Oceanogr.*, *45*(5), 1426–1445, doi:10.1175/JPO-D-14-0217.1.

Moon, T., I. Joughin, B. Smith, M. R. van den Broeke, W. J. van de Berg, B. Noël, and M. Usher (2014), Distinct patterns of seasonal Greenland glacier velocity, *Geophys. Res. Lett.*, *41*(20), 2014GL061836, doi:10.1002/2014GL061836.

Morlighem, M., E. Rignot, H. Seroussi, E. Larour, H. Ben Dhia, and D. Aubry (2011), A mass conservation approach for mapping glacier ice thickness, *Geophys. Res. Lett.*, *38*, L19503, doi:10.1029/2011GL048659.

Morlighem, M., E. Rignot, J. Mouginot, H. Seroussi, and E. Larour (2014), Deeply incised submarine glacial valleys beneath the Greenland ice sheet, *Nat. Geosci.*, *7*(6), 418–422, doi:10.1038/ngeo2167.

Morriss, B. F., R. L. Hawley, J. W. Chipman, L. C. Andrews, G. A. Catania, M. J. Hoffman, M. P. Lüthi, and T. A. Neumann (2013), A ten-year record of supraglacial lake evolution and rapid drainage in West Greenland using an automated processing algorithm for multispectral imagery, *The Cryosphere*, *7*(6), 1869–1877, doi:10.5194/tc-7-1869-2013.

Motyka, R. J., M. Fahnestock, and M. Truffer (2010), Volume change of Jakobshavn Isbræ, West Greenland:: 1985–1997–2007, *J. Glaciol.*, *56*(198), 635–646, doi:10.3189/002214310793146304.

Müller, F., and A. Iken (1973), Velocity fluctuations and water regime of Arctic valley glaciers, *Int. Assoc. Sci. Hydrol. Publ.*, *95*, 165–182.

Murray, T., and G. K. C. Clarke (1995), Black-box modeling of the subglacial water system, *J. Geophys. Res. Solid Earth*, *100*(B6), 10231–10245, doi:10.1029/95JB00671.

Nienow, P. W., M. J. Sharp, and I. Willis (1998), Seasonal change in the morphology of the subglacial drainage system, Haut Glacier D'Arolla, Switzerland, *Earth Surf. Process. Landf.*, *23*, 825–843.

Noh, M.-J., and I. M. Howat (2015), Automated stereo-photogrammetric DEM generation at high latitudes: Surface Extraction with TIN-based Search-space Minimization (SETSM) validation and demonstration over glaciated regions, *GIScience Remote Sens.*, *52*(2), 198–217, doi:10.1080/15481603.2015.1008621.

Nye, J. F. (1969), A calculation on the sliding of ice over a wavy surface using a Newtonian viscous approximation, *Proc. R. Soc. Lond. Math. Phys. Eng. Sci.*, *311*(1506), 445–467, doi:10.1098/rspa.1969.0127.

Nye, J. F. (1970), Glacier sliding without cavitation in a linear viscous approximation, *Proc. R. Soc. Lond. Math. Phys. Eng. Sci.*, *315*(1522), 381–403, doi:10.1098/rspa.1970.0050.

Nye, J. F. (1973), Water at the bed of a glacier, in *Symposium on the Hydrology of Glaciers*, vol. 95, pp. 189–194, IAHS Publishers.

Nye, J. F. (1976), Water flow in glaciers: jökulhlaups, tunnels and veins, *J. Glaciol.*, *17*, 181–207.

Palmer, S., A. Shepherd, P. Nienow, and I. Joughin (2011), Seasonal speedup of the Greenland Ice Sheet linked to routing of surface water, *Earth Planet. Sci. Lett.*, *302*(3–4), 423–428, doi:10.1016/j.epsl.2010.12.037.

Pellicciotti, F., B. Brock, U. Strasser, P. Burlando, M. Funk, and J. Corripio (2005), An enhanced temperature-index glacier melt model including the shortwave radiation balance: development and testing for Haut Glacier d'Arolla, Switzerland, *J. Glaciol.*, *51*(175), 573–587, doi:10.3189/172756505781829124.

Phillips, T., S. Leyk, H. Rajaram, W. Colgan, W. Abdalati, D. McGrath, and K. Steffen (2011), Modeling moulin distribution on Sermeq Avannarleq glacier using

ASTER and WorldView imagery and fuzzy set theory, *Remote Sens. Environ.*, *115*(9), 2292–2301, doi:10.1016/j.rse.2011.04.029.

Phillips, T., H. Rajaram, W. Colgan, K. Steffen, and W. Abdalati (2013), Evaluation of cryo-hydrologic warming as an explanation for increased ice velocities in the wet snow zone, Sermeq Avannarleq, West Greenland, *J. Geophys. Res. Earth Surf.*, *118*(3), 1241–1256, doi:10.1002/jgrf.20079.

Pimentel, S., and G. E. Flowers (2011), A numerical study of hydrologically driven glacier dynamics and subglacial flooding, *Proc. R. Soc. Lond. Math. Phys. Eng. Sci.*, *467*(2126), 537–558, doi:10.1098/rspa.2010.0211.

Poinar, K., I. Joughin, S. B. Das, M. D. Behn, J. T. M. Lenaerts, and M. R. van den Broeke (2015), Limits to future expansion of surface-melt-enhanced ice flow into the interior of western Greenland, *Geophys. Res. Lett.*, *42*(6), 2015GL063192, doi:10.1002/2015GL063192.

Price, S. F., A. J. Payne, G. A. Catania, and T. A. Neumann (2008), Seasonal acceleration of inland ice via longitudinal coupling to marginal ice, *J. Glaciol.*, *54*(185), 213–219, doi:10.3189/002214308784886117.

Rea, B. R., and W. B. Whalley (1994), Subglacial observation from Øksfjordjøkelen, North Norway, *Earth Surf. Process. Landf.*, *19*, 659–673.

Reeh, N., and O. B. Olesen (1986), Velocity measurements on Daugaard-Jensen Gletscher, Scoresby Sund, East Greenland, *Ann Glaciol*, *8*, 146–150.

Rennermalm, A. K., L. C. Smith, V. W. Chu, J. E. Box, R. R. Forster, M. R. Van den Broeke, D. Van As, and S. E. Moustafa (2013a), Evidence of meltwater retention within the Greenland ice sheet, *The Cryosphere*, *7*(5), 1433–1445, doi:10.5194/tc-7-1433-2013.

Rennermalm, A. K. et al. (2013b), Understanding Greenland ice sheet hydrology using an integrated multi-scale approach, *Environ. Res. Lett.*, *8*(1), 015017.

Rippin, D., I. Willis, N. Arnold, A. Hodson, J. Moore, J. Kohler, and H. Björnsson (2003), Changes in geometry and subglacial drainage of Midre Lovénbreen, Svalbard, determined from digital elevation models, *Earth Surf. Process. Landf.*, *28*(3), 273–298, doi:10.1002/esp.485.

Ritz, C., A. Fabre, and A. Letréguilly (1997), Sensitivity of a Greenland ice sheet model to ice flow and ablation parameters: Consequences for the evolution through the last climatic cycle, *Clim. Dyn.*, *13*, 11–24.

Röthlisberger, H. (1972), Water pressure in intra- and subglacial channels, *J. Glaciol.*, *11*, 177–203.

Ryser, C., M. P. Lüthi, L. C. Andrews, G. A. Catania, M. Funk, R. Hawley, M. Hoffman, and T. A. Neumann (2014a), Caterpillar-like ice motion in the ablation zone of the Greenland ice sheet, *J. Geophys. Res. Earth Surf.*, *119*(10), 2258–2271, doi:10.1002/2013JF003067.

Ryser, C., M. P. Lüthi, L. C. Andrews, M. J. Hoffman, G. A. Catania, R. L. Hawley, T. A. Neumann, and S. S. Kristensen (2014b), Sustained high basal motion of the Greenland ice sheet revealed by borehole deformation, *J. Glaciol.*, *60*(222), 647–660, doi:10.3189/2014JoG13J196.

Schoof, C. (2005), The effect of cavitation on glacier sliding, *Proc. R. Soc. Math. Phys. Eng. Sci.*, *461*(2055), 609–627, doi:10.1098/rspa.2004.1350.

Schoof, C. (2010), Ice-sheet acceleration driven by melt supply variability, *Nature*, *468*(7325), 803–806, doi:10.1038/nature09618.

Schoof, C., I. J. Hewitt, and M. A. Werder (2012), Flotation and free surface flow in a model for subglacial drainage. Part 1. Distributed drainage, *J. Fluid Mech.*, *702*, 126–156, doi:10.1017/jfm.2012.165.

Schweizer, J., and A. Iken (1992), The role of bed separation and friction in sliding over an undeformable bed, *J. Glaciol.*, *38*, 77–92.

Shannon, S. R. et al. (2013), Enhanced basal lubrication and the contribution of the Greenland ice sheet to future sea-level rise, *Proc. Natl. Acad. Sci.*, *110*(35), 14156–14161, doi:10.1073/pnas.1212647110.

Shepherd, A., A. Hubbard, P. Nienow, M. King, M. McMillan, and I. Joughin (2009), Greenland ice sheet motion coupled with daily melting in late summer, *Geophys. Res. Lett.*, *36*(1).

Shreve, R. L. (1972), Movement of water in glaciers, *J. Glaciol.*, *11*(62), 205–214.

Smith, L. C. et al. (2015), Efficient meltwater drainage through supraglacial streams and rivers on the southwest Greenland ice sheet, *Proc. Natl. Acad. Sci.*, *112*(4), 1001–1006, doi:10.1073/pnas.1413024112.

Sole, A., P. Nienow, I. Bartholomew, D. Mair, T. Cowton, A. Tedstone, and M. A. King (2013), Winter motion mediates dynamic response of the Greenland Ice Sheet to warmer summers, *Geophys. Res. Lett.*, *40*(15), 3940–3944, doi:10.1002/grl.50764.

Steffen, K., J. E. Box, and W. Abdalati (1996), Greenland Climate Network: GC-Net, in *Glaciers, Ice Sheets and Volcanoes: A Tribute to Mark F. Meier*, vol. Special Report 96-27, CRREL.

Stevens, L. A., M. D. Behn, J. J. McGuire, S. B. Das, I. Joughin, T. Herring, D. E. Shean, and M. A. King (2015), Greenland supraglacial lake drainages triggered by hydrologically induced basal slip, *Nature*, *522*(7554), 73–76, doi:10.1038/nature14480.

Stroeve, J. C., J. E. Box, and T. Haran (2006), Evaluation of the MODIS (MOD10A1) daily snow albedo product over the Greenland Ice Sheet, *Remote Sens. Environ.*, *105*(2), 155–171, doi:10.1016/j.rse.2006.06.009.

Sugiyama, S., and H. Gudmundsson (2004), Short-term variations in glacier flow controlled by subglacial water pressure at Lauteraargletscher, Bernese Alps, Switzerland, *J. Glaciol.*, *50*(170), 353–362, doi:10.3189/172756504781829846.

Sundal, A. V., A. Shepherd, P. Nienow, E. Hanna, S. Palmer, and P. Huybrechts (2011), Melt-induced speed-up of Greenland ice sheet offset by efficient subglacial drainage, *Nature*, *469*(7331), 521–524, doi:10.1038/nature09740.

Tarboton, D. G., R. L. Bras, and I. Rodriguez-Iturbe (1991), On the extraction of channel networks from digital elevation data, *Hydrol. Process.*, *5*(1), 81–100, doi:10.1002/hyp.3360050107.

Tedesco, M., X. Fettweis, M. R. van den Broeke, R. S. W. van de Wal, C. J. P. P. Smeets, W. J. van de Berg, M. C. Serreze, and J. E. Box (2011), The role of albedo and accumulation in the 2010 melting record in Greenland, *Environ. Res. Lett.*, *6*(1), 014005, doi:10.1088/1748-9326/6/1/014005.

Tedesco, M., X. Fettweis, T. Mote, J. Wahr, P. Alexander, J. E. Box, and B. Wouters (2013a), Evidence and analysis of 2012 Greenland records from spaceborne observations, a regional climate model and reanalysis data, *The Cryosphere*, *7*(2), 615–630, doi:10.5194/tc-7-615-2013.

Tedesco, M., I. C. Willis, M. J. Hoffman, A. F. Banwell, P. Alexander, and N. S. Arnold (2013b), Ice dynamic response to two modes of surface lake drainage on the Greenland ice sheet, *Environ. Res. Lett.*, *8*(3), 034007, doi:10.1088/1748-9326/8/3/034007.

Tedstone, A. J., P. W. Nienow, A. J. Sole, D. W. F. Mair, T. R. Cowton, I. D. Bartholomew, and M. A. King (2013), Greenland ice sheet motion insensitive to exceptional meltwater forcing, *Proc. Natl. Acad. Sci.*, *110*(49), 19719–19724, doi:10.1073/pnas.1315843110.

Tedstone, A. J., P. W. Nienow, N. Gourmelen, and A. J. Sole (2014), Greenland ice sheet annual motion insensitive to spatial variations in subglacial hydraulic structure, *Geophys. Res. Lett.*, *41*(24), 2014GL062386, doi:10.1002/2014GL062386.

Tedstone, A. J., P. W. Nienow, N. Gourmelen, A. Dehecq, D. Goldberg, and E. Hanna (2015), Decadal slowdown of a land-terminating sector of the Greenland Ice Sheet despite warming, *Nature*, *526*(7575), 692–695, doi:10.1038/nature15722.

Thomsen, H. H. (1986), Photogrammetric and satellite mapping of the margin of the inland ice, West Greenland, *Ann. Glaciol.*, *8*, 164–167.

Thomsen, H. H., L. Thorning, and R. J. Braithwaite (1988), *Glacier-hydrological conditions on the inland ice northeast of Jakobshavn/Illulisat, West Greenland*, Groenlands Geoloiske Undersoegelse.

Tsai, V. C., and J. R. Rice (2010), A model for turbulent hydraulic fracture and application to crack propagation at glacier beds, *J. Geophys. Res. Earth Surf.*, *115*(F3), F03007, doi:10.1029/2009JF001474.

Vaughan, D. G. et al. (2013), Observations: Cryosphere, in *Climate Change 2013: The Physical Science Basis. Contribution of Working Group I to the Fifth Assessment Report of the Inter governmental Panel on Climate Change*, pp. 317–382, Cambridge University Press, Cambridge, United Kingdom and New York, NY USA.

van der Veen, C. J. (1999), *Fundamentals of Glacier Dynamics*, A. A. Balkena Publishers, Rotterdam, Netherlands.

Velicogna, I. (2009), Increasing rates of ice mass loss from the Greenland and Antarctic ice sheets revealed by GRACE, *Geophys. Res. Lett.*, *36*(19), L19503, doi:10.1029/2009GL040222.

Velicogna, I., T. C. Sutterley, and M. R. van den Broeke (2014), Regional acceleration in ice mass loss from Greenland and Antarctica using GRACE time-variable gravity data, *Geophys. Res. Lett.*, *41*(22), 8130–8137, doi:10.1002/2014GL061052.

Vieli, A., J. Jania, H. Blatter, and M. Funk (2004), Short-term velocity variations on Hansbreen, a tidewater glacier in Spitsbergen, *J. Glaciol.*, *50*(170), 389–398, doi:10.3189/172756504781829963.

Walder, J., and A. Fowler (1994), Channelized subglacial drainage over a deformable bed, *J. Glaciol.*, *40*(134).

Walder, J. S. (1986), Hydraulics of subglacial cavities, *J. Glaciol.*, *32*(112), 439–445.

Walder, J. S., and B. Hallet (1979), Geometry of former subglacial water channels and cavities, *J. Glaciol.*, *23*(89), 335–346.

van de Wal, R. S. W. et al. (2015), Self-regulation of ice flow varies across the ablation area in south-west Greenland, *The Cryosphere*, *9*(2), 603–611, doi:10.5194/tc-9-603-2015.

van de Wal, R. S. W. van de, W. Boot, M. R. van den Broeke, C. J. P. P. Smeets, C. H. Reijmer, J. J. A. Donker, and J. Oerlemans (2008), Large and Rapid Melt-Induced Velocity Changes in the Ablation Zone of the Greenland Ice Sheet, *Science*, *321*(5885), 111–113, doi:10.1126/science.1158540.

Walter, F., J. Chaput, and M. P. Lüthi (2014), Thick sediments beneath Greenland's ablation zone and their potential role in future ice sheet dynamics, *Geology*, *42*(6), 487–490, doi:10.1130/G35492.1.

Weertman, J. (1957), On the sliding of glaciers, *J Glaciol.*, *3*(21), 33–38.

Weertman, J. (1964), The theory of glacier sliding, *J. Glaciol.*, *5*, 287–303.

Weertman, J. (1966), Effect of a basal water layer on the dimensions of ice sheets, *J. Glaciol.*, *6*, 191–207.

Weertman, J. (1969), Water lubrication mechanism of glacier surges, *Can. J. Earth Sci.*, *6*(4), 929–942, doi:10.1139/e69-097.

Weertman, J. (1979), The unsolved general glacier sliding problem, *J. Glaciol.*, *23*, 97–115.

Werder, M. A., A. Loye, and M. Funk (2009), Dye tracing a jökulhlaup: I. Subglacial water transit speed and water-storage mechanism, *J. Glaciol.*, *55*(193), 889–898.

Werder, M. A., I. J. Hewitt, C. G. Schoof, and G. E. Flowers (2013), Modeling channelized and distributed subglacial drainage in two dimensions, *J. Geophys. Res. Earth Surf.*, *118*(4), 2140–2158, doi:10.1002/jgrf.20146.

Willis, I. C., C. D. Fitzsimmons, K. Melvold, L. M. Andreassen, and R. H. Giesen (2012), Structure, morphology and water flux of a subglacial drainage system, Midtdalsbreen, Norway, *Hydrol. Process.*, *26*(25), 3810–3829, doi:10.1002/hyp.8431.

Yang, K., L. C. Smith, V. W. Chu, C. J. Gleason, and M. Li (2015), A Caution on the Use of Surface Digital Elevation Models to Simulate Supraglacial Hydrology of the Greenland Ice Sheet, *IEEE J. Sel. Top. Appl. Earth Obs. Remote Sens.*, 1–13, doi:10.1109/JSTARS.2015.2483483.

Zwally, H. J., W. Abdalati, T. Herring, K. Larson, J. Saba, and K. Steffen (2002), Surface Melt-Induced Acceleration of Greenland Ice-Sheet Flow, *Science*, *297*(5579), 218–222, doi:10.1126/science.1072708.